



Universiteit  
Leiden  
The Netherlands

## **Diagnostic challenges of today's lung cancer pathology: personalizing therapy by immunohistochemical and molecular biomarkers**

Hondelink, L.M.

### **Citation**

Hondelink, L. M. (2023, November 8). *Diagnostic challenges of today's lung cancer pathology: personalizing therapy by immunohistochemical and molecular biomarkers*. Retrieved from <https://hdl.handle.net/1887/3656465>

Version: Publisher's Version

License: [Licence agreement concerning inclusion of doctoral thesis in the Institutional Repository of the University of Leiden](#)

Downloaded from: <https://hdl.handle.net/1887/3656465>

**Note:** To cite this publication please use the final published version (if applicable).

# DIAGNOSTIC CHALLENGES OF TODAY'S LUNG CANCER PATHOLOGY

LIESBETH HONDELINK



# Diagnostic challenges of today's lung cancer pathology

Liesbeth Hondelink

Diagnostic challenges of today's lung cancer pathology

Personalizing therapy by immunohistochemical and molecular biomarkers

ISBN: 978-94-6483-512-0

Copyright 2023, Liesbeth Hondelink

# Diagnostic challenges of today's lung cancer pathology

Personalizing therapy by immunohistochemical  
and molecular biomarkers

Proefschrift

ter verkrijging van  
de graad van doctor aan de Universiteit Leiden,  
op gezag van rector magnificus prof.dr.ir. H. Bijl,  
volgens besluit van het college voor promoties  
te verdedigen op woensdag 8 november 2023  
klokke 13:45 uur

door

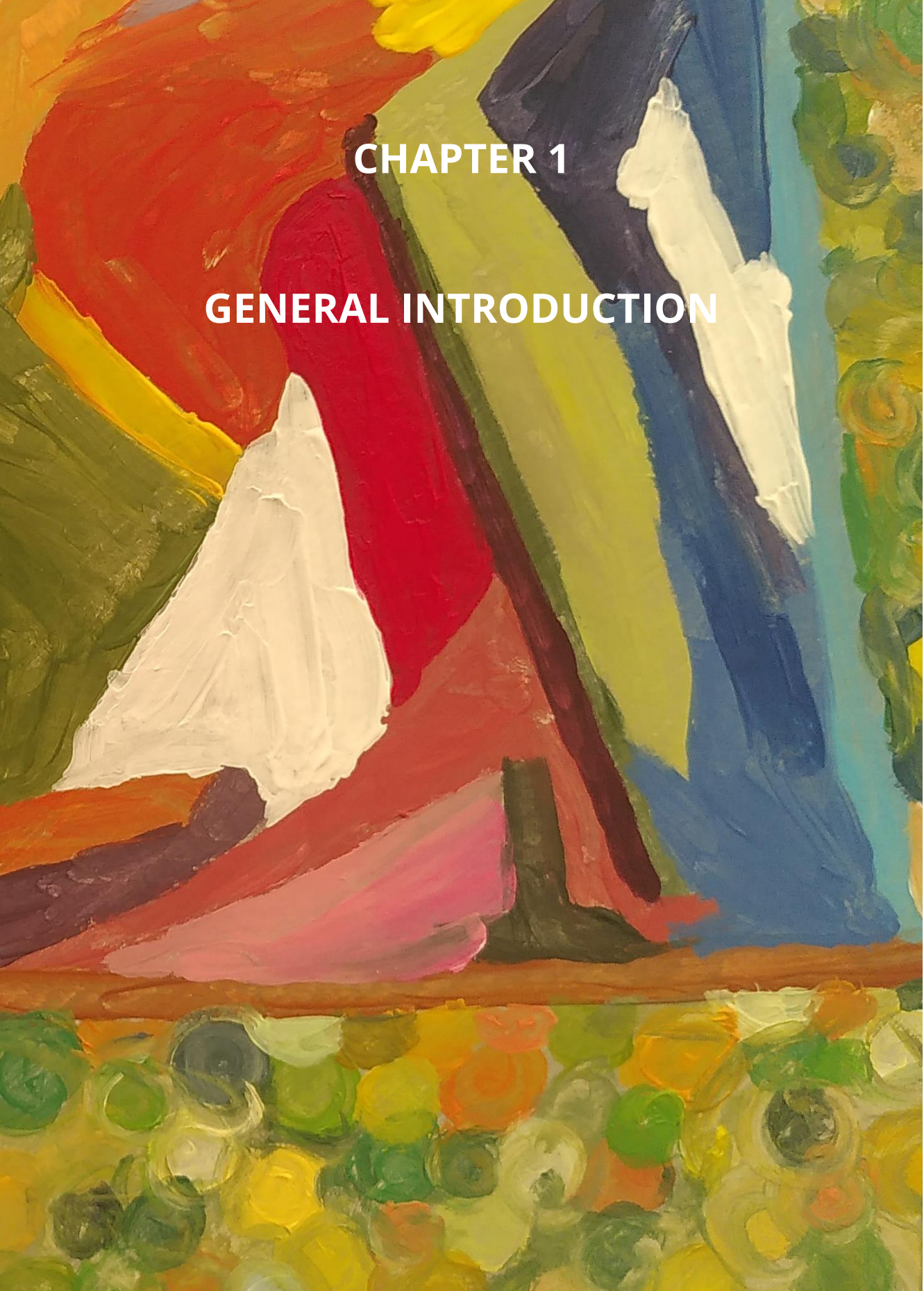
Liesbeth Hondelink

Promotor	Prof.dr. P.E. Postmus
Co-promotores	Dr. D. Cohen Dr. J.H. von der Thüsen
Promotiecommissie	Prof.dr. A.C. Dingemans, Erasmus MC Prof.dr. M. van den Heuvel, Radboud UMC Dr. T. Radonic, Amsterdam UMC Prof.dr. W. Dinjens, Erasmus MC

## Table of contents

Chapter 1	page 7
<i>General Introduction</i>	
Chapter 2	page 31
<i>Early stage EGFR mutations: Prevalence, clinical and molecular characteristics of early-stage EGFR-mutated lung cancer in a real-life West-European cohort: implications for adjuvant therapy.</i>	
Chapter 3	page 51
<i>Treatment-naïve stage IV NSCLC molecular workup: Optimizing mutation and fusion detection in Non-Small Cell Lung Cancer by sequential DNA and RNA sequencing.</i>	
Chapter 4	page 83
<i>PD-L1 algorithm: Development and validation of a supervised deep learning algorithm for automated whole-slide programmed death-ligand 1 tumour proportion score assessment in non-small cell lung cancer.</i>	
Chapter 5	page 109
<i>NTRK immunohistochemistry: The sensitivity of pan-TRK immunohistochemistry in solid tumors: a meta-analysis.</i>	
Chapter 6	page 127
<i>EGFR TKI resistance molecular workup: Real-World Approach for Molecular Analysis of Acquired EGFR Tyrosine Kinase Inhibitor Resistance Mechanisms in NSCLC.</i>	
Chapter 7	page 155
<i>Discussion, summary and future challenges</i>	
Appendices	page 173
<i>Nederlandse samenvatting</i>	
<i>List of publications</i>	
<i>Curriculum vitae</i>	
<i>Dankwoord</i>	



An abstract painting featuring bold, expressive brushstrokes in a variety of colors including red, white, blue, green, yellow, and pink. The composition is dynamic, with thick layers of paint creating a sense of depth and movement. The background is a mix of these colors, with some areas appearing more saturated than others. The overall style is reminiscent of modernist or expressionist art.

# CHAPTER 1

## GENERAL INTRODUCTION

# Chapter 1: General introduction

## 1.1 Case presentation, a patient journey anno 2023

A 62-year old former smoker visits the pulmonologist because a pulmonary node in the left upper lobe is discovered. His symptoms are limited, only a dry cough that he has had for a few weeks. A CT-guided biopsy is taken, which leads to the diagnosis of non-small cell lung cancer (NSCLC). Specifically a TTF-1 positive adenocarcinoma with lepidic, papillary and micropapillary growth patterns is diagnosed. After comprehensive staging with PET-CT and EBUS, it's established that the patient has a T1bN0M0 tumor. He undergoes a lobectomy of the left upper lobe. The resection margins are tumor-free and the carcinoma has not infiltrated the visceral pleura.

After 2 years and 3 months, a liver nodule is revealed, and a biopsy confirms that it is a metastasis of the prior lung adenocarcinoma. Thus, the patient is now stage IV, which warrants additional molecular and immunohistochemical tests. The PD-L1 tumor proportion score is 5% and mutations in EGFR p. L858R and TP53 p. V157S are identified with DNA NGS. The patient is treated with Osimertinib. Following an 18-month period of stable disease, growing lesions are discovered in the adrenal gland and lymph nodes. A new biopsy is taken from one of the growing mediastinal lymph nodes via fine needle aspiration, in which an EML4:ALK fusion is identified, in addition to the EGFR p. L858R and TP53 p. V157S mutations. The patient is treated with chemoradiation and dies within 9 months. (Figure 1)

This case, of which there are hundreds of similar ones in the Netherlands each year, illustrates the complexity of the current NSCLC patient journey. The pathologist is prominently involved, and is required to assess the case at key decision-making moments in the disease process: at the early-stage diagnosis, at the late-stage diagnosis and at the moment of acquired resistance.

## 1.2 Introduction Outline

In this introduction, the characteristics of NSCLC, including the molecular makeup and genomic heterogeneity are comprehensively addressed. The most important novel treatments are outlined: targeted tyrosine kinase inhibitors (TKIs) and immune-checkpoint inhibitors (immunotherapy), including a

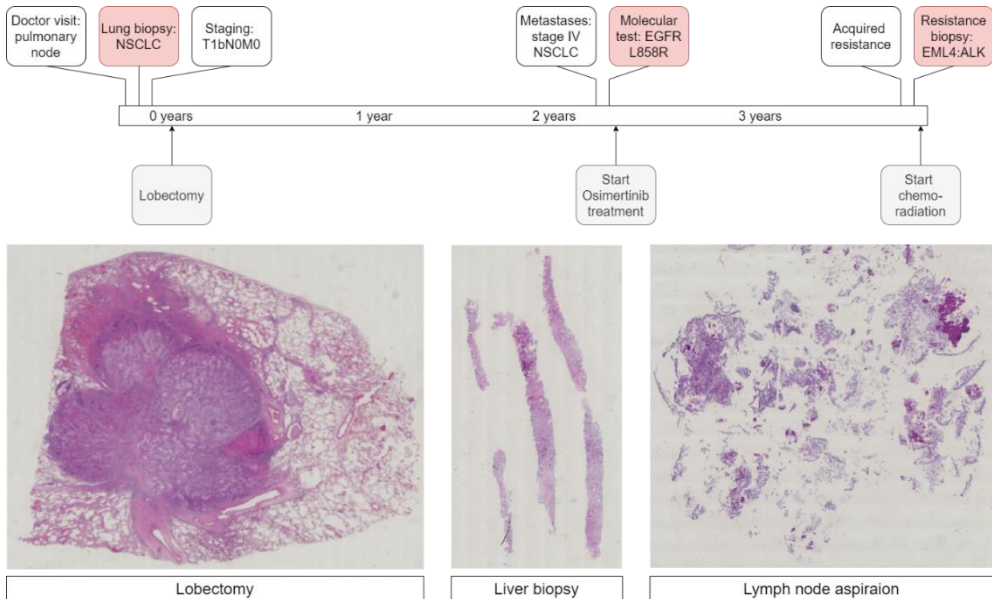


**Figure 1:** Case patient journey. Red: pathologist tasks. Grey: New treatment.

detailed description of testing techniques to select patients for either of these therapies. In the final paragraph, the societal impact of lung cancer research will be discussed.

### 1.3 Lung Cancer demographics

Lung cancers are one of the most common and deadly cancers worldwide, with 1.6 million deaths annually. [1] In the Netherlands, approximately 13,000 new lung cancer patients are diagnosed each year, the majority of which suffer from non-small cell lung cancer (NSCLC). [2]

The high death rate of NSCLC is in part due to the late stage at diagnosis: due to the localization, many tumors remain asymptomatic until after the tumor has metastasized. Approximately 50% of patients are therefore diagnosed in stage IIIB or IV. In addition, early stage tumors are not always successfully cured. Approximately 50% of patients who undergo surgical resection die of lung cancer within 5 years, likely due to the presence of occult metastasis at the time of surgery.

NSCLC can be divided into two main subtypes: lung adenocarcinoma and lung squamous cell carcinoma. [3, 4] Adenocarcinomas can be further divided using growth patterns or differentiation grade, leading to a stratification of patients in low risk (well differentiated, lepidic growth), intermediate risk (moderately

differentiated, papillary or acinar growth) and high risk (poorly differentiated, solid, complex glandular or micropapillary growth). [5]

Up to 90% of lung cancers can be attributed to tobacco smoking. [6] In 2019, 21.7% of adults and 8% of children aged 12-16 in the Netherlands were smokers. [7] Worldwide, 20% of individuals aged 15 or above are smokers. (Figure 2) In 2019, 7.7 million deaths were attributable to tobacco smoking worldwide, making smoking the cause of 13.6% of all deaths that year. [8] In the Netherlands, 13.1% of deaths are still attributed to smoking in 2019, which is only just below the global average.

Smoking is more common in people in a lower socio-economic class, making tobacco addiction a true poverty disease. In the Netherlands, 15.4% of HBO and University-educated people were smokers, versus 26.2% of people who attended VMBO, MAVO, LBO or primary school only. [7] Remarkably, although smoking prevalence is slowly decreasing in the Netherlands, the number of smokers is still rising in many other countries, which are often low- to middle-income countries: Azerbaijan, Georgia, Kyrgyzstan, Mongolia, Uzbekistan, Albania, Bosnia and Herzegovina, North Macedonia, Serbia, Belarus, Lithuania, Moldova, Russia, Antigua and Barbuda, Belize, Grenada, El Salvador, Afghanistan, Egypt, Iran, Jordan, Lebanon, Saudi Arabia, Federated States of Micronesia, Kiribati, Solomon Islands, Tuvalu, Indonesia, Laos, Congo, Equatorial Guinea, Gabon, Djibouti, Lesotho, Côte d'Ivoire, Guinea-Bissau, Mali, Niger and São Tomé and Príncipe. [8]

Therefore, perhaps the most important aspect of lung cancer management is prevention. Smoking eradication, together with screening (heavy) smokers for pulmonary nodules is paramount. It was recently demonstrated that low-dose CT screening in heavy smokers aged 50-74 reduces lung cancer related mortality by 24%, which is an important argument in favor of population screening. [9]

#### 1.4 Molecular landscape of NSCLC; smokers versus non-smokers

The vast majority of NSCLCs are caused by the inhalation of carcinogens (tobacco smoke, air pollution and occupational carcinogens). These carcinogens lead to an accumulation of DNA-mutations, which drives cells to

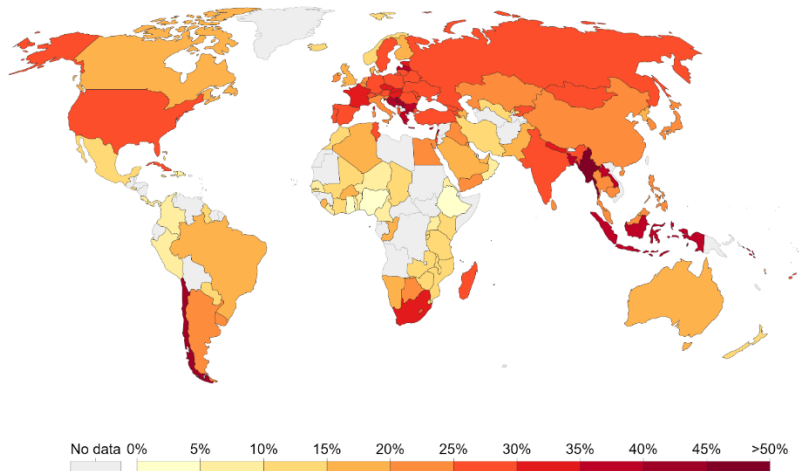


**Figure 2:** Worldwide prevalence of smoking in 2018, measured in individuals aged 15 and older. Adapted from Ritchie et al, *Our World In Data*. [10]

malignant behavior via the alteration oncogenic driver genes (such as KRAS and EGFR) or tumor-suppressor genes (such as TP53 and CTNNB1). [3, 4, 11] Due to this mechanism of carcinogenesis, tobacco-related lung cancers can harbor many different DNA-alterations and are highly heterogeneous in their molecular makeup. [3, 12] Typical smoking-related DNA-alterations are KRAS, BRAF, PTEN, PIK3CA and TP53. [13]

A minority of NSCLCs arises in never-smokers. These tumors have a different molecular signature and more frequently harbor mutations in ALK, ROS1, RET, HER2 and EGFR. [3, 13, 14] Tumors in never-smokers generally have a lower tumor mutational burden (TMB) and fewer co-mutations in tumor suppressor genes such as TP53. [13, 14] Never-smokers respond differently to treatment with TKIs, [15] immunotherapy [16] and chemotherapy. [17]

When assessing the smokers and never-smokers together, it's clear that NSCLC is a highly heterogeneous disease, both in the clinical and genomic aspect. Known driver alterations, their prevalence and common NSCLC growth patterns are outlined in Figure 3.

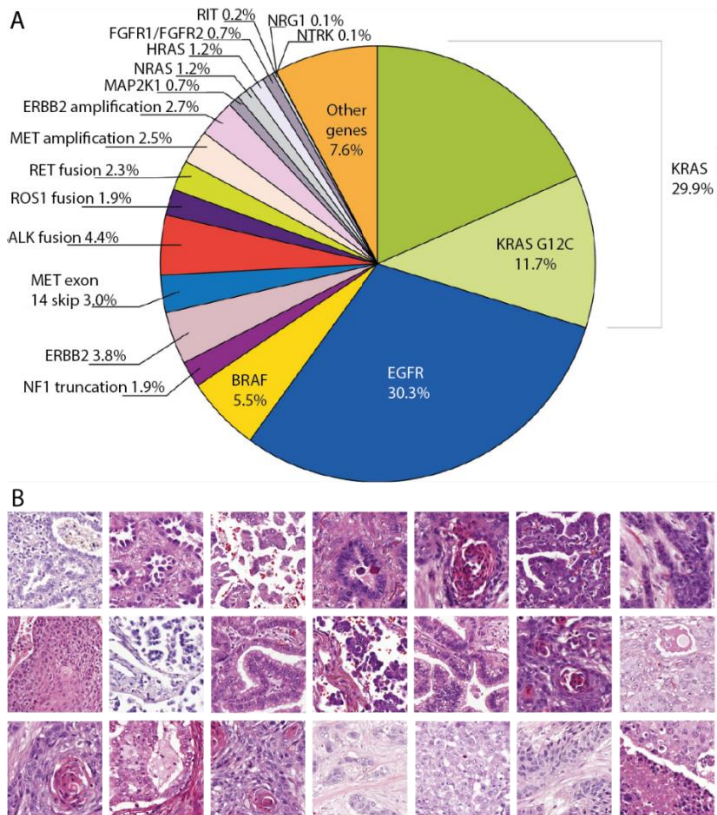


**Figure 3:** Lung cancer heterogeneity. A: oncogenic driver mutations in metastatic lung adenocarcinoma. Adapted from Addeo et al. [18] B: morphological heterogeneity in surgical NSCLC specimens.

#### 1.4.1 Intratumor genomic heterogeneity and tumor evolution

In addition to these differences *between* tumors, there is substantial genetic heterogeneity *within* tumors as well. Recent studies have reported that genomic aberrations often occur only in subclonal portions of lung cancer cells, which is called 'intratumor genomic heterogeneity'. This is observed for all mutations, including oncogenic drivers. [19, 20] Using multi-region tissue sequencing experiments, a distinction can be made between 'trunk mutations', that are homogenously present in all tumor sequencing regions, 'branch mutations', that are only present in part of the tumor sequencing regions, and germline mutations, present in all tumor and benign sequencing regions. (Figure 4) [20] It's hypothesized that intratumor genomic heterogeneity could

be the substrate for mixed response, acquired resistance, morphologic heterogeneity and tumor progression. [19]

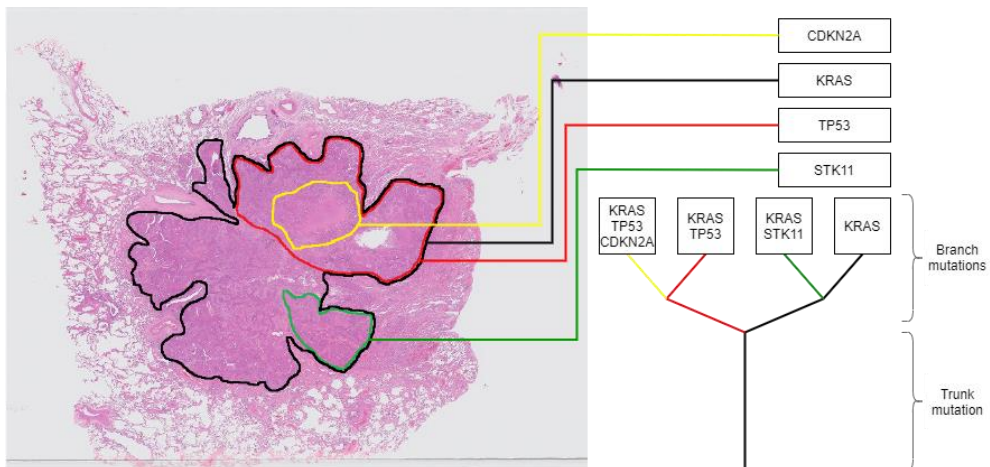


**Figure 4:** Example of intratumor genetic heterogeneity (ITH), with one trunk mutations (in this case: KRAS) and multiple branch mutations (in this case: STK11, TP53, CDKN2A).

### 1.5 Targeted therapy and acquired resistance

For decades, the treatment of NSCLC was limited to surgery, radiation and chemotherapy, with limited survival benefit and substantial co-morbidity and mortality. [3, 4, 21, 22] An important change started in 2003, with the registration of gefitinib for chemotherapy-refractory metastatic NSCLC.

#### 1.5.1 History: Gefitinib and other TKIs

Gefitinib, an antagonist for the endothelial growth factor receptor (EGFR), was first intended as a generic cancer growth inhibitor, but its introduction in the clinic in 2003 led to unexpected results. Whereas a small portion of chemotherapy-refractory NSCLC patients (10-19%) showed remarkable response to gefitinib, no effect was observed at all in the majority of patients. Later, in 2004, activating EGFR-mutations, such as L858R and exon 19 deletion, were identified in gefitinib-sensitive patients and showed to be absent in gefitinib-insensitive patients. [23]

These data formed the basis of a new and optimistic field of cancer research – targeted DNA-therapy. Simply finding the tumor’s driver mutation and

inhibiting it with a specific antagonist – the cancer’s kryptonite – would be the key to achieve durable response or even curation for all lung cancer patients.

In addition to EGFR, there are now tyrosine kinase inhibitors (TKIs) routinely available, targeting alterations in BRAF V600, [24] ALK, [25] MET, [26] HER2, [27] ROS1, [28] NTRK [29] and RET [30]. (Figure 5) For many other targets, such as BRAF non-V600, KRAS G12C and NRG1, new TKIs are available in the experimental context or via compassionate use or early access programs. However, for some targets, it has been difficult to find an effective TKI, and not all TKIs are perhaps as effective as we hoped: although progression-free survival has become significantly longer for stage IV patients with targetable mutations, complete curation is still far away.

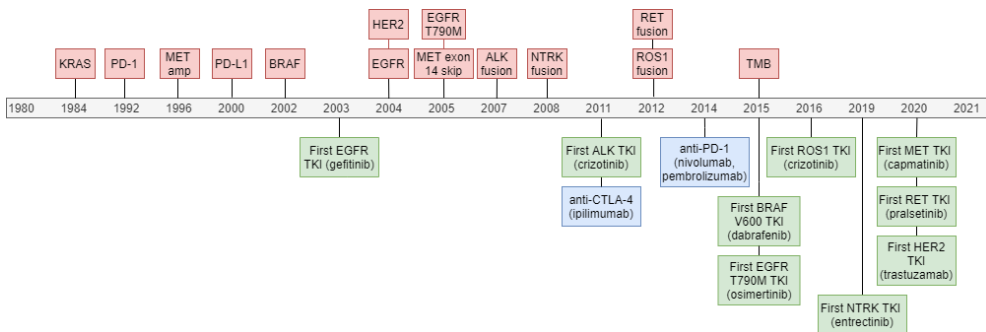


**Figure 5:** timeline novel targets and therapies NSCLC. Red: Targets. Green: TKIs. Blue: immunotherapy.

### 1.5.2 Acquired resistance

It has also become clear that, although many patients respond excellent to TKIs, eventually tumors bypass these inhibitory drugs and become resistant, often by acquiring additional oncogenic mutations. From that moment, one or more lesions will continue to grow and the disease progresses. [31-33] The mechanism by which the tumor acquires resistance can, in turn, be a targetable genomic aberration (such as EML4:ALK fusion), for which yet another TKI might be administered. [34]

A famous example is, again, EGFR. After the early successes of gefitinib and the discovery of mutations in the EGFR gene, the resistance mechanism EGFR p. T790M was discovered in 2005. The T790M mutation makes it impossible for gefitinib, afatinib and erlotinib to bind to EGFR, and prohibits its antagonistic effects. T790M therefore leads to reactivation of mutant EGFR and perfectly

explains the acquired resistance phenotype. In addition to T790M, many other resistance mechanisms have been discovered since, in part oncogenic driver mutations that we know, such as KRAS p. G12C, ALK fusion, HER2 amplification and MET amplification, but also novel mutations, such as EGFR p. C797S after treatment with Osimertinib. [35] Treatment with other TKIs, such as crizotinib, seems to follow the same principles as EGFR TKI treatment. [32, 36]

### 1.5.3 NTRK

An especially interesting, relatively novel target is NTRK. For most genetic targets, TKIs are first established in one cancer type and then translated to others. This is true for HER2, which was first discovered and treated in breast cancers; BRAF V600E, which was first discovered and treated in melanomas, and RET fusions, which were first discovered and treated in thyroid carcinomas. This tissue-oriented approach is a distinct disadvantage for patients with rare cancers, who are often the last to benefit from these new treatments.

Fusions in NTRK are extremely rare in NSCLC and in most cancers, whereas they are common in others (e.g. secretory carcinoma). Entrectinib and Larotrectinib trials therefore included all NTRK-rearranged metastatic solid tumors from the start, which has led to the registration of NTRK TKIs as first-line therapy for all solid tumors. [29, 37] This registration clearly marks the beginning of a shift from diagnosis-based to gene-based treatment.

### 1.6 Towards personalized medicine: selecting the right patients

There are many methods available for TKI and immunotherapy susceptibility testing, and finding the most optimal sequence can certainly be challenging. Often, there are significant time constraints, as the performance state of patients can be poor and waiting is not optimal, especially when brain metastases are present. In addition, the tissue available for genetic testing is rarely abundant; in some cases only cytology or small biopsy specimens are available, holding a limited number of tumor cells for molecular testing. When the tissue runs out before a definitive diagnosis is established, the patient has to undergo another biopsy, which can cause serious side effects and delay the diagnosis. Additionally, there can be financial limitations as well, since comprehensive genetic testing is costly. The pathologist therefore has to

identify the diagnosis method that minimizes time, tissue and expenses, while still achieving high effectiveness in finding targetable DNA-mutations.

As outlined in the patient journey figure (Figure 1), testing to select patients for immunotherapy or TKI treatment is now required at two specific moments: right after the diagnosis of metastatic lung cancer (1) and when acquired resistance occurs (2). In the future, testing will be implemented in the early stage as well, since there are indications in the literature that immunotherapy and treatment with TKIs could give early stage, surgical patients a survival benefit as well. [38, 39] In addition, as the management of acquired resistance mechanisms continues to evolve, patients could be treated with multiple lines of TKI treatment, which would further increase the number of testing moments.

### 1.6.1 A history of molecular testing

Since the discovery of the structure and function of DNA and specifically the Watson-Crick DNA model in 1953, molecular testing has taken off. In the 1980s, molecular testing became routed in routine diagnostics, via the application of Southern blotting to identify DNA alterations in Duchenne and fragile X syndrome.

In the 1993, the invention of polymerase chain reaction (PCR) [40] and the following introduction into clinical diagnostics was an important milestone, that enabled large-scale testing for HIV, hepatitis and other infectious diseases. In the late 1990s, genetic testing was applied to population screening for the first time, when testing newborns for cystic fibrosis mutations became the standard.

The first application of genetic testing for oncology occurred with the testing for the BCR:ABL translocation, the most common driver of chronic myelogenous leukemia (95%) and associated with acute lymphoblastic leukemia (ALL). With a novel and potent ABL TKI [41, 42] available – the first TKI ever described – all CML patients were required to undergo testing for the BCR:ALB fusion product, widely known as the ‘Philadelphia gene’. This testing was first implemented using Sanger sequencing, a widely used and relatively fast technique, [43] which was later also commonly used to detect the first pathogenic EGFR mutations, including p. L858R.

However, it was only after the completion of the Human Genome Project in 2003, that the focus of molecular diagnostics research truly shifted from infectious and hereditary diseases to cancer. With the approval of Herceptin for HER2-amplified breast cancer, testing for HER2 amplifications suddenly became a requirement, which led to the implementation of fluorescent in situ hybridization in many Pathology laboratories. [44] Additionally, the discovery of gefitinib-sensitizing EGFR mutations became an incentive for testing metastatic NSCLC for exon 19 deletions and L858R mutations in EGFR. [45]

Around the same time, PCR and automated Sanger sequencing were slowly replaced by next-generation DNA sequencing, a high-throughput multi-target method with wide applicability. In the mid-2010s, many laboratories started using DNA NGS to routinely screen for frequently occurring somatic oncogene mutations in KRAS, EGFR, BRAF, etc. [46] Although DNA NGS is well suited to find point mutations, small deletions, insertions and (when the tumor cell percentage is sufficient) amplifications, the identification of fusions and exon skipping events was always performed with in situ hybridization. In recent years, RNA NGS has replaced ISH in many laboratories.

The newest step in this rapid succession of molecular panels is the transfer to whole genome sequencing (WGS) and whole exome sequencing (WES). WGS and WES utilize massive sequencing panels covering the entire genome or exome. Although not yet routinely used for diagnostics in all clinical laboratories, WGS and WES are routinely applied for research purposes.

### 1.6.2 Current molecular testing methods

Testing methods currently available in routine diagnostic laboratories in the Netherlands include: immunohistochemistry (IHC), in situ hybridization (ISH), DNA NGS and RNA NGS. Each method has distinct advantages and disadvantages, as discussed below, which makes choosing the optimal workup challenging and complex.

#### 1.6.2.1 Immunohistochemistry

IHC can be used to measure expression of a specific protein. (Figure 6A) In NSCLC, literature indicates that several genetic targets can be identified with IHC (ALK fusion, [47] ROS1 fusion, [48] NTRK fusion, [49] HER2 amplification [50]), as well as susceptibility to immunotherapy (PD-L1 expression). [51, 52]

The most important advantage of IHC is its speed and price – IHC is a relatively fast and cheap method. A distinct downside is the fact that IHC is a single-target assay. In addition, IHC results can be subjective, and thus less than 100% sensitive and specific.

#### 1.6.2.2 *In situ hybridization*

ISH can be used to identify translocation or amplification of a specific gene. (Figure 6B, 6C) In NSCLC, ISH is frequently used, to detect amplifications in MET, [53] EGFR [54] and HER2, [50] as well as fusions in ALK, [47] ROS1, [48] RET [55] and NTRK. [49] As ISH is a single-target assay, a separate analysis is required for each target gene, which is a disadvantage. In addition, information about the breakpoint and fusion partner is generally not provided by ISH. An important advantage over DNA NGS, however, is the ability to detect polysomy and amplifications in part of the tumor cells, which is an important benefit when dealing with intratumor genetic heterogeneity in TKI resistance cases.

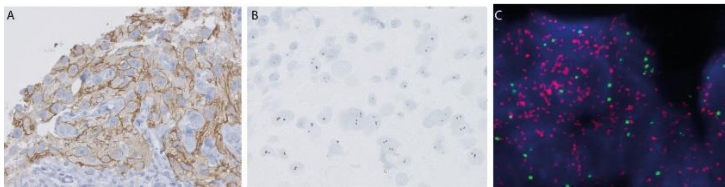


**Figure 6:** IHC and ISH examples. A: HER2 IHC. B: HER2 silver ISH. C: MET:C7 fluorescent ISH. Adapted from Chapter 3.

#### 1.6.2.3 DNA NGS

DNA NGS panels are able to identify alterations on a single nucleotide level within the DNA. DNA NGS can detect point mutations, small deletions and insertions with high accuracy. To some extent, DNA NGS also detects copy number variance, exon skipping and fusions. However, DNA NGS detections are highly dependent on which targets are included in the panel. Whole genome sequencing covers the entire genome, and is well suited to detect copy number variance, exon skipping and fusions, but also requires a much higher tissue input. Most laboratories therefore use a much smaller panel, which covers hotspots in cancer genes, but excludes introns and non-hotspot areas. Most clinically used DNA NGS panels therefore can't detect fusions and exon skipping. The ability to detect amplifications with smaller DNA NGS panels greatly depends on the tumor cell percentage. When the tumor cell

percentage is too low, amplifications can easily be missed, especially in tumors with intratumor genetic heterogeneity.

#### 1.6.2.4 RNA NGS

RNA NGS identifies alterations on a single nucleotide level within the RNA. RNA NGS therefore identifies fusions, exon skipping events, point mutations and small insertions and deletions of covered regions. In contrast to ISH and IHC, DNA NGS and RNA NGS are multi-target assays. An important advantage of RNA NGS over ISH is the ability to detect fusion partners and breakpoint. Although RNA NGS uses more tissue than one ISH analysis, RNA NGS is a multi-target assay, meaning that multiple genes can be screened for translocations in one test. RNA NGS is less effective in bone lesions, as RNA quality decreases from the chemicals used in the decalcification process. The applications of RNA NGS and the techniques discussed above are summarized in Figure 7.

### 1.7 Immunotherapy

Immunotherapy is based on the interaction between programmed death ligand 1 (PD-L1) and programmed death 1 (PD-1). (Figure 8) When tumor cells express PD-L1, and this binds to the PD-1 receptor on T-cells, T-cells deactivate or undergo apoptosis, thus providing an effective method of immune evasion for the tumor. [56] Blocking this PD-1/PD-L1 interaction with monoclonal antibodies such as anti-PD-1 (nivolumab, pembrolizumab) constitutes an effective anti-tumor therapy, that has been reported to lead to a substantial survival benefit. [52, 57-60]

#### 1.7.1 Immunotherapy, a brief history

The first mention of cancer immune therapy in the scientific literature was in 1891, when sarcoma and lymphoma patients were treated with live, inactivated *Streptococcus pyogenes* and *Serratia marcescens* by dr. Coley, in an attempt to activate the immune system against the tumor. [61, 62] Since then, the idea of activating the immune system and using it as a weapon against cancer, has taken root, and pan-cancer immunotherapy became a distant dot on the horizon. Since the discovery of the PD-1/PD-L1 interaction and its role in the immune evasion in cancer became clear in 2002, [56] that dot has become a lot closer. Years of murine models and preclinical testing

finally resulted in the approval of ipilumab in 2011 [63] and nivolumab [59, 64] and pembrolizumab in 2014 [58].

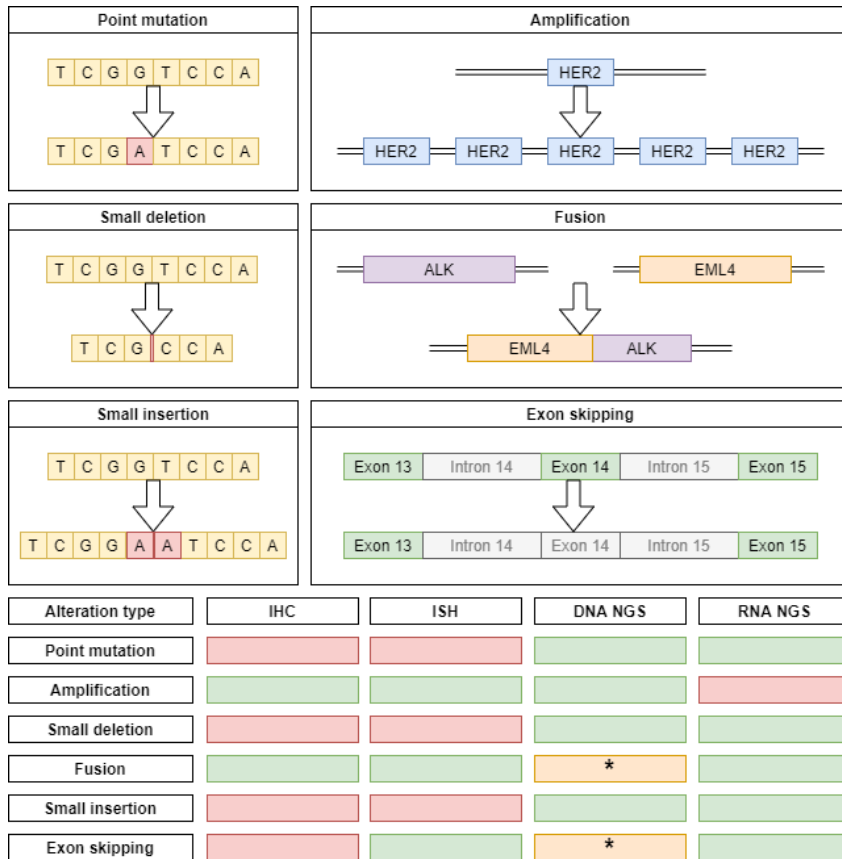


**Figure 7:** testing for molecular alterations per alteration type. Green rectangle: testing is possible; red rectangle: testing is not possible; orange rectangle: sometimes possible. \*: only with good coverage of introns, for example whole genome sequencing (WGS).

Being high-volume and high-mutational burden tumors, most of these immunotherapy regimens were registered for advanced metastatic NSCLC and melanoma first, but are now expanding to other cancers as well, including breast cancer and head- and neck squamous cell carcinoma, with promising results. Immune regulatory drugs have opened up an entirely new avenue for cancer treatment and research, which is a true game changer for the field of Medical Oncology, and was thus awarded the Nobel Prize in 2018. [65]

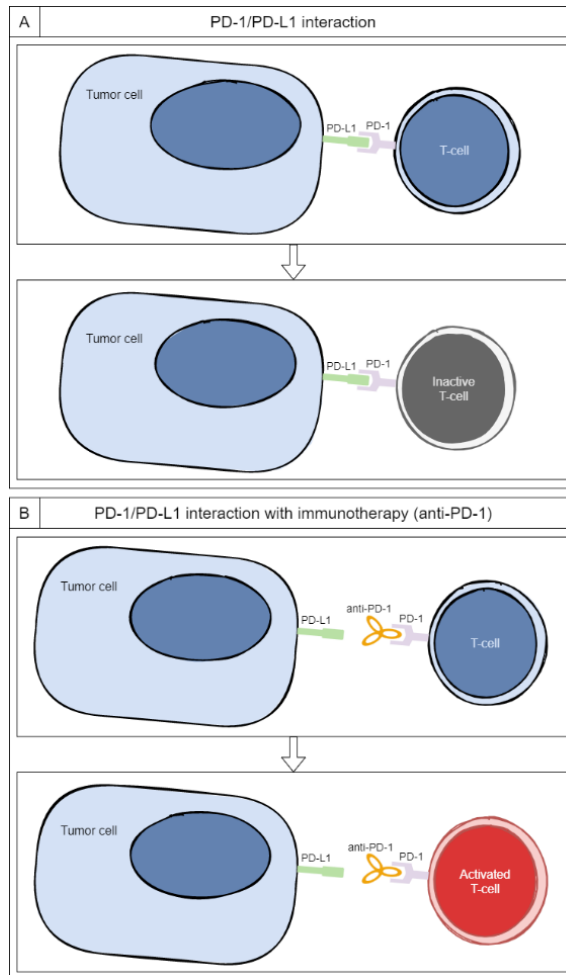


**Figure 8:** PD-1/PD-L1 interaction and immunotherapy. A: interaction between tumoral PD-L1 and T-cell PD-1, resulting in T-cell apoptosis. B: inhibition of the PD-L1/PD-1 interaction by immunotherapy (monoclonal anti-PD-1 antibodies, pembrolizumab or nivolumab), resulting in T-cell activation.

### 1.7.2 Immunohistochemical PD-L1 as a biomarker for immunotherapy response

However, not all patients respond to immunotherapy to the same extent. Whereas some patients achieve durable progression-free survival, others have limited or no benefit from immunotherapy. [58, 59] The most important predictive biomarkers are the expression of immunohistochemical PD-L1 on tumor cell membranes [52, 58] and the tumor mutational burden (TMB), [66]

which have, since the introduction of immunotherapy in the clinic, become tremendously important in routine diagnostics.

However, both biomarkers are problematic. Both are non-perfect predictors of immunotherapy response: some patients with high PD-L1 expression or TMB fail to respond, and vice versa. In addition, PD-L1 is subject to substantial interobserver variance due to human limitations in estimating percentages, and there is a risk of sampling error, due to the intratumor heterogeneity of PD-L1 expression. (Formula 1) TMB can be assessed with multiple bioinformatics methods and NGS panels, each leading to a different 'mutations per megabase' score. Most of the currently used (lung) cancer panels are too small to determine the TMB, only the bigger panels (with higher drop-out) are able to, which means not all laboratories are able to assess TMB yet. And finally, due to intratumor genomic heterogeneity, (1.4.1) the TMB is not the same in all tumor regions, which could lead to sampling error.

$$PD - L1 \text{ score} = \frac{PD - L1 \text{ positive tumor cells}}{PD - L1 \text{ positive tumor cells} + PD - L1 \text{ negative tumor cells}}$$

**Formula 1:** *PD-L1 tumor proportion score.*

### 1.7.3 Future biomarkers

Therefore, the search for new biomarkers for immunotherapy response continues. Most efforts have been focused on the makeup of the tumor immune microenvironment (TME), which is one of the key elements of an anti-tumor response. Important potential biomarkers, which have already shown to be associated with immunotherapy response in lung cancer are: tumor-infiltrating cytotoxic (CD8+) T-cells, [61, 67] M2-polarized macrophages, [67, 68] plasmablasts, [67, 69] IFN $\gamma$  messenger RNA, [67, 70] dendritic cells [67, 71] and macrophage PD-L1 expression. [67, 72] In addition, there are numerous potential biomarkers correlated to immunotherapy response in other cancers, such as tertiary lymphoid structures. [67]

What this quantity of TME studies illustrates, is that the interaction between cancer and immune system is complex – perhaps even more so than we now realize. Efforts to compress this complexity into a single-target biomarker such as PD-L1 are ambitious but also slightly naïve. In the future, we might be able to comprehensively assess the TME and come with personalized and accurate

immunotherapy response predictions, but for now, patient selection remains imperfect.

## 1.8 Thesis Outline and Aims

To summarize, there are more treatment options for NSCLC than ever before, which makes selecting the treatment regimens an increasingly complex task. Pulmonary pathologists are faced with the difficult challenge of testing patients for a wide range of molecular alterations and predicting immunotherapy susceptibility. For this task, they can use a number of tests: IHC, ISH, DNA NGS and RNA NGS. However, in this rapidly changing field of molecular diagnostics and cancer immunology, the optimal testing method is not always clear. A balance must be found between tissue-efficiency, time, costs and comprehensiveness of testing.

The general aim of this thesis is therefore to retrospectively investigate the current testing landscape, and identify the most optimal testing sequence for NSCLC patients, at three key decision making moments:

1. Early stage NSCLC
2. Late stage NSCLC, treatment-naïve
3. Late stage NSCLC after acquired resistance

**Chapter 2** describes the yield of molecular testing in early stage NSCLC.

**Chapter 3** discusses the optimal workup in stage IV NSCLC. **Chapter 4** investigates the role of AI in PD-L1 immunoscore. **Chapter 5** describes the sensitivity of NTRK IHC, and whether it should be used in routine diagnostics.

**Chapter 6** describes the molecular workup after acquired resistance to EGFR TKIs.

## References

1. Bray F, Ferlay J, Soerjomataram I, et al., *Global cancer statistics 2018: GLOBOCAN estimates of incidence and mortality worldwide for 36 cancers in 185 countries*. *CA Cancer J Clin*, 2018. **68**: p. 394-424.
2. IKNL. *Nederlandse Kankerregistratie (NKR)*. 4-11-2021]; Available from: [iknl.nl/nkr-cijfers](http://iknl.nl/nkr-cijfers).
3. Herbst RS, Morgensztern D and Boshoff C, *The biology and management of non-small cell lung cancer*. *Nature*, 2018. **553**(7689): p. 446-454.
4. Molina JR, Yang P, Cassivi SD, et al., *Non-small cell lung cancer: epidemiology, risk factors, treatment, and survivorship*. *Mayo Clin Proc*, 2008. **83**(5): p. 584-594.
5. Moreira AL, Ocampo PSS, Xia Y, et al., *A Grading System for Invasive Pulmonary Adenocarcinoma: A Proposal From the International Association for the Study of Lung Cancer Pathology Committee*. *J Thorac Oncol*, 2020. **15**(10): p. 1599-1610.
6. Walser T, Cui X, Yanagawa J, et al., *Smoking and lung cancer: the role of inflammation*. *Proc Am Thorac Soc*, 2008. **5**(8): p. 811-815.
7. Nationaal Expertisecentrum Tabaksontmoediging, *Kerncijfers Roken 2019: De laatste cijfers over roken, stoppen met roken en het gebruik van elektronische sigaretten.*, Trimbos Instituut. 2020.
8. GBD 2019 Chewing Tobacco Collaborators, *Spatial, temporal, and demographic patterns in prevalence of chewing tobacco use in 204 countries and territories, 1990-2019: a systematic analysis from the Global Burden of Disease Study 2019*. *Lancet Public Health*, 2021. **6**(7): p. e482-e499.
9. De Koning HJ, Van der Aalst CM, De Jong PA, et al., *Reduced Lung-Cancer Mortality with Volume CT Screening in a Randomized Trial*. *N Engl J Med*, 2020. **382**(6): p. 503-513.
10. Ritchie H and Roser M, *Smoking*. Our World In Data, 2013.
11. Pfeifer GP, Denissenko MF, Olivier M, et al., *Tobacco smoke carcinogens, DNA damage and p53 mutations in smoking-associated cancers*. *Oncogene*, 2002. **21**(48): p. 7435-51.
12. The Cancer Genome Atlas Research Network, *Comprehensive molecular profiling of lung adenocarcinoma*. *Nature*, 2014. **511**(7511): p. 543-550.
13. Gou LY, Niu FY, Wu YL, et al., *Differences in driver genes between smoking-related and non-smoking-related lung cancer in the Chinese population*. *Cancer*, 2015. **121 Suppl 17**: p. 3069-79.
14. Dias M, Linhas R, Campainha S, et al., *Lung cancer in never-smokers - what are the differences?* *Acta Oncol*, 2017. **56**(7): p. 931-935.
15. Kim IA, Lee JS, Kim HJ, et al., *Cumulative smoking dose affects the clinical outcomes of EGFR-mutated lung adenocarcinoma patients treated with EGFR-TKIs: a retrospective study*. *BMC Cancer*, 2018. **18**(1): p. 768.

16. Zhao W, Jiang W, Wang H, et al., *Impact of Smoking History on Response to Immunotherapy in Non-Small-Cell Lung Cancer: A Systematic Review and Meta-Analysis*. *Front Oncol*, 2021. **11**(3273).
17. Tsao AS, Liu D, Lee JJ, et al., *Smoking affects treatment outcome in patients with advanced nonsmall cell lung cancer*. *Cancer*, 2006. **106**(11): p. 2428-36.
18. Addeo A, Passaro A, Malapelle U, et al., *Immunotherapy in non-small cell lung cancer harbouring driver mutations*. *Cancer Treat Rev*, 2021. **96**: p. 102179.
19. McGranahan N and Swanton C, *Clonal Heterogeneity and Tumor Evolution: Past, Present, and the Future*. *Cell*, 2017. **168**(4): p. 613-628.
20. Zhang Y, Chang L, Yang Y, et al., *Intratumor heterogeneity comparison among different subtypes of non-small-cell lung cancer through multi-region tissue and matched ctDNA sequencing*. *Mol Cancer*, 2019. **18**(1): p. 7.
21. Chabner BA and Roberts TG, *Chemotherapy and the war on cancer*. *Nat Rev Cancer*, 2005. **5**(1): p. 65-72.
22. Alberti W, Anderson G, Bartolucci A, et al., *Chemotherapy in non-small cell lung cancer: a meta-analysis using updated data on individual patients from 52 randomised clinical trials*. *BMJ*, 1995. **311**(7010): p. 899-909.
23. Lynch TJ, Bell DW, Sordella R, et al., *Activating mutations in the epidermal growth factor receptor underlying responsiveness of non-small-cell lung cancer to gefitinib*. *N Engl J Med*, 2004. **350**(21): p. 2129-39.
24. Planchard D, Kim TM, Mazieres J, et al., *Dabrafenib in patients with BRAF(V600E)-positive advanced non-small-cell lung cancer: a single-arm, multicentre, open-label, phase 2 trial*. *Lancet Oncol*, 2016. **17**(5): p. 642-50.
25. Shaw AT, Kim DW, Nakagawa K, et al., *Crizotinib versus Chemotherapy in Advanced ALK-Positive Lung Cancer*. *N Engl J Med*, 2013. **368**(25): p. 2385-2394.
26. Wolf J, Seto T, Han JY, et al., *Capmatinib in MET Exon 14-Mutated or MET-Amplified Non-Small-Cell Lung Cancer*. *N Engl J Med*, 2020. **383**(10): p. 944-957.
27. Swanton C, Futreal A and Eisen T, *Her2-Targeted Therapies in Non-Small Cell Lung Cancer*. *Clin Cancer Res*, 2006. **12**(14): p. 4377s.
28. Shaw AT, Ou SHI, Bang YJ, et al., *Crizotinib in ROS1-Rearranged Non-Small-Cell Lung Cancer*. *N Engl J Med*, 2014. **371**(21): p. 1963-1971.
29. Drilon A, Laetsch TW, Kummar S, et al., *Efficacy of Larotrectinib in TRK Fusion-Positive Cancers in Adults and Children*. *N Engl J Med*, 2018. **378**(8): p. 731-739.
30. Subbiah V, Gainor JF, Rahal R, et al., *Precision Targeted Therapy with BLU-667 for RET-Driven Cancers*. *Cancer Discov*, 2018. **8**(7): p. 836-849.
31. Kobayashi S, Boggon TJ, Dayaram T, et al., *EGFR mutation and resistance of non-small-cell lung cancer to gefitinib*. *N Engl J Med*, 2005. **352**(8): p. 786-92.
32. Shaw AT, Solomon BJ, Besse B, et al., *ALK Resistance Mutations and Efficacy of Lorlatinib in Advanced Anaplastic Lymphoma Kinase-Positive Non-Small-Cell Lung Cancer*. *J Clin Oncol*, 2019. **37**(16): p. 1370-1379.

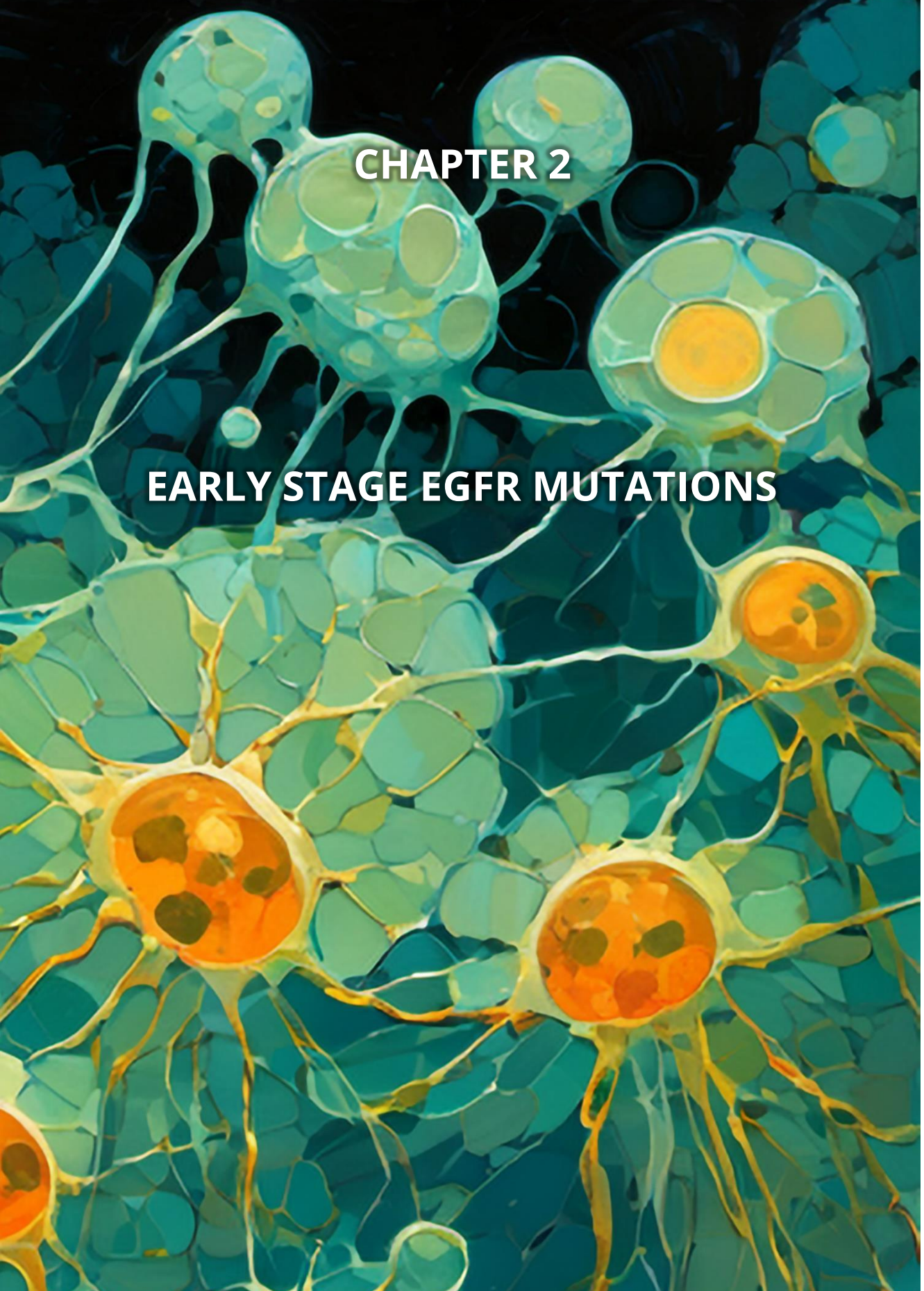
33. Gainor JF, Tseng D, Yoda S, et al., *Patterns of Metastatic Spread and Mechanisms of Resistance to Crizotinib in ROS1-Positive Non-Small-Cell Lung Cancer*. JCO Precis Oncol, 2017. **2017**.
34. Piotrowska Z, Isozaki H, Lennerz JK, et al., *Landscape of Acquired Resistance to Osimertinib in EGFR-Mutant NSCLC and Clinical Validation of Combined EGFR and RET Inhibition with Osimertinib and BLU-667 for Acquired RET Fusion*. Cancer Discov, 2018. **8**(12): p. 1529-1539.
35. Leonetti A, Sharma S, Minari R, et al., *Resistance mechanisms to osimertinib in EGFR-mutated non-small cell lung cancer*. Br J Cancer, 2019. **121**(9): p. 725-737.
36. Lin JJ, Choudhury NJ, Yoda S, et al., *Spectrum of Mechanisms of Resistance to Crizotinib and Lorlatinib in ROS1 Fusion-Positive Lung Cancer*. Clin Cancer Res, 2021. **27**(10): p. 2899.
37. Doebele RC, Drilon A, Paz-Ares L, et al., *Entrectinib in patients with advanced or metastatic NTRK fusion-positive solid tumours: integrated analysis of three phase 1-2 trials*. Lancet Oncol, 2020. **21**(2): p. 271-282.
38. Wu YL, Tsuboi M, He J, et al., *Osimertinib in Resected EGFR-Mutated Non-Small-Cell Lung Cancer*. N Engl J Med, 2020. **383**(18): p. 1711-1723.
39. Gainor JF, *Adjuvant PD-L1 blockade in non-small-cell lung cancer*. Lancet, 2021. **398**(10308): p. 1281-1283.
40. Mullis K, Faloona F, Scharf S, et al., *Specific enzymatic amplification of DNA in vitro: the polymerase chain reaction*. Cold Spring Harbor symposia on quantitative biology, 1986. **51 Pt 1**: p. 263-273.
41. Druker BJ, Tamura S, Buchdunger E, et al., *Effects of a selective inhibitor of the Abl tyrosine kinase on the growth of Bcr-Abl positive cells*. Nat Med, 1996. **2**(5): p. 561-6.
42. Zimmermann J, Buchdunger E, Mett H, et al., *Potent and selective inhibitors of the Abl-kinase: phenylamino-pyrimidine (PAP) derivatives*. Bioorganic & Medicinal Chemistry Letters, 1997. **7**(2): p. 187-192.
43. Sanger F, Nicklen S and Coulson AR, *DNA sequencing with chain-terminating inhibitors*. Proc Natl Acad Sci U S A, 1977. **74**(12): p. 5463-7.
44. Tsongalis GJ and Silverman LM, *Molecular diagnostics: A historical perspective*. Clin Chim Acta, 2006. **369**(2): p. 188-192.
45. Sordella R, Bell DW, Haber DA, et al., *Gefitinib-sensitizing EGFR mutations in lung cancer activate anti-apoptotic pathways*. Science, 2004. **305**(5687): p. 1163-7.
46. Goodwin S, McPherson JD and McCombie WR, *Coming of age: ten years of next-generation sequencing technologies*. Nat Rev Genet, 2016. **17**(6): p. 333-351.
47. Selinger CI, Rogers TM, Russell PA, et al., *Testing for ALK rearrangement in lung adenocarcinoma: a multicenter comparison of immunohistochemistry and fluorescent in situ hybridization*. Mod Pathol, 2013. **26**(12): p. 1545-1553.

48. Sholl LM, Sub H, Butaney M, et al., *ROS1 immunohistochemistry for detection of ROS1-rearranged lung adenocarcinomas*. Am J Surg Pathol, 2013. **37**(9): p. 1441-9.
49. Solomon JP and Hechtman JF, *Detection of NTRK Fusions: Merits and Limitations of Current Diagnostic Platforms*. Cancer Res, 2019. **79**(13): p. 3163-3168.
50. Yoshizawa A, Sumiyoshi S, Sonobe M, et al., *HER2 status in lung adenocarcinoma: a comparison of immunohistochemistry, fluorescence in situ hybridization (FISH), dual-ISH, and gene mutations*. Lung Cancer, 2014. **85**(3): p. 373-8.
51. Diggs LP and Hsueh EC, *Utility of PD-L1 immunohistochemistry assays for predicting PD-1/PD-L1 inhibitor response*. Biomark Res, 2017. **5**(1): p. 12.
52. Mok TSK, Wu YL, Kudaba I, et al., *Pembrolizumab versus chemotherapy for previously untreated, PD-L1-expressing, locally advanced or metastatic non-small-cell lung cancer (KEYNOTE-042): a randomised, open-label, controlled, phase 3 trial*. Lancet, 2019. **393**(10183): p. 1819-1830.
53. Park S, Choi YL, Sung CO, et al., *High MET copy number and MET overexpression: poor outcome in non-small cell lung cancer patients*. Histol Histopathol, 2012. **27**(2): p. 197-207.
54. Sholl, L.M., et al., *Validation of chromogenic in situ hybridization for detection of EGFR copy number amplification in nonsmall cell lung carcinoma*. Mod Pathol, 2007. **20**(10): p. 1028-1035.
55. Radonic T, Geurts-Giele WRR, Samsom KG, et al., *RET Fluorescence In Situ Hybridization Analysis Is a Sensitive but Highly Unspecific Screening Method for RET Fusions in Lung Cancer*. J Thorac Oncol, 2021. **16**(5): p. 798-806.
56. Dong H, Strome SE, Salomao DR, et al., *Tumor-associated B7-H1 promotes T-cell apoptosis: a potential mechanism of immune evasion*. Nat Med, 2002. **8**(8): p. 793-800.
57. Gadgeel S, Rodriguez-Abreu D, Speranza G, et al., *Updated Analysis From KEYNOTE-189: Pembrolizumab or Placebo Plus Pemetrexed and Platinum for Previously Untreated Metastatic Nonsquamous Non-Small-Cell Lung Cancer*. J Clin Oncol, 2020. **38**(14): p. 1505-1517.
58. Reck M, Rodriguez-Abreu D, Robinson AG, et al., *Pembrolizumab versus Chemotherapy for PD-L1-Positive Non-Small-Cell Lung Cancer*. N Engl J Med, 2016. **375**(19): p. 1823-1833.
59. Borghaei H, Paz-Ares L, Horn L, et al., *Nivolumab versus Docetaxel in Advanced Nonsquamous Non-Small-Cell Lung Cancer*. N Engl J Med, 2015. **373**(17): p. 1627-1639.
60. Gettinger S, Rizvi NA, Chow LQ, et al., *Nivolumab Monotherapy for First-Line Treatment of Advanced Non-Small-Cell Lung Cancer*. J Clin Oncol, 2016. **34**(25): p. 2980-7.

61. Zhang Y and Zhang Z, *The history and advances in cancer immunotherapy: understanding the characteristics of tumor-infiltrating immune cells and their therapeutic implications*. Cell Mol Immunol, 2020. **17**(8): p. 807-821.
62. Starnes CO, *Coley's toxins*. Nature, 1992. **360**(6399): p. 23-23.
63. Tomasini P, Khobta N, Greillier L, et al., *Ipilimumab: its potential in non-small cell lung cancer*. Ther Adv Med Oncol, 2012. **4**(2): p. 43-50.
64. Brahmer J, Reckamp KL, Baas P, et al., *Nivolumab versus Docetaxel in Advanced Squamous-Cell Non-Small-Cell Lung Cancer*. N Engl J Med, 2015. **373**(2): p. 123-135.
65. Guo ZS, *The 2018 Nobel Prize in medicine goes to cancer immunotherapy (editorial for BMC cancer)*. BMC cancer, 2018. **18**(1): p. 1086-1086.
66. Marabelle A, Rakih M, Lopez J, et al., *Association of tumour mutational burden with outcomes in patients with advanced solid tumours treated with pembrolizumab: prospective biomarker analysis of the multicohort, open-label, phase 2 KEYNOTE-158 study*. Lancet Oncol, 2020. **21**(10): p. 1353-1365.
67. Petitprez F, Meylan M, De Reynies A, et al., *The Tumor Microenvironment in the Response to Immune Checkpoint Blockade Therapies*. Front Immunol, 2020. **11**: p. 784.
68. Cao L, Che X, Qiu X, et al., *M2 macrophage infiltration into tumor islets leads to poor prognosis in non-small-cell lung cancer*. Cancer Manag Res, 2019. **11**: p. 6125-6138.
69. DeFalco J, Harbell M, Manning-Bog A, et al., *Non-progressing cancer patients have persistent B cell responses expressing shared antibody paratopes that target public tumor antigens*. Clin Immunol, 2018. **187**: p. 37-45.
70. Higgs BW, Morehouse CA, Streicher K, et al., *Interferon Gamma Messenger RNA Signature in Tumor Biopsies Predicts Outcomes in Patients with Non-Small Cell Lung Carcinoma or Urothelial Cancer Treated with Durvalumab*. Clin Cancer Res, 2018. **24**(16): p. 3857-3866.
71. Mayoux M, Roller A, Pulko V, et al., *Dendritic cells dictate responses to PD-L1 blockade cancer immunotherapy*. Sci Transl Med, 2020. **12**(534).
72. Liu Y, Zugazagoitia J, Ahmed FS, et al., *Immune Cell PD-L1 Colocalizes with Macrophages and Is Associated with Outcome in PD-1 Pathway Blockade Therapy*. Clin Cancer Res, 2020. **26**(4): p. 970-977.





A microscopic image showing a cluster of cells. The cells are arranged in a somewhat organized pattern, with some cells having prominent nuclei. The color of the cells transitions from a light blue/cyan at the top to a bright orange at the bottom. The background is dark, making the cells stand out. The text 'CHAPTER 2' is overlaid in white, bold, sans-serif font at the top center.

**CHAPTER 2**

**EARLY STAGE EGFR MUTATIONS**

## Chapter 2: Early stage EGFR mutations

### 2.1 Title page

Prevalence, clinical and molecular characteristics of early-stage *EGFR*-mutated lung cancer in a real-life West-European cohort: implications for adjuvant therapy.

Short running title: *EGFR* in early-stage lung cancer

*Published: European Journal of Cancer, 2023. DOI: 10.1016/j.ejca.2022.12.010*

### 2.1.1 Authors

Authors: Liesbeth M. Hondelink<sup>1</sup>, Sophie M. Ernst<sup>2</sup>, Peggy Atmodimedjo<sup>3</sup>, Danielle Cohen<sup>1</sup>, Janina L. Wolf<sup>3</sup>, Anne-Marie C. Dingemans<sup>2</sup>, Hendrikus J. Dubbink<sup>3</sup>, Jan H. von der Thüsen<sup>3</sup>

### 2.1.2 Affiliations

1. Department of Pathology, Leiden University Medical Center, the Netherlands
2. Department of Respiratory Medicine, Erasmus MC Cancer Institute, Erasmus University Medical Center, Rotterdam, the Netherlands
3. Department of Pathology and Clinical Bioinformatics, Erasmus Medical Center, the Netherlands
- 4.

### 2.1.4 Acknowledgement

The authors thank the molecular diagnostics team at the Department of Pathology and Clinical Bioinformatics, Erasmus Medical Center.

### 2.1.5 Funding

This study received funding from AstraZeneca for the generation of data.

## 2.2 Abstract

### 2.2.1 Objectives

The landmark ADAURA study recently demonstrated a significant disease-free survival benefit of adjuvant osimertinib in patients with resected EGFR-mutated lung adenocarcinoma. However, data on prevalence rates and stage distribution of EGFR mutations in NSCLC in Western populations are limited since upfront EGFR testing in early-stage lung adenocarcinoma is not common practice. Here we present a unique, real-world, unselected cohort of lung adenocarcinoma to aid in providing a rationale for routine testing of early-stage lung cancers for EGFR mutations in the West-European population.

### 2.2.2 Material and Methods

We performed routine unbiased testing of all cases, regardless of TNM stage, with targeted next generation sequencing (NGS) on 486 lung adenocarcinoma cases between 01-01-2014 and 01-02-2020. Clinical and pathological data, including co-mutations and morphology, were collected. *EGFR*-mutated cases were compared to *KRAS*-mutated cases to investigate *EGFR*-specific characteristics.

### 2.2.3 Results

53 of 486 lung adenocarcinomas (11%) harbored an *EGFR* mutation. In early-stages (stage 0-IIIa) the prevalence was 13%, versus 9% in stage IIIB-IV. 9 out of 130 (7%) stage IB-IIIa patients fit the ADAURA criteria. Early-stage cases harbored more *L858R* mutations ( $p = 0.02$ ), fewer exon 20 insertions ( $p = 0.048$ ), fewer *TP53* co-mutations ( $p = 0.007$ ), and were more frequently never smokers ( $p = 0.04$ ) compared to late-stage cases with *EGFR* mutations. The *KRAS*-mutated cases were distributed more evenly across TNM stages compared to the *EGFR*-mutated cases.

### 2.2.4 Conclusion

As (neo-)adjuvant targeted therapy regimes enter the field of lung cancer treatment, molecular analysis of early-stage NSCLC becomes relevant. Testing for *EGFR* mutations in early-stage lung adenocarcinoma holds a substantial yield in our population, as our number needed to test ratio for adjuvant osimertinib was 14.4. The observed differences between early- and late-stage

disease warrants further analysis to work towards better prognostic stratification and more personalized treatment.

## 2.3 Introduction

Almost 30% of patients with non-small cell lung cancer (NSCLC) present with resectable early-stage disease. [1] Unfortunately, recurrence rates after resection are high: up to 50% of patients present with lung cancer recurrence within 5 years, which underscores the need for effective (neo)adjuvant treatment strategies. [2] Currently, in most patients with completely resected stage II-IIIa disease adjuvant platinum-based chemotherapy is recommended. However, the 5-year survival benefit of adjuvant chemotherapy remains limited. [3] Therefore, certain therapies that have proven to be effective in the advanced setting, such as immunotherapy and tyrosine kinase inhibitors (TKI), are now also of interest for the adjuvant setting. For instance, the landmark ADAURA trial has recently led to the approval of osimertinib, a third generation TKI, as adjuvant treatment after complete resection in patients with stage IB-IIIa NSCLC harboring EGFR exon 19 deletions or L858R substitution mutations. [4]

Pathogenic mutations in the *EGFR* gene are one of the most common oncogene driver mutations in metastatic NSCLC. The incidence of *EGFR* mutations in advanced non-squamous NSCLC varies greatly, from around 10% in West-European populations, to as high as 64% in the East Asian population. [5-11] The introduction of TKIs that inhibit the downstream pathways of *EGFR*, have greatly improved the outcome of patients with metastatic *EGFR*-mutated NSCLC. [12, 13] Osimertinib increased the median progression-free survival to 18.9 months [12] and the overall survival to 38.6 months. [14] Recently, the ADAURA investigators also demonstrated a substantial clinical benefit of adjuvant osimertinib in patients with resected *EGFR*-mutated lung adenocarcinoma. The study was discontinued early due to a significant efficacy benefit shown at interim analysis: patients with stage IB-IIIa disease receiving adjuvant osimertinib had a 24-month disease-free survival of 89%, versus only 52% in the placebo group ( $p < 0.001$ ), with a hazard ratio of 0.20 for disease recurrence and death. [15] However, currently the secondary endpoint of overall survival remains immature, and is hampered by the early unblinding of the study.

Until now, molecular screening for *EGFR* has only been routinely performed as part of standard care in stage IIIB and IV disease to select patients for treatment with osimertinib or other *EGFR* TKIs. [5, 6, 16] The expansion of routine molecular analysis to all early-stage lung adenocarcinomas to select patients for adjuvant treatment warrants a well-founded approach. To construct such an approach, several questions still need to be answered. There is a considerable amount of literature available on the prevalence of *EGFR* mutations in late-stage NSCLC and in the East Asian population. [17] However, as upfront *EGFR* testing in early-stage disease is not common practice, most reports on early-stage *EGFR*-mutated lung adenocarcinoma are from preselected cohorts, often enriched for *EGFR* mutations. [18] Therefore, it is still unclear how prevalent *EGFR* mutations are in early-stage *EGFR*-mutated lung adenocarcinomas in the Western population, and how to identify the patients who are at higher risk of recurrence and would therefore potentially have greater benefit of adjuvant treatment. These lacunae are essential to fill, as they could have implications for justified patient selection for adjuvant TKI treatment.

In the Erasmus Medical Center in Rotterdam, the Netherlands, all lung adenocarcinomas are subject to targeted next generation sequencing (NGS) testing regardless of TNM stage, so-called 'reflex-testing'. This provides a unique opportunity to investigate the real-world prevalence of *EGFR* mutations in early-stage NSCLC in a West-European patient population. Here we present our prospective unselected cohort of consecutive lung adenocarcinomas that were diagnosed in our center over the course of 6 years, using patients with *KRAS*-mutated NSCLC as a comparator for *EGFR*-mutated NSCLC. Additionally, we investigated the clinicopathological features, such as co-mutations and morphology, that are potentially associated with a higher risk for disease recurrence in early-stage *EGFR*-mutated NSCLC.

## **2.4 Materials and methods**

### **2.4.1 Case collection and study setup**

All in-house lung adenocarcinoma core needle biopsies, cytology specimens or resection samples of the Erasmus Medical Center Rotterdam (EMC) that were submitted to the pathology department for routine diagnostic purposes between 01-01-2014 and 01-02-2020 were evaluated for inclusion. Cases had

to have been analyzed with targeted DNA NGS with a customized oncogene-panel and have complete TNM staging for inclusion. In the case of multiple primary tumors per patient, each primary adenocarcinoma was eligible for inclusion if NGS had been performed. Both cytology and histology specimens were included, consisting of metastatic as well as primary tumor specimens. Only primary diagnostic specimens were allowed; liquid biopsy specimens and sequential biopsies after start of systemic treatment were excluded. Cases with insufficient tissue for DNA NGS or without complete TNM staging were excluded, which for example occurred if the patient opted to be referred to another medical center for staging, or if the patient was terminally ill with a concurrent disease.

To investigate whether possible differences between early- and late-stage cases are *EGFR*-specific, we compared the *EGFR* cases to the *KRAS*-mutated cases of our cohort.

#### 2.4.2 DNA isolation

Formalin-fixed paraffin-embedded (FFPE) tissue, including cytology cell blocks, was used for DNA isolation. The DNA was isolated as previously described. [19] The acquired DNA was stored at -20°C until analysis.

#### 2.4.3 DNA NGS

For targeted DNA NGS, an IonTorrent custom targeted NGS panel was used, including the following genes: *CDKN2A* (coverage 98%), *PTEN* (coverage 94%), *TP53* (coverage 100%) and mutation hotspots in *AKT1* (exon 3), *ALK* (20, 22-25), *APC* (14), *ARAF* (7), *BRAF* (11, 15), *CTNNB1* (3, 7, 8), *EGFR* (18-21), *HER2* (19-21), *EZH2* (16), *FBWX7* (9, 10), *FGFR1* (4, 7, 12), *FGFR2* (7, 9, 12), *FGFR3* (7, 9), *FOXL2* (1), *GNA11* (4, 5), *GNAQ* (4, 5), *GNAS* (8, 9), *HRAS* (2-4), *IDH1* (4), *IDH2* (4), *KIT* (8, 9, 11, 13, 14, 17), *KRAS* (2-4), *MAP2K1* (2, 3), *MET* (2, 14, 19), *MYD88* (5), *NOTCH1* (26, 27), *NRAS* (2-4), *PDGFRA* (12, 14, 18), *PIK3CA* (10, 21), *POLD1* (12), *POLE* (9, 13), *RAF1* (7), *RET* (11, 16), *RNF43* (3, 4, 9), *ROS1* (38, 41), *SMAD4* (3, 9, 12), *STK11* (4, 5, 8) and *TERT* promotor, as previously described. [20] Copy number calling was performed with SNPitty. [21, 22]

Genomic alterations were classified according to the ACMG/AMP consensus paper in 5 classes of ascending likelihood of pathogenicity. [23] For *EGFR* mutations, both class 4 or 5 pathogenic mutations and variants of unknown

significance (VUS) were included. We considered non-*EGFR* and non-*KRAS* mutations as co-mutations, including other driver mutations. Only class 4 and 5 pathogenic mutations were included, VUS were not considered co-mutations. Pathogenicity was assessed with reference databases, including Alamut, ClinVar, IARC, CKB and cBioportal. *KRAS* mutations were classified in G12C, G12D, G12V, Q61H and other mutations.

Additionally, we assessed the immunohistochemical expression pattern of *p53* in the *EGFR*-mutated cases if available.

#### 2.4.4 Clinical parameters

For all cases, clinical data regarding age at diagnosis, TNM stage (7<sup>th</sup> edition) and sex were collected. For patients with *EGFR*-mutated adenocarcinoma, we collected additional data on the smoking history, recurrence-free survival (RFS) for early-stage cases, previous cytotoxic therapy for another malignancy, follow up time, symptoms at the time of diagnosis and prior lung cancer screening or monitoring. Stage 0-III A were considered early-stage disease, and stage III B and IV were considered late-stage disease. RFS was defined as time from date of diagnosis until disease recurrence.

Patients were categorized as 'current smokers' if they smoked in the month before diagnosis. Patients were considered to be 'former smokers' if they quit smoking at least one month before diagnosis. Patients were considered to be 'never smokers' if they had accumulated less than one pack year and had not smoked in the month before diagnosis.

#### 2.4.5 Morphology

Growth patterns were assessed by one or multiple experienced thoracic pathologists, using a continuous score for each of the following categories: percentage lepidic, percentage acinar-papillary, percentage micropapillary-solid. The continuous scores for each category were used to assess the 'most prevalent growth pattern' and the 'worst growth pattern'. The 'most prevalent growth pattern' was the pattern which was most prevalent. If two patterns were equally prevalent, the worst growth pattern was used as the most prevalent growth pattern.

Literature has previously suggested that the type of growth pattern has potential prognostic value, with micropapillary-solid having the worst

prognosis, followed by acinar-papillary, and a lepidic growth pattern having the most favorable prognosis. [24] We therefore also scored the cases according to the pattern with the assumed worst prognosis, i.e. the 'worst growth pattern', to evaluate whether the presence of a less favorable growth pattern indeed has prognostic value. Growth pattern assessment was only performed for cases in which tissue from the primary tumor was available. Cytology specimens and metastasis biopsies were not scored for growth pattern. Examples of these scoring systems are outlined in Supplementary Table 1.

#### 2.4.6 Statistics

We used IBM SPSS Statistics software, version 25 for statistical analysis. Statistical significance was set at  $p < 0.05$ . Categorical data were compared using the Chi Square test or Fisher Exact test, as appropriate. For t-distributed stochastic neighbor embedding (t-SNE) data visualization, we adapted the dataset. We normalized all continuous and ordinal data, such as age and TNM stage to values between 0 and 1. We used one-hot-encoding for non-ordinal categorical data, including *EGFR* mutations and co-mutations. We performed Mean Imputation for missing values in normally distributed continuous data and binary data. We performed Median Imputation for missing non-normally distributed continuous data and categorical data. [25] T-SNE was created with Python 3.7, using scikit-learn and perplexity values of 4 and 12 to plot these t-SNE figures. [26] The stage labels were excluded from the t-SNE data.

#### 2.4.7 Ethics

This study was approved by the local medical ethical committee, registration number: MEC-2020-0732. Informed consent was not necessary and patient data were anonymized before processing.

## 2.5 Results

### 2.5.1 Case characteristics

We included 486 new lung adenocarcinoma cases, 53 (11%) harbored an *EGFR* mutation and 129 (27%) harbored a *KRAS* mutation. Cases were spread unevenly across TNM stages, with fewer patients in stage 0 (in situ carcinoma) and II and more patients in stage I and IV (Table 1).

CASE CHARACTERISTICS	ALL CASES (N = 486)	EGFR-MUTATED (N = 53)	KRAS-MUTATED (N = 129)
STAGE 0	11 (2%)	3 (6%)	3 (2%)
STAGE IA	114 (23%)	21 (40%)	31 (24%)
STAGE IB	38 (8%)	4 (8%)	13 (10%)
STAGE IIA	16 (3%)	2 (4%)	3 (2%)
STAGE IIB	17 (3%)	0	5 (4%)
STAGE IIIA	59 (12%)	3 (6%)	13 (10%)
STAGE IIIB	25 (5%)	1 (2%)	7 (5%)
STAGE IV	206 (42%)	19 (36%)	54 (42%)
EARLY-STAGE (0-III A)	255 (52%)	33 (62%)	68 (53%)
LATE-STAGE (IIIB-IV)	231 (48%)	20 (38%)	61 (47%)

**Table 1:** Case overview per TNM stage (TNM 7<sup>th</sup> edition).

### 2.5.2 Prevalence of EGFR mutations per TNM stage

*EGFR* mutations were more prevalent in early-stage adenocarcinoma (13% of stage 0-III A patients harbored an *EGFR* mutation), compared to late-stage (9% of stage IIIB-IV patients harbored an *EGFR* mutation). The percentage of patients harboring *EGFR* mutations was especially high in stage 0 (27%) and 1A (18%), compared to the other stages ( $p = 0.03$ ) (Figure 1). Of the 33 patients with early-stage *EGFR*-mutated NSCLC, 9 (27%) fit the ADAURA criteria (*L858R* mutation or exon 19 deletion, stage IB-III A). Since we included 130 stage IB-III A in our EMC cohort, the number of stage IB-III A cases needed to test in order to identify one patient eligible for adjuvant osimertinib following the ADAURA regimen, is 14.4.

### 2.5.3 Characteristics of early versus late-stage EGFR-mutated adenocarcinoma

We compared clinical, molecular and morphological parameters between the early-stage and the late-stage *EGFR* cases (Table 2), as well as between *EGFR* and *KRAS* cases (Figure 2). *EGFR*-mutated, early-stage cases harbored significantly more *EGFR L858R* mutations (45% vs 15%,  $p = 0.02$ ), and were more likely to have a predominantly lepidic growth pattern (65% versus 0%,  $p = 0.003$ ) than the late-stage *EGFR*-mutated cases. Late-stage cases more often harbored *EGFR* exon 20 insertions (25% versus 6%,  $p = 0.048$ ) and were enriched for *TP53* co-mutations (65% versus 27%,  $p = 0.007$ ). Within the *TP53* mutated cases, late-stage harbored more disruptive *TP53* mutations than early-stage cases (40% versus 0%,  $p < 0.001$ ). The *KRAS* early- and late-stage cohorts

differed with regard to *TP53* mutation prevalence (31% versus 52%, respectively,  $p = 0.02$ ), with late-stage cases again harboring more disruptive *TP53* mutations, though not significantly (15% versus 9%,  $p = 0.4$ ).

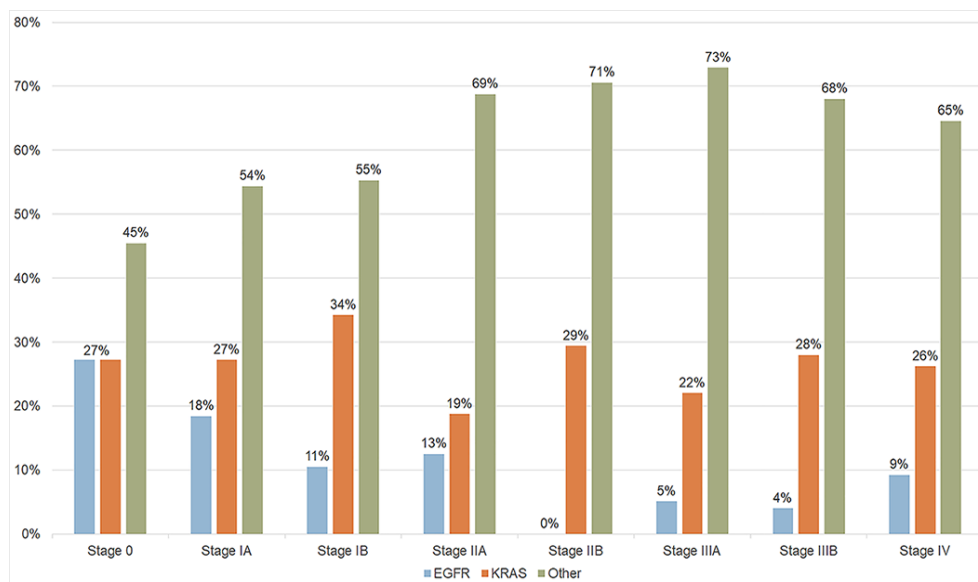


**Figure 1:** Mutation prevalence across stages. Prevalence of *EGFR*-mutated cases, *KRAS*-mutated cases and Other cases per TNM stage (TNM 7<sup>th</sup> edition). Blue: *EGFR*; Orange: *KRAS*; Green: other cases. *KRAS* is evenly distributed across stages, whereas *EGFR* prevalence differs across stages.

Additionally, early- and late-stage *EGFR*-mutated cases differed significantly with regard to smoking history ( $p = 0.04$ ). We did not identify differences in age, sex, and worst growth pattern between early- and late-stage disease. In 8 of the *TP53* mutated cases *p53* immunohistochemistry was performed: 7 showed strong nuclear expression for *p53*, whereas one had absent nuclear expression.

Prior to diagnosis, 9 patients (27% of all early-stage *EGFR*-mutated cases) were monitored with computed tomography (CT) scans for a 'ground glass' lesion or pulmonary node, for an average time period of 3.1 years (range 1-7 years). Of these cases, 4 harbored a *L858R* mutation, 4 an exon 19 deletion, and one an exon 20 insertion. 4 cases harbored a non-disruptive *TP53* mutation. 7 had a predominantly lepidic growth pattern, and the remaining 2 cases had acinar growth patterns. Two other patients were not monitored, but the tumor had in

retrospect been visible on previous imaging, 15 and 17 years prior to the diagnosis, respectively.

From the 486 included cases, 129 were *KRAS*-mutated, including 68 early-stage and 61 late-stage cases. The characteristics for the *KRAS* cohort are outlined in Supplementary Table 2. The *EGFR*-mutated and *KRAS*-mutated cohorts differ with regard to smoking history and pre-diagnosis follow up, with more current smokers in the *KRAS* cohort (42% versus 11%,  $p < 0.001$ ), more never-smokers in the *EGFR* cohort (28% versus 2%,  $p < 0.001$ ) and more often pre-diagnosis follow-up in the *EGFR* cohort (17% versus 5%,  $p = 0.03$ ). In contrast to the *EGFR*-mutated cases, the *KRAS*-mutated cases were distributed more evenly across TNM stages (Figure 1). Also, *EGFR* early- and late-stage cases differed significantly with regard to mutation type, predominant growth pattern, and co-mutation prevalence, whereas this was not the case for the *KRAS* cohort.

FEATURE N (%)	EARLY- STAGE <i>EGFR</i> (N = 33)	LATE- STAGE <i>EGFR</i> (N = 20)	P- VALUE	EARLY- STAGE <i>KRAS</i> (N = 68)	LATE- STAGE <i>KRAS</i> (N = 61)	P- VALUE
<i>EGFR</i> L858R	15 (45%)	3 (15%)	0.02 <sup>a</sup>	N/A	N/A	N/A
<i>EGFR</i> EXON 20 INS	2 (6%)	5 (25%)	0.048 <sup>a</sup>	N/A	N/A	N/A
<i>EGFR</i> EXON 19 DEL	13 (39%)	9 (45%)	0.7	N/A	N/A	N/A
OTHER <i>EGFR</i>	3* (9%)	3* (15%)	0.5 <sup>a</sup>			
<i>TP53</i>	9 (27%)	13 (65%)	0.007 <sup>a</sup>	21 (31%)	32 (52%)	0.02 <sup>a</sup>
<i>TP53</i> DISRUPTIVE	0	8 (40%)	<0.001 <sup>a</sup>	6 (9%)	9 (15%)	0.4 <sup>a</sup>
MOST PREVALENT GROWTH PATTERN			0.003 <sup>b</sup>			0.6 <sup>b</sup>
LEPIDIC	20 (65%)	0 (0%)		22 (38%)	6 (33%)	
ACINAR OR PAPILLARY	9 (29%)	3 (15%)		31 (53%)	9 (50%)	
SOLID OR MICROPAPILLARY	2 (6%)	3 (15%)		5 (9%)	3 (17%)	
NOT SCORED	2 (6%)	14 (70%)				
SMOKING STATUS			<0.001 <sup>b</sup>			0.4 <sup>b</sup>

NEVER SMOKER	21 (64%)	1 (5%)	2 (3%)	0
FORMER SMOKER	10 (30%)	15 (75%)	34 (56%)	27 (48%)
CURRENT SMOKER	2 (6%)	4 (20%)	25 (41%)	29 (52%)
UNKNOWN	0	0	7 (10%)	5 (8%)
PRIOR TO DIAGNOSIS			0.02 <sup>a</sup>	0.7 <sup>a</sup>
PRIOR FOLLOW-UP	9 (27%)	0	5 (7%)	1 (2%)
NO PRIOR FOLLOW-UP	24 (73%)	19 (95%)	52 (76%)	26 (43%)
UNKNOWN	0	1 (5%)	11 (16%)	34 (56%)

**Table 2:** Significant differences between early-stage EGFR-mutated lung adenocarcinomas (n = 33) and late-stage EGFR-mutated lung adenocarcinomas (n = 20). Co-mutations were assessed only in cases with complete coverage of the panel, as described in the Methods. Predominant growth pattern was not available for cytology and metastasis specimens. P-values were calculated with (a) Fisher's Exact test or (b) Chi-squared test. For categories 'Smoking status' and 'Prior to diagnosis', missing data was omitted from percentage calculations and statistic testing. \* 'Other' EGFR mutations included p.G779F, p.G719A and p.L861R. • 'Other' EGFR mutations included p.G719A, concomitant p.G719S and p.S768I, and p.V774L.

#### 2.5.4 Recurrence free survival (RFS)

Within the early-stage EGFR cases (n = 33), 3 patients (9%) had presented with disease recurrence after 7, 48 and 60 months respectively, 12 patients (36%) were recurrence-free for at least 2 years after resection, and 18 (55%) patients had a follow-up duration of less than 2 years. Type of EGFR mutation, presence of TP53 mutations and clinical characteristics for the recurrence-free, recurrence and late-stage cases are summarized in Supplementary Figure 1. This illustrates that most late-stage cases harbor similar clinicopathological features (EGFR exon 20 insertions, presence of (TP53) co-mutations, growth pattern, previous or current tobacco smoke exposure), which can also partly be identified in the early-stage cases with recurrence although in a limited number of cases, and in some recurrence-free cases. With regard to the growth patterns, the recurrence-free cases were predominantly characterized by a lepidic growth pattern (67%), followed by an acinar growth pattern (10%).

Growth patterns differed in the 3 cases with recurrence: one case had a predominantly solid, one predominantly acinar and one predominantly lepidic growth pattern. The patient with the solid growth pattern had a RFS of 7 months, versus 48 months in the patient with predominantly acinar growth pattern and 60 months in the patient with the lepidic growth pattern.

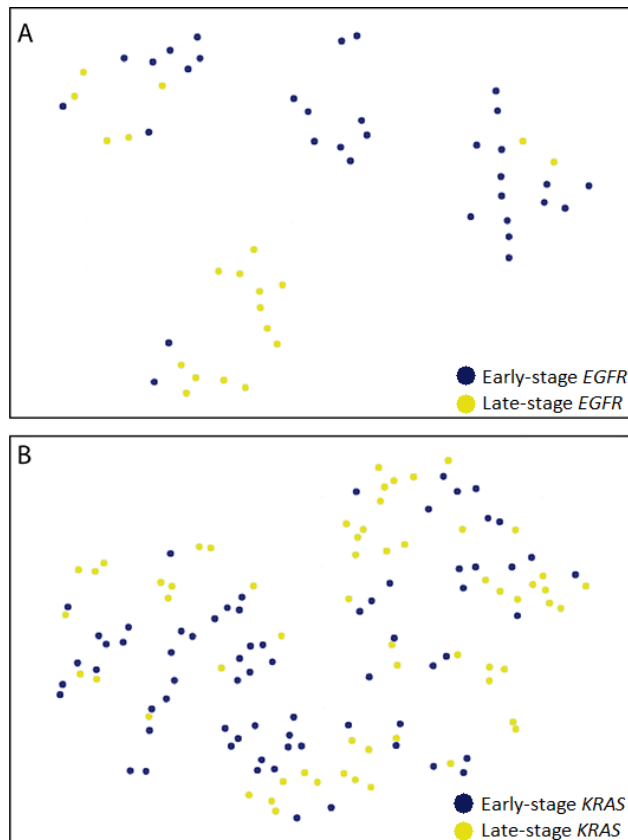


**Figure 2:** Unsupervised clustering of EGFR- and KRAS-mutated cases. Unsupervised clustering, using *t*-distributed stochastic neighbor embedding (*t*-SNE). A: *t*-SNE of EGFR-mutated lung adenocarcinoma features, perplexity value 4. B: *t*-SNE of KRAS-mutated lung adenocarcinoma features, perplexity value 12. Blue dots: early-stage (0-III A, TNM 7<sup>th</sup> edition); yellow dots: late-stage (IIIB-IV). Features used for this *t*-SNE include: smoking history, symptoms, prior follow-up, T-stage, sex, age, growth pattern, EGFR mutations, KRAS mutations and co-mutations.

To illustrate these different growth patterns, figure 3A depicts the aforementioned case with a solid growth pattern and disease recurrence after 7 months. This 64-year-old woman was referred to the pulmonologist with an

asymptomatic pulmonary nodule, discovered via a coincidental finding. She was a former smoker and had accumulated 22 pack years. A lung biopsy was taken (Figure 3A), and the patient was diagnosed with a lung adenocarcinoma with 100% solid growth pattern. Staging showed that the tumor is stage cT2aN0M0, and the patient is eligible for surgical resection. In the resection specimen, the tumor had infiltrated the visceral pleura (pT2aN0M0PL1) and harbored an *EGFR* L858R mutation. After 7 months, she was diagnosed with bone metastases, and treated with *EGFR* TKIs.

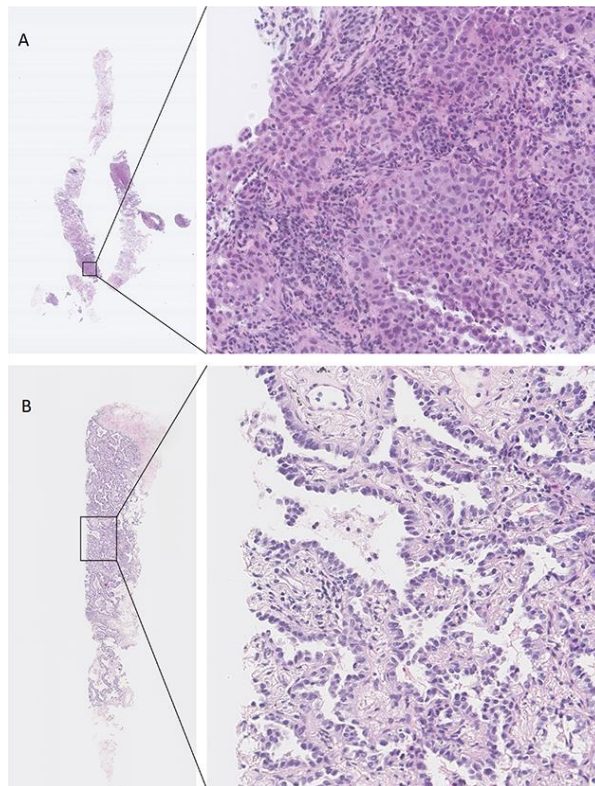


**Figure 3:** Case descriptions. A: Case 1 biopsy. First image: 4x, close-up: 40x. B: Case 2 biopsy. First image: 4x, close-up: 40x.

In contrast, figure 3B illustrates a case with a lepidic growth pattern in which no disease recurrence occurred. This 65-year-old woman was referred to the pulmonologist with a pulmonary lesion on CT-scan, discovered via a coincidental finding. She had smoked in the past, but had accumulated less than 10 pack years. On CT, a 'ground glass' lesion was identified, not suspicious for invasive malignancy. She was followed every 6 months with a CT-scan. After

2 years, the lesion had grown a few millimeters, and now had a small solid component. A lung biopsy (Figure 3B) revealed a 100% lepidic lung adenocarcinoma (IASLC grade 1). The patient was diagnosed with a cT1aN0M0 lung adenocarcinoma. Next-generation sequencing revealed an exon 19 deletion in *EGFR*, and no co-mutations. After surgical resection of the tumor, the patient is now recurrence free for 6 years.

## 2.6 Discussion

In this study, we investigated the prevalence of *EGFR* mutations across TNM stages in an unselected West-European cohort of 486 lung adenocarcinomas in which NGS reflex testing was performed. We found that *EGFR* mutations are unevenly spread over TNM stages, with a prevalence of 13% in early-stage, and 9% in late-stage. The latter is in line with previously reported prevalence rates of *EGFR* mutations in metastatic NSCLC in the Netherlands. [9, 11] 9 out of 130 (7%) stage IB-IIIa cases met the ADAURA inclusion criteria (*L858R* or exon 19 deletion), [15] which indicates that the number of stage IB-IIIa tumors needed to test in order to identify one patient eligible for adjuvant osimertinib is 14.4. Of note, we found that 36% of early-stage *EGFR*-mutated cases had current or previous tobacco smoke exposure. This highlights that selection for molecular analysis in the early-stage setting should also not be guided by clinical characteristics such as smoking history. These real-world data provide a rationale for routine testing of early-stage lung cancers for *EGFR* mutations in the West-European population.

Additionally, we provided a descriptive analysis of the characteristics of *EGFR*-mutated NSCLC over disease stages. We found that early-stage *EGFR*-mutated cases differ from late-stage cases with respect to clinical, genomic, and morphological characteristics. The late-stage group harbors more exon 20 insertions and fewer *L858R* mutations, more *TP53* mutations, more patients with previous or current tobacco smoke exposure, and more high-grade growth patterns. Although the *KRAS*-mutated late-stage cases also had a higher prevalence of *TP53* mutations than the early-stage cases, the *KRAS*-mutated cohort seemed more homogeneous over tumor stages. This could imply that the differences between early- and late-stage disease in the *EGFR*-mutated cohort are *EGFR*-specific.

In our *EGFR*-mutated early-stage cases, three patients presented with disease recurrence after an average of 3.2 years. This is longer than the average time to recurrence in NSCLC, as in most post-surgical NSCLC cases occult metastases present within 2 years after surgery. [27, 28] In addition, we found that 27% of all early-stage *EGFR*-mutated cases had been monitored prior to diagnosis because of 'ground glass' lesions. Recent data showed a 5-year overall survival rate of 100% in patients with surgically resected clinical stage 1A *EGFR*-mutated lung adenocarcinoma with ground glass opacity component [29]. In the *KRAS* cohort significantly less patients were followed up prior to diagnosis. This could suggest that some *EGFR*-mutated tumors are 'slow growers', and occult metastases – if present – are only identified after a long follow-up. Therefore, further studies with long survival data could aid in optimizing the timing of resection and surveillance strategies of resected *EGFR*-mutated carcinomas.

In all, these results suggest that *EGFR*-mutated lung adenocarcinoma is not one homogeneous disease, but rather that there are subgroups that could be defined by their different phenotypes. Although we have a limited sample size, it seems that some patients with (high) tobacco exposure, high grade growth pattern, *EGFR* exon 20 insertion and *TP53* mutation often present at a higher TNM stage and often progress to a higher stage. On the other hand, patients who have never smoked, with common *EGFR* mutations without co-mutations and with a low-grade growth pattern are rare in the high TNM stage group and the metastasis group. We should further investigate whether these findings truly indicate a 'high risk' and 'low risk' subtype in larger case series, as this could potentially help clinicians and pathologists identify patients who are at a higher risk of recurrence after surgery than others. It can be hypothesized that 'high risk' patients could derive more benefit from adjuvant TKI treatment than patients who were already at a low risk of recurrence, which could have implications for the prevention of over- and undertreatment.

The main limitation of our study is the sample size. While we screened a substantial number of cases (n = 486), 53 cases harbored an *EGFR* mutation. This is a limited dataset, especially in subset analyses. Consequently, our comparison between, for example, early-stage recurrence and recurrence free disease only included a small number of patients. Therefore, it is possible that our analysis lacked the power to detect smaller differences. However, this did

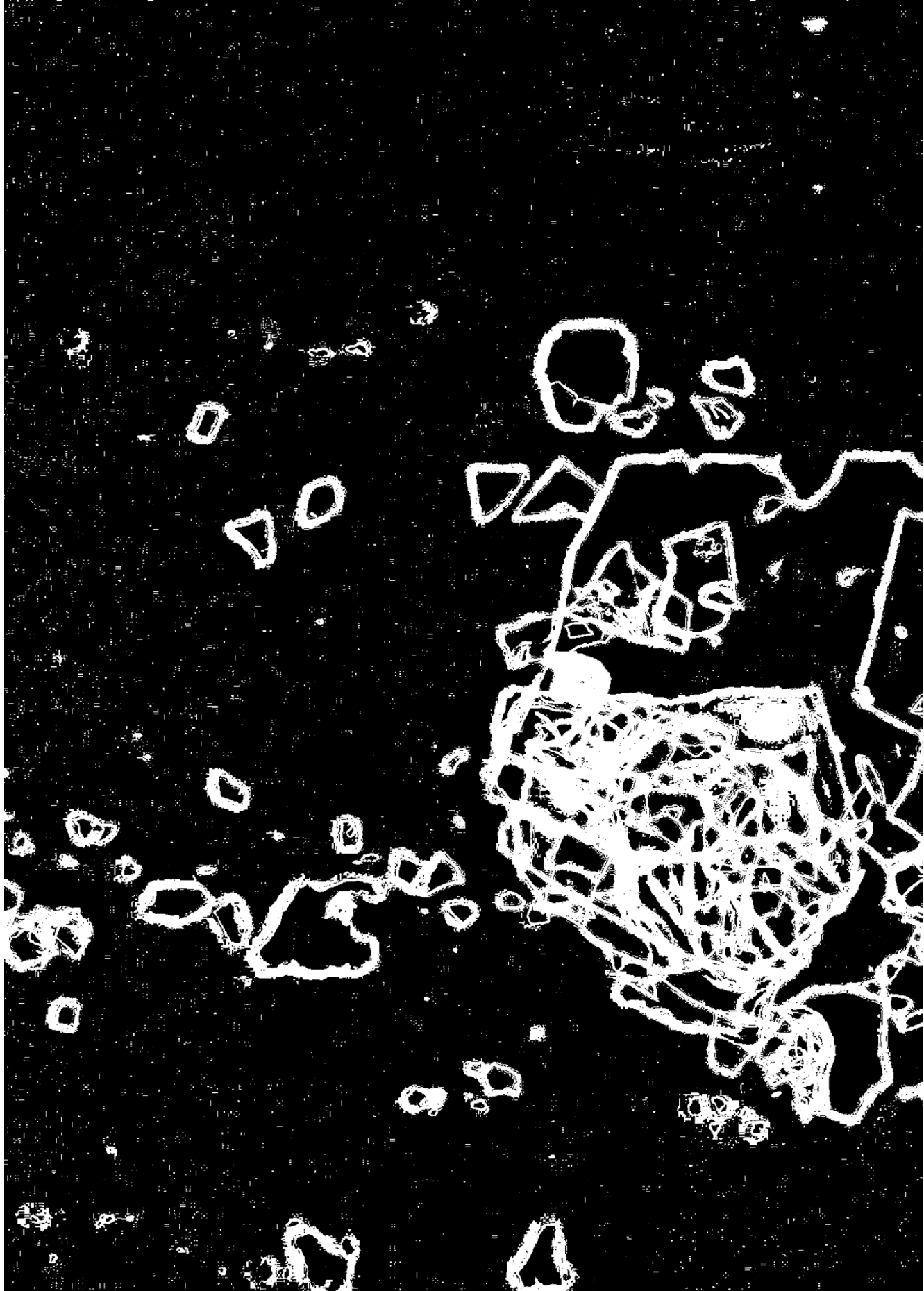
not limit our primary objective of determining *EGFR* prevalence rates across TNM stages.

In conclusion, the prevalence of *EGFR* mutations in early-stage lung adenocarcinoma in our West-European patient population is 13%, and the prevalence of ADAURA-eligible *EGFR* mutations in stage IB-III A is 7%, which constitutes a substantial yield when combining this number with the demonstrated benefit of adjuvant osimertinib. [15] However, we must emphasize that screening for *EGFR* mutations in early-stage lung adenocarcinoma is only a first step. Our data adds to a growing body of evidence that suggests that *EGFR*-mutated lung cancer, although seemingly one homogeneous group, actually consists of several genomic and clinical subgroups, in which we can potentially start to define low-risk and high-risk phenotypes that are correlated to clinical disease behavior. This underlines the intrinsic heterogeneity in NSCLC and the importance of comprehensive tumor characterization in clinical practice, as well as in future research. It would be of interest to investigate potential differences in outcomes between patients with low and high-risk phenotypes receiving adjuvant TKIs such as osimertinib, in order to guide future therapy decisions.

## References

1. Le Chevalier T, *Adjuvant chemotherapy for resectable non-small-cell lung cancer: where is it going?* Ann Oncol, 2010. **21 Suppl 7**: p. vii196-8.
2. Kratz JR, He J, Van den Eeden SK, et al., *A practical molecular assay to predict survival in resected non-squamous, non-small-cell lung cancer: development and international validation studies.* The Lancet, 2012. **379**(9818): p. 823-832.
3. Pignon JP, Tribodet H, Scagliotti GV, et al., *Lung adjuvant cisplatin evaluation: a pooled analysis by the LACE Collaborative Group.* J Clin Oncol, 2008. **26**(21): p. 3552-9.
4. Wu YL, Tsuboi M, He J, et al., *Osimertinib in Resected EGFR-Mutated Non-Small-Cell Lung Cancer.* N Engl J Med, 2020. **383**(18): p. 1711-1723.
5. Barlesi F, Mazieres J, Merlio JP, et al., *Routine molecular profiling of patients with advanced non-small-cell lung cancer: results of a 1-year nationwide programme of the French Cooperative Thoracic Intergroup (IFCT).* Lancet, 2016. **387**(10026): p. 1415-1426.
6. Cohen D, Hondelink LM, Solleveld-Westerink N, et al., *Optimizing Mutation and Fusion Detection in NSCLC by Sequential DNA and RNA Sequencing.* J Thorac Oncol, 2020. **15**(6): p. 1000-1014.
7. The Cancer Genome Atlas Research Network, *Comprehensive molecular profiling of lung adenocarcinoma.* Nature, 2014. **511**: p. 543-550.
8. Shi Y, Au JSK, Thongprasert S, et al., *A prospective, molecular epidemiology study of EGFR mutations in Asian patients with advanced non-small-cell lung cancer of adenocarcinoma histology (PIONEER).* J Thorac Oncol, 2014. **9**(2): p. 154-62.
9. Ten Berge D, Aarts MJ, Groen HJM, et al., *A population-based study describing characteristics, survival and the effect of TKI treatment on patients with EGFR mutated stage IV NSCLC in the Netherlands.* Eur J Cancer, 2022. **165**: p. 195-204.
10. Gao B, Sun Y, Zhang J, et al., *Spectrum of LKB1, EGFR, and KRAS mutations in chinese lung adenocarcinomas.* J Thorac Oncol, 2010. **5**(8): p. 1130-5.
11. Koopman B, Garcia BNC, Kuijpers CCHJ, et al., *A Nationwide Study on the Impact of Routine Testing for EGFR Mutations in Advanced NSCLC Reveals Distinct Survival Patterns Based on EGFR Mutation Subclasses.* Cancers (Basel), 2021. **13**(14).
12. Soria J, Ohe Y, Vansteenkiste J, et al., *Osimertinib in Untreated EGFR-Mutated Advanced Non-Small-Cell Lung Cancer.* N Engl J Med, 2018. **378**: p. 113-125.
13. Mok TS, Wu YL, Ahn MJ, et al., *Osimertinib or Platinum-Pemetrexed in EGFR T790M-Positive Lung Cancer.* N Engl J Med., 2017. **376**(7): p. 629-640.
14. Ramalingam SS, Vansteenkiste J, Planchard D, et al., *Overall Survival with Osimertinib in Untreated, EGFR-Mutated Advanced NSCLC.* N Engl J Med, 2019. **382**(1): p. 41-50.
15. Herbst RS, Morgensztern D, Boshoff C, *The biology and management of non-small cell lung cancer.* Nature, 2018. **553**(7689): p. 446-454.

16. Pi C, Xu CR, Zhang MF, et al., *EGFR mutations in early-stage and advanced-stage lung adenocarcinoma: Analysis based on large-scale data from China*. Thorac Cancer, 2018. **9**(7): p. 814-819.
17. Saw SPL, Zhou S, Chen J, et al., *Association of Clinicopathologic and Molecular Tumor Features With Recurrence in Resected Early-Stage Epidermal Growth Factor Receptor-Positive Non-Small Cell Lung Cancer*. JAMA Netw Open, 2021. **4**(11): p. e2131892.
18. van Lier MG, Wagner A, van Leerdam ME, et al., *A review on the molecular diagnostics of Lynch syndrome: a central role for the pathology laboratory*. J Cell Mol Med, 2010. **14**: p. 181-97.
19. Pruis MA, Geurts-Giele WRR, von der Thusen JH, et al., *Highly accurate DNA-based detection and treatment results of MET exon 14 skipping mutations in lung cancer*. Lung Cancer, 2020. **140**: p. 46-54.
20. van Riet J, Krol NMG, Atmodimedjo PN, et al., *SNPitty: An Intuitive Web Application for Interactive B-Allele Frequency and Copy Number Visualization of Next-Generation Sequencing Data*. J Mol Diagn, 2018. **20**(2): p. 166-176.
21. Dubbink HJ, Atmodimedjo PN, van Marion R, et al., *Diagnostic Detection of Allelic Losses and Imbalances by Next-Generation Sequencing: 1p/19q Co-Deletion Analysis of Gliomas*. J Mol Diagn, 2016. **18**(5): p. 775-786.
22. Boyd JA, Hubbs JL, Kim DW, et al., *Timing of local and distant failure in resected lung cancer: implications for reported rates of local failure*. J Thorac Oncol, 2010. **5**(2): p. 211-4.
23. Demicheli R, Fornili M, Ambrogi F, et al., *Recurrence Dynamics for Non-Small-Cell Lung Cancer: Effect of Surgery on the Development of Metastases*. J of Thorac Oncol, 2012. **7**(4): p. 723-730.
24. Li M, Xi J, Zhang H, et al., *Pan-Driver-Negatives versus Epidermal Growth Factor Receptor Mutants for C-Stage IA Lung Adenocarcinoma with Ground-Glass Opacity*. Ann Thorac Cardiovasc Surg, 2022.



**CHAPTER 3**  
**TREATMENT-NAÏVE STAGE IV**  
**NSCLC MOLECULAR WORKUP**



## Chapter 3: Treatment-naïve stage IV NSCLC molecular workup

### 3.1 Title page

Title: Optimizing mutation and fusion detection in NSCLC by sequential DNA and RNA sequencing.

*Published: Journal of Thoracic Oncology, 2020. DOI: 10.1016/j.jtho.2020.01.019*

#### 3.1.1 Authors

Cohen D<sup>\*1</sup>, Hondelink LM<sup>\*1</sup>, Solleveld-Westerink N<sup>1</sup>, Uljee SM<sup>1</sup>, Ruano D<sup>1</sup>, AM Cleton-Jansen<sup>1</sup>, von der Thüsen JH<sup>1</sup>, Ramai SRS<sup>2</sup>, Postmus PE<sup>2</sup>, Graadt van Roggen JF<sup>3</sup>, Hoppe BPC<sup>4</sup>, Clahsen PC<sup>5</sup>, Maas KW<sup>6</sup> Ahsmann EJM<sup>7</sup>, ten Heuvel A<sup>8</sup>, Smedts F<sup>9</sup>, van Rossem RN<sup>10</sup>, van Wezel T<sup>1</sup>.

#### 3.1.2 Affiliations

1. Department of Pathology, Leiden University Medical Centre (LUMC)
2. Department of Pulmonology, Leiden University Medical Centre (LUMC)
3. Department of Pathology, Alrijne Hospital
4. Department of Pulmonology, Alrijne Hospital
5. Department of Pathology, Haaglanden Medical Centre (HMC)
6. Department of Pulmonology, Haaglanden Medical Centre (HMC)
7. Department of Pathology, Groene Hart Hospital (GHZ)
8. Department of Pulmonology, Groene Hart Hospital (GHZ)
9. Department of Pathology, Reinier de Graaf gasthuis (RdGG)
10. Department of Pulmonology, Reinier de Graaf gasthuis (RdGG)

\* Both authors contributed equally to this article

#### 3.1.4 Acknowledgements

Karin Kleiverda, Katherine Vahl-Harding, Juanita Ippel, Kim van Elst.

#### 3.1.5 Funding.

JT van Wezel received a research grant from ArcherDX Inc. ArcherDX Inc. supplied 24 reactions free of charge to finish this study.

## 3.2 Abstract

### 3.2.1 Background

Frequently, patients with locally advanced or metastatic NSCLC are screened for mutations and fusions. In most laboratories, molecular workup includes a multitude of tests: immunohistochemistry (ALK, ROS1, and programmed death-ligand 1 testing), DNA sequencing, in situ hybridization for fusion, and amplification detection. With the fast-emerging new drugs targeting specific fusions and exon-skipping events, this procedure harbors a growing risk of tissue exhaustion.

### 3.2.2 Materials and methods

In this study, we evaluated the benefit of anchored, multiplexed, polymerase chain reaction-based targeted RNA sequencing (RNA next-generation sequencing (NGS)) in the identification of gene fusions and exon-skipping events in patients, in which no pathogenic driver mutation was found by DNA-based targeted cancer hotspot NGS (DNA NGS). We analyzed a cohort of stage IV NSCLC cases from both in-house and referral hospitals, consisting 38.5% cytology samples and 61.5% microdissected histology samples, mostly core needle biopsies. We compared molecular findings in a parallel workup (DNA NGS and RNA NGS, cohort 1, n = 198) with a sequential workup (DNA NGS followed by RNA NGS in selected cases, cohort 2, n = 192). We hypothesized the sequential workup to be the more efficient procedure.

### 3.2.3 Results

In both cohorts, a maximum of one oncogenic driver mutation was found per case. This is in concordance with large, whole-genome databases and suggests that it is safe to omit RNA NGS when a clear oncogenic driver is identified in DNA NGS. In addition, this reduced the number of necessary RNA NGS to only 53% of all cases. The tumors of never smokers, however, were enriched for fusions and exon-skipping events (32% versus 4% in former and current smokers,  $p = 0.00$ ), and therefore benefited more often from the shorter median turnaround time of the parallel approach (15 d versus only 9 d in the parallel workup).

### 3.2.4 Conclusion

We conclude that sequentially combining DNA NGS and RNA NGS is the most efficient strategy for mutation and fusion detection in smoking-associated NSCLC, whereas for never smokers we recommend a parallel approach. This approach was shown to be feasible on small tissue samples including for cytology tests, can drastically reduce the complexity and cost of molecular workup, and also provides flexibility in the constantly evolving landscape of actionable targets in NSCLC.

## 3.3 Introduction

The incidence of lung cancer worldwide is high, with over 2 million new cases diagnosed in 2018 [1]. Most patients present with advanced-stage, unresectable disease. The 5-year survival rate in metastatic disease is only 4.7%, making lung cancer the number one cause of cancer deaths globally [1, 2].

In current practice, all patients with locally advanced or metastatic NSCLC (nonsquamous type) should be tested for pathogenic driver mutations in EGFR [3, 4], BRAF [5-7], ERBB2 [8, 9], KRAS [10, 11] and MET (including exon 14 skipping) [12-15]; amplifications in EGFR [16, 17], ERBB2 and MET [12]; fusions in RET [18-20], ALK [21-23], NTRK [24, 25] and ROS1 [26, 27]; as well as for programmed death-ligand 1 (PD-L1) expression [28-31]. This is especially important in NSCLC in nonsmokers, which as a group is a distinct molecular entity, harboring different driver mutations. [32] In the past few years, targeted therapy aimed at specific driver mutations has become possible with increasing frequency, making personalized medicine universally accepted and greatly improving prognosis in advanced metastatic disease [33-39].

To facilitate the accompanying need for more extensive molecular diagnostics, there have been major and rapid advances in the field of DNA sequencing. In recent years, next-generation sequencing (NGS) has become a typically used method of molecular diagnostics in daily clinical practice of pathology. Although it is now possible to analyze tumor DNA and RNA on the basis of cytology, histology, and even plasma samples, the limited amount of tissue for NSCLC diagnostics remains a common problem for molecular pathologists and requires a molecular workup that covers all potential targets, including

mutations, fusions, and exon-skipping events, while using as little tissue as possible.

Although many laboratories have switched to DNA NGS for mutation detection, oncogenic fusion detection is most often performed by fluorescence in situ hybridization (FISH) or reverse transcription polymerase chain reaction (PCR), and is limited to one fusion site per amplicon or probe. This method often fails to provide useful information regarding the fusion partner and the breakpoint; in FISH, it is not possible to identify the fusion partner, and in reverse transcription PCR, only known partners can be found. [40, 41]. The identification of fusion partners is becoming increasingly important because the partners can influence treatment choices and can be of prognostic importance. [42-45]

Archer Anchored Multiplex PCR (Archer) technology (RNA NGS) was previously found to efficiently find genomic aberrations, including novel partners, in routine diagnostics for sarcoma [40] and experimentally in cholangiocarcinoma, glioblastoma and thyroid carcinoma. [41] In addition, it was noted that RNA NGS was able to identify both known and novel fusion partners for ALK [46], ROS1 [41, 47], RET [21, 41] and NTRK [26, 41] and to identify MET exon 14 skipping [48] in small groups of NSCLC samples.

In a recent study by Benayed et al., [49] it was shown that additional Archer-based RNA NGS is required to detect targetable kinase fusions and exon-skipping events that are otherwise missed in their large hybrid capture DNA NGS panel (MSK-IMPACT). This study illustrates that even in large hybrid capture panels, not all fusions and exon-skipping events can be identified owing to the length of introns and blind spots within the targeted areas. Combining hybrid capture DNA NGS with RNA NGS seems the ideal method; however, this procedure is both expensive and probably not feasible in a real-world case-mix of ca. 30% to 40% small histology or cytology samples. Indeed, in this study by Benayed et al., [49] only 47% of cases had available tissue left for RNA extraction, suggesting the need for improvement.

In addition, implementing NGS panels in daily practice can be quite expensive. In large-scale, cost-effectiveness analyses, it has been reported that the mean total cost of targeted DNA-based NGS is estimated to be around €607 per patient. [50] For RNA-based NGS, large-scale cost-effectiveness analysis has not

been performed yet, and we estimated our own costs at €500 to €700 per patient.

We herewith present the route to our current molecular workup of advanced-stage and metastatic NSCLC, combining DNA-based targeted PCR-based NGS (DNA NGS) with Archer-based RNA NGS for the detection of mutations and genetic translocations in routine diagnostics for advanced NSCLC. Our case-mix includes both in-house cases and cases from referral centers with both cytology samples and microdissected histology cases, mostly small core needle biopsies or transbronchial biopsies.

### **3.4 Materials and methods**

#### 3.4.1 Patients and samples

For this study, we included all NSCLC samples from March 2018 until January 2019 (n = 390) for which a molecular NSCLC workup was performed before first-line treatment at the Leiden University Medical Center. Cases originated from both in-house and referred patients. Cases referred with a different diagnostic goal (e.g., clonality with a second tumor or osimertinib resistance) were excluded. Both histology and cytology specimens were included. Squamous cell carcinoma and large cell neuroendocrine carcinoma were not included. In some cases, the workup could not be completed owing to tissue exhaustion. These cases were not excluded from this study but analyzed separately.

The parallel workup was executed from March 2018 to September 2018 (n = 192). For these cases, we performed both DNA NGS and RNA NGS in addition to immunohistochemical staining for ALK, ROS1, and PD-L1. After this 6-month period, we switched from this parallel approach to a sequential approach, performing RNA NGS only when no pathogenic driver mutation in KRAS, BRAF, EGFR, or ERBB2 (including ERBB2 amplification) or MET exon 14 skipping were found in DNA NGS. The sequential approach was performed from September 2018 until January 2019 (n = 198). These cohorts will be henceforth referred to as cohort 1 (parallel approach) and cohort 2 (sequential approach) (Figure 1).

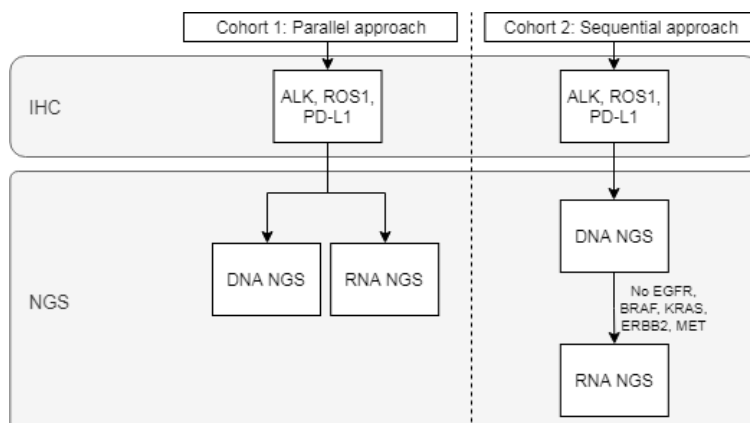


**Figure 1:** Study design and NSCLC diagnostic workup. Cohort 1 (left): DNA next-generation sequencing (NGS) and RNA NGS in parallel. Cohort 2 (right): DNA NGS and RNA NGS only when no pathogenic mutations are found in KRAS, EGFR, BRAF, and ERBB2 and no MET exon 14 skipping is found (including ERBB2 and EGFR amplification). In both cohorts, immunohistochemical staining for ROS1, ALK, and programmed death-ligand 1 (PD-L1) was performed before molecular analyses. Both cytology and histology samples were eligible. Nucleic acid was isolated from blocks by microdissection or punching or from slides.

All samples were isolated from material that had been formalin-fixed, paraffin embedded (FFPE) and preserved. For hematoxylin and eosin and immunohistochemistry (IHC) staining, 1- to 10- $\mu$ m thick slides were cut using a Leica RM2255 Automated Microtome. Staining for ALK fusion (clone D5F3, laboratory-developed test), ROS1 (clone D4D6, laboratory-developed test), and PD-L1 (clone22C3, laboratory-developed test) was performed using a Dako Omnis immunostainer and Dako EnVision Flex+.

The smoking status was extracted from patient records. Patients who had never smoked or had ceased smoking more than 1 month earlier and had accumulated fewer than 5 pack-years were included in the never-smoker category. If they had smoked in the month before diagnosis, they were included in the current-smoker category. The patients with more than 5 pack-years who had not smoked in the month before diagnosis were included in the former-smoker category.

The turnaround time was measured in molecular diagnostics time in workdays (MD time), MD-to-sign time, and received-to-sign time. MD time is the time from the start of molecular analysis until all the results from all molecular

analyses are returned to the pathologist. The MD-to-sign time is the time from the start of molecular analysis until the final report (stating all molecular testing results) is completed and becomes available for the clinician. The received-to-sign time is the time from the receipt of the tissue by the pathology department until the final report is completed.

#### 3.4.2 RNA/DNA isolation

To isolate RNA and DNA for NGS, we collected tumor cells from FFPE blocks by microdissection in cases of core needle biopsies and cytology cell blocks, or by punching resection material. Five 10- $\mu$ m slides were used for the isolation of total nucleic acids from a single extraction process using a tissue preparation system robot (Siemens), as described previously in the literature. [51] The same total nucleic acid sample was used for both the DNA and RNA NGS assays, and in most cases, was sufficient to execute the parallel and sequential workflows without additional isolation. When no tissue block was available or when the tissue block did not contain enough tumor cells, tumor cells were scraped off cytology or hematoxylin and eosin slides. After total nucleic acid isolation, the nucleic acid solution was stored in a freezer at  $-20^{\circ}\text{C}$  for use in DNA NGS and subsequent RNA NGS. Material that was no longer needed for molecular diagnostic testing was stored at  $-70^{\circ}\text{C}$  for future use.

#### 3.4.3 DNA NGS

DNA NGS was performed with a customized Cancer Hotspot Panel, covering hotspots in 75 genes, including ABL1, AKT1, ALK, APC, ARAF, ATM, BRAF, CARD11, CD79A, CD79B, CDH1, CDK4, CDKN2A, CIC, CSF1R, CTNNB1, EGFR, EIF1AX, ERBB2, ERBB3, ERBB4, EZH2, FAK (PTK2), FBXW7, FGFR1, FGFR2, FGFR3, FLT3, FOXL2, GNA11, GNAQ, GNAS, H3F3A, H3F3B, HNF1A, HRAS, IDH1, IDH2, JAK2, JAK3, KDR, KIT, KRAS, MAP2K1, MAP2K2, MAP2K4, MAP3K1, MDM2, MED12, MET, MLH1, MPL, MUTYH, MYC, MYD88, NOTCH1, NPM1, NRAS, PDGFRA, PDGFRB, PIK3CA, POLE, PTEN, PTPN11, RB1, RET, SMAD4, SMARCB1, SMO, SRC, STK11, TP53, and VHL. DNA NGS required 15 ng of input DNA per reaction.

The unaligned bam files generated by the Ion Torrent sequencer were mapped against the human reference genome (GRCh37/hg19) using the TMAP 5.0.7 software with default parameters (<https://github.com/iontorrent/TS>).

Subsequently, variant calling was done using the Ion Torrent specific caller,

Torrent Variant Caller (TVC)-5.0.2, using the recommended Variant Caller Parameter for Cancer Hotspot Panel version 2.

Variant interpretation was done using Genetic Assistant, which assigns functional prediction, conservation scores, and disease-associated information to each variant ([http://softgenetics.com/GeneticistAssistant\\_2.php](http://softgenetics.com/GeneticistAssistant_2.php)). Once a pathogenicity classification is assigned to a variant, the same pathogenicity is automatically attributed the next time the variant is observed. Integrative Genomics Viewer was used for visually inspecting variants. [52]

Chromosomal gains and losses (copy number changes) were also assessed. In short, the median base coverage per amplicon was calculated. The amplicon coverage was then normalized using the median value of all amplicons in that sample. Low quality samples and samples with a high coverage variability were removed. Then, systematic differences among amplicons were normalized. Copy number gains and losses were identified using 99% confidence intervals calculated per gene. The algorithm does not require normal samples to be included; but to obtain reliable results, multiple tumor samples should be included for a more robust and accurate normalization, and to make a better estimation of the 99% confidence intervals per gene. In addition, the algorithm assumes that each amplicon or gene is gained or deleted in a minority of the samples. Copy number analysis, visualization of results, loss of heterozygosity, and chromosomal imbalances were done using the Next-Generation Sequencing Expert shiny app (<https://git.lumc.nl/druano/NGSE>)

The detection of copy number variation by DNA NGS was validated by comparing the data from in situ hybridization and IHC (Figure 2). Sample-to-data time is 5 to 7 days.

#### 3.4.4 RNA NGS

RNA NGS was performed with the Archer Comprehensive Thyroid and Lung panel. This method is capable of detecting fusions with a novel or unknown fusion partner using gene-specific primers in conjunction with molecular barcoded adapters. The RNA NGS panel produces NGS libraries targeting ALK, AXL, BRAF, CCND1, EGFR, FGFR1, FGFR2, FGFR3, MET, NTRK1, NTRK2, NTRK3,

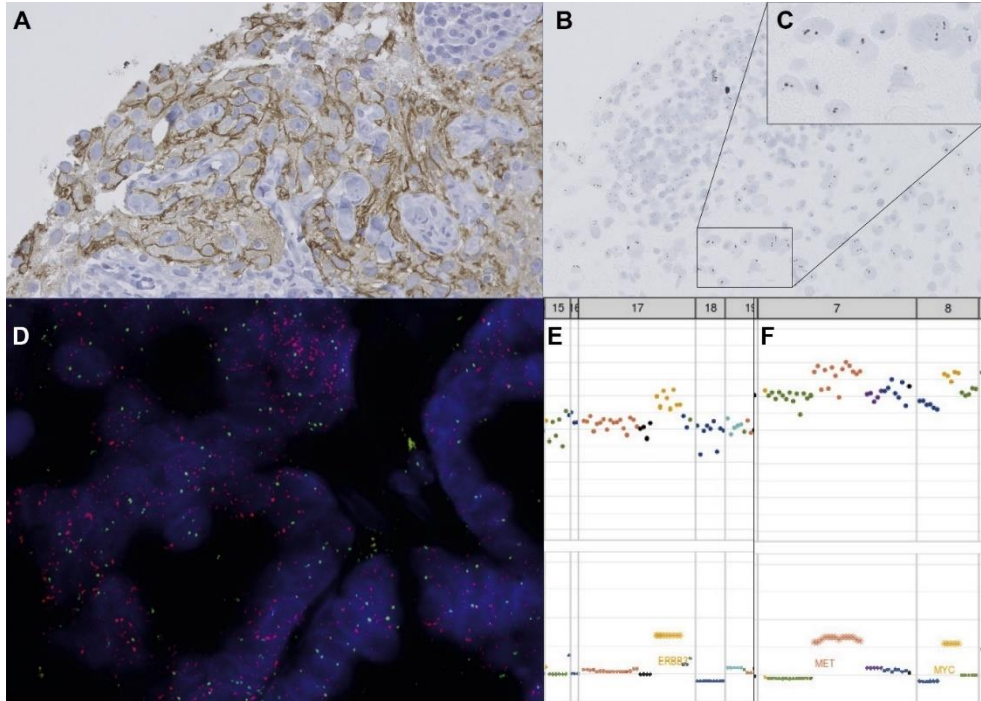


**Figure 2:** Copy number variation analysis for ERBB2 and MET amplification. (A) ERBB2 staining using immunohistochemistry; (B) ERBB2 silver-stained in situ hybridization; (C) enlargement of (B). (D) MET fluorescence in situ hybridization: green, centromere SE7 probe on chromosome 7; red, MET probe showing high MET amplification with >10 signals per cluster per cell; (E) DNA next-generation sequencing read count of chromosome 13 to 21, with ERBB2 amplification on chromosome 17 (upper panel: logarithmic scale, each dot representing the median read count per amplicon, lower panel: normalized read counts); (F) DNA next-generation sequencing read count of chromosome five to eight, with MET amplification on chromosome 7 and MYC amplification on chromosome 8 (upper panel: logarithmic scale, each dot representing the median read count per amplicon, lower panel: normalized read counts).

NRG1, PPARG, RAF1, RET, ROS1, and THADA, including detection of MET exon 14 skipping events. In addition, the RNA NGS panel can detect mutations in ALK, AKT1, BRAF, CTNNB1, DDR2, EGFR, ERBB2, FGFR1, GNAS, HRAS, IDH1, IDH2, KRAS, MAP2K1, NRAS, NTRK1, PIK3CA, RET, and ROS1. Moreover, imbalances in ALK, NTRK1, NTRK2, NTRK3, RET, and ROS1 can be identified. RNA NGS required 20 ng to 200 ng nucleic acid per reaction. Both fresh frozen and FFPE tissue were used. The generated libraries were sequenced using an

Ion Torrent platform and the produced reads were analyzed using the Comprehensive Thyroid and Lung Target Region File and the vendor supplied software (Archer Analysis, version 5.1.7). The sample-to-data time was 5 days.

### 3.4.5 Statistical Analysis

Statistical analysis was performed using IBM SPSS Statistics software, version 25. We defined pathogenic driver mutations as class 4 or 5 pathogenic mutations in KRAS, EGFR, BRAF, ERBB2; high amplifications in ERBB2 and EGFR; fusions in ALK, ROS1, RET, NTRK1, 2, and 3, and FGFR1, 2, and 3; MET exon 14 skipping and BRAF exon skipping. Class 3 mutations of unknown pathogenicity were not taken into account.

### 3.4.6 Ethics

Informed consent was obtained from the patients in the two illustrative cases. The rest of the data were obtained from routine diagnostic reports and were anonymized before processing.

## 3.5 Results

### 3.5.1 Case characteristics

Cases from March 2018 until January 2019 were included. From March 2018 until September 2018, 192 cases were enrolled in cohort 1 and were evaluated with the parallel approach (Figure 1). From September 2018 until January 2019, 198 cases were enrolled in cohort 2 and were evaluated with the sequential approach. Both groups had similar characteristics as outlined in Table 1.

CHARACTERISTIC	COHORT 1: PARALLEL APPROACH (N=192)	COHORT 2: SEQUENTIAL APPROACH (N=198)	P-VALUE
<b>PATIENT CHARACTERISTICS</b>			
AGE	67.3 (43-86)	67.5 (31-90)	0.83
FEMALE	82 (43%)	99 (50%)	0.16
MALE	110 (57%)	99 (50%)	0.16
<b>SMOKING STATUS</b>			0.49
NEVER SMOKER	22 (11%)	24 (12%)	
FORMER SMOKER	73 (38%)	89 (45%)	
CURRENT SMOKER	80 (42%)	71 (36%)	
UNKNOWN	17 (9%)	14 (7%)	
<b>TUMOR TYPE</b>			0.46

ADENOCARCINOM A	174 (91%)	182 (92%)	
NSCLC NOS	14 (7%)	11 (6%)	
ADENOSQUAMO S	4 (2%)	3 (2%)	
PLEIOMORPHIC	0	2 (1%)	
<b>TISSUE ORIGIN</b>			0.61
PRIMARY TUMOR	63 (33%)	70 (35%)	
LYMPH NODE	59 (31%)	68 (34%)	
PLEURAL FLUID	22 (11%)	17 (9%)	
DISTANT METASTASIS	48 (25%)	43 (22%)	
<b>SAMPLE TYPE</b>			0.68
CYTOLOGY	76 (40%)	74 (37%)	
HISTOLOGY	116 (60%)	124 (63%)	
<b>PDL1 STATUS</b>			0.37
NEGATIVE (<1%)	88 (46%)	83 (42%)	
LOW POSITIVITY (1- 49%)	33 (17%)	43 (22%)	
HIGH POSITIVITY (50-100%)	47 (25%)	52 (26%)	
INSUFFICIENT TISSUE AVAILABLE	6 (3%)	9 (5%)	
UNKNOWN (PERFORMED ELSEWHERE)	18 (9%)	11 (6%)	

**Table 1:** Case characteristics. In cohort 1, both DNA NGS and RNA NGS were performed on all specimens. In cohort 2, DNA NGS was performed on all specimens, and when no pathogenic driver mutation in KRAS, BRAF, EGFR, or ERBB2; MET exon 14 skipping; or amplification in EGFR and ERBB2 was found, RNA NGS was performed. P-value for age was calculated with an unpaired T test, all other p-values were calculated with Pearson chi-square test.

### 3.5.2 DNA Next-Generation Sequencing

DNA NGS identified mutations in oncogenes in 241 of the 375 successfully screened cases (64.3%), as also outlined in Table 2, including: KRAS (33.3%), EGFR (11.2% mutation and 2.9% amplification), ERBB2 (2.1% mutation and 1.1% amplification), BRAF (5.1%), PIK3CA (2.9%), NRAS (1.6%), MAP2K1 (1.1%), MET (0.8% mutation, 1.1% amplification, and 0.3% exon 14 skipping).

Genomic aberrations were also found in tumor suppressor genes, for example, in TP53 (48.8%), STK11 (8.3%), CDKN2A (4.0% mutation and 5.6% homozygous

deletion), CTNNB1 (2.1%), PTEN (1.9%), and RB1 (1.1% mutation and 0.5% deletion).

CHARACTERISTIC	NEVER-SMOKERS (N = 46)	FORMER AND CURRENT SMOKERS (N = 313)	P-VALUE
<b>PATIENT CHARACTERISTICS</b>			
FEMALE	26 (61%)	138 (44%)	0.04
MALE	18 (39%)	175 (56%)	0.04
AGE	67.9 (31-89)	67.5 (43-90)	0.81
<b>DNA NGS</b>			0.01
DRIVER IDENTIFIED	26 (59%)	175 (58%)	
TUMOR SUPPRESSOR OR COPY NUMBER VARIANCE ONLY	7 (16%)	95 (32%)	
NO MUTATIONS	11 (35%)	32 (11%)	
<b>RNA NGS</b>			0.00
FUSION/EXON SKIPPING	10 (32%)	7 (4%)	
NO FUSIONS	21 (68%)	182 (96%)	

**Table 2:** different characteristics and outcomes for never-smokers compared to former and current smokers. DNA NGS was performed successfully in never-smokers in 44 cases and in former and current smokers in 302 cases. RNA NGS was performed successfully in never-smokers in 31 cases and in former and current smokers in 270 cases.

MET exon 14 skipping was detected by DNA NGS in only one case. The ability to detect MET exon 14 skipping in DNA NGS depends on the location of the splice-inducing mutation at the splice acceptor site in intron 13 or the splice donor site at intron 14. DNA NGS using the applied cancer hotspot panel does not cover the complete splice region involved in MET exon 14 skipping, explaining the four additional cases of MET exon 14 skipping identified with RNA NGS.

When comparing our data with The Cancer Genome Atlas (TCGA) [53] and Memorial Sloan Kettering-Integrated Mutation Profiling of Actionable Targets (MSK-IMPACT) [36] datasets, we found that our data were mostly concordant with data from these databases. The observed differences were most likely because of the inclusion in TCGA of a more limited range of TNM stages and, therefore, include fewer tumor progression-related mutations. TCGA and MSK-IMPACT included tumors from patients with more diverse international origins,

whereas we received cases from hospitals in only the western part of the Netherlands. In addition, we excluded EGFR tyrosine kinase inhibitor (TKI)-resistant cases, but the MSK-IMPACT database included tumors harboring EGFR T790M mutations, resulting in MSK-IMPACT having a higher percentage of EGFR mutations than our dataset. In Figure 3, we provide a chart showing the most frequently seen and the most therapeutic relevant pathogenic mutations.

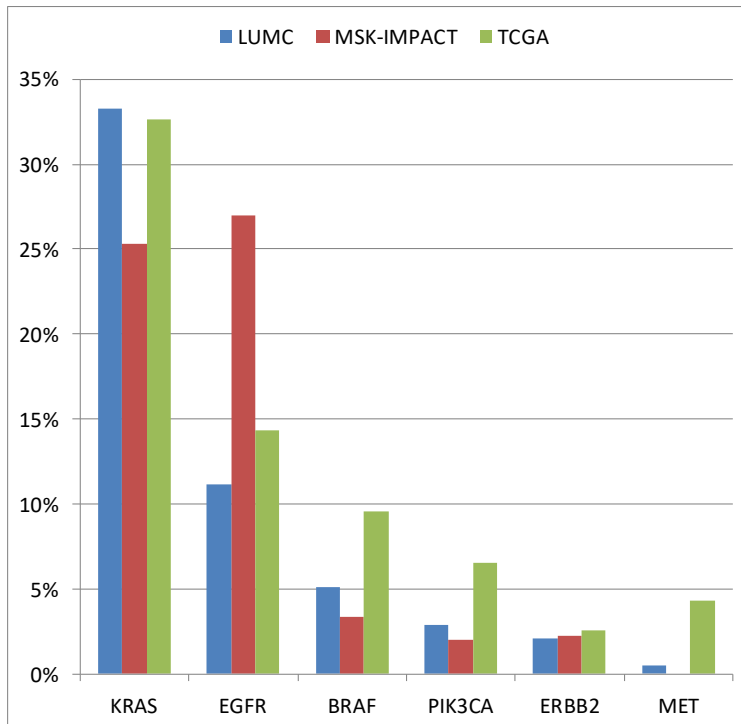


**Figure 3:** Comparison of mutation prevalence in the dataset from The Cancer Genome Atlas-NSCLC adenocarcinoma, Memorial Sloan Kettering-Integrated Mutation Profiling of Actionable Targets, and Leiden University Medical Centre (both cohorts combined). Y axis: percentage of all cases, x axis: oncogenic somatic mutation.

### 3.5.3 RNA Next-Generation Sequencing

In the sequential approach, additional RNA NGS was necessary in 105 of 198 cases without a mutagenic driver (53%), whereas it was performed in all 192 cases in the parallel approach.

In both cohorts combined, RNA NGS was performed in 297 cases. Fusions were found in 19 cases, representing 6.4% of all RNA NGS cases and 4.9% of the total cohort. ALK fusions were detected in eight cases, of which EML4 was the most common fusion partner (n = 6). In one case, ALK was fused to STRN3, and in another case to RPTOR. In all EML4 and STRN3 fusion cases, the ALK breakpoint was at exon 20. In the RPTOR fusion case, the breakpoint was at ALK exon 10 and the fusion protein was out of frame, which also explains the ALK-negative IHC. Because there was no other pathogenic mutation, this fusion was reported, but it is not certain if this is an oncogenic driver. Therefore, the patient has not been treated with TKIs and response data are not available. KIF5B-RET fusion occurred in two cases, FGFR3 fusion occurred in two cases (with TACC3 and WHSC1), MET exon 14 skipping occurred in four additional cases (one case already identified with DNA NGS), and CD74-ROS1 fusion occurred in one case (Figure 4).

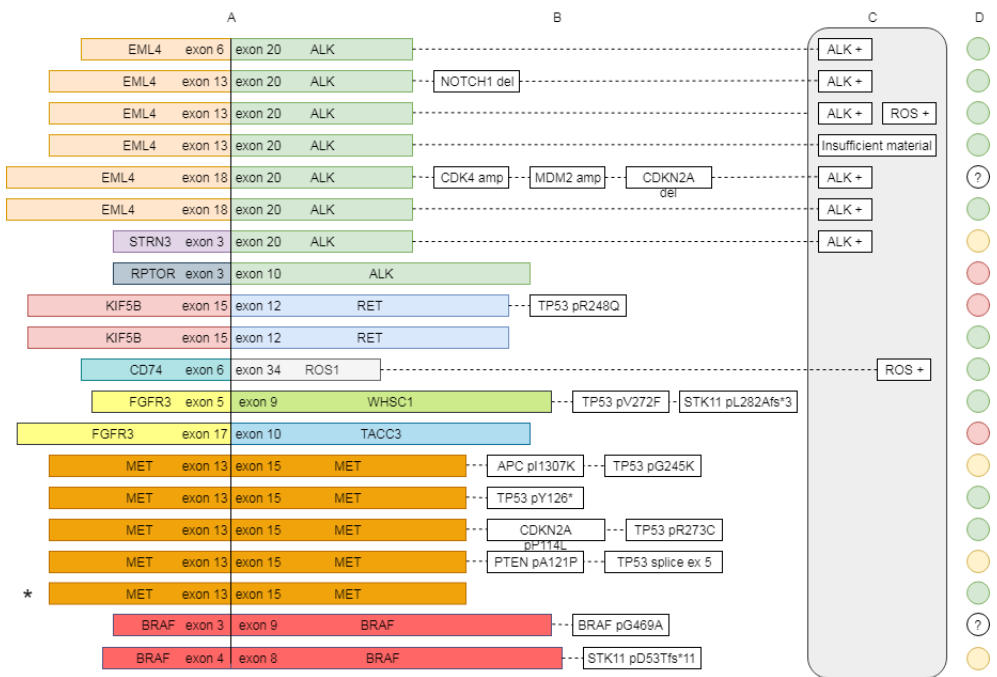


**Figure 4:** Fusions and exon-skipping events found through RNA next-generation sequencing (NGS) for cohorts 1 and 2. The total number of fusions and MET splicing events identified was 19 (5% of the total cohort). (A) RNA NGS findings; (B) DNA NGS findings; (C) immunohistochemistry findings; (D) smoking status: green: never smoker; yellow: former smoker; red: current smoker; white with "?": unknown. \*: event found through DNA NGS.

Fusion-positive cases were mutually exclusive with pathogenic driver mutations in both cohorts, as shown in Figure 4. We did, however, find co-occurrence of ALK fusions with CDKN2A and NOTCH1 deletions and MDM2 and CDK4 amplifications. MET exon 14 skipping co-occurred with CDKN2A deletions, and TP53, APC, and PTEN mutations, RET fusion with TP53 mutations, and FGFR3 fusion coincided with TP53 and STK11 mutations. BRAF exon skipping coincided with non-V600 BRAF mutations and STK11 mutations. However, the non-V600 BRAF mutation was a very low frequency variant and was only observed in RNA NGS.

#### 3.5.4 Never smoking status

In this study, 22 never smokers were included in the parallel cohort and 24 in the sequential cohort. These patients had significantly different characteristics (more often female,  $p = 0.04$ ) and demonstrated a different outcome from DNA NGS and RNA NGS, compared with former and current smokers ( $n = 313$ ), as outlined in Table 2. Smoking history was unknown in 31 cases, which were not included in Table 2.

Although a driver mutation was identified by DNA NGS equally often in never smokers, the types of driver mutations compared with former and current smokers were more often EGFR (41% in never smokers versus 7% in former- and current smokers,  $p = 0.00$ ) and less often KRAS (9% in never smokers versus 37% in former- and current smokers,  $p = 0.00$ ). Furthermore, a fusion was more often in never smokers (32%) versus former and current smokers (4%) ( $p = 0.00$ ) (Figure 5).

In never smokers, DNA NGS failed and a new biopsy was recommended in two cases. In the cases in which DNA NGS was successful, an oncogenic driver was identified in 26 cases (59%). In the 18 cases (41%) in which no oncogenic driver was found in DNA NGS, an oncogenic fusion was found in 10 of 13 successfully analyzed cases (77%). RNA NGS failed in five cases, and a new biopsy was recommended.

In some of the patients included in the never-smoking group, we registered smoking-associated mutations, for example four KRAS mutations. One patient

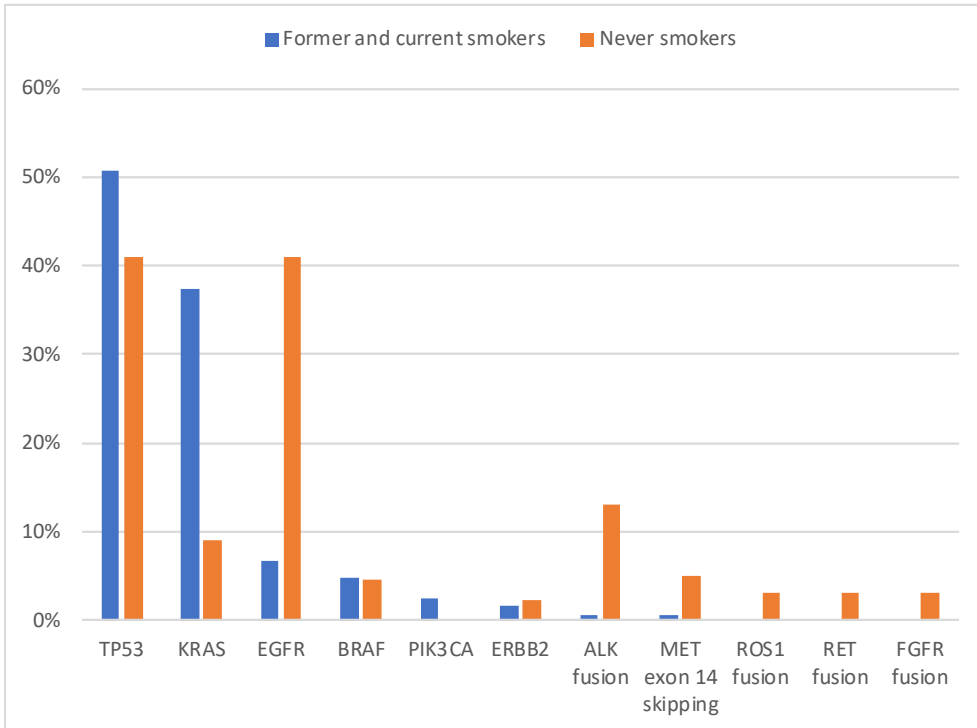


**Figure 5:** Mutations found in smokers (blue) versus never smokers (orange). The difference is significant for KRAS ( $p = 0.00$ ), EGFR ( $p = 0.00$ ), and ALK ( $p = 0.00$ ). Only successful next-generation sequencing (NGS) analyses were taken into account. For smokers  $n = 375$  for DNA NGS targets and  $n = 270$  for RNA NGS targets; for never smokers  $n = 44$  for DNA NGS targets and  $n = 31$  for RNA NGS targets.

with KRAS mutation had never smoked, but it was mentioned in the file that this patient had had frequent exposure to second-hand smoke. This might also have been the case in other patients with KRAS mutations; but this was not always registered extensively in their case file.

### 3.5.5 Turnaround time

In molecular diagnostics for NSCLC, time is an important factor and a possible disadvantage for the sequential approach. We have outlined the turnaround times in Table 3. The median MD time (time from the start of molecular diagnostics until the results are issued to the pathologist) was equal in both cohorts: both had 9 working days.

COHORT	CHARACTERISTIC	MD TIME	MD TO SIGN TIME	RECEIVED TO SIGN TIME
--------	----------------	---------	-----------------	-----------------------

<b>OVERALL (N = 390)</b>	Mean (range)	1906 (2-364)	21.1 (2-365)	33.6 (7-2285)
	Median	9	10	13
<b>PARALLEL COHORT (N = 192)</b>	Mean (range)	14.3 (5-364)	15.7 (6-365)	19.7 (7-365)
	Median	9	10	13
<b>SEQUENTIAL COHORT (N = 198)</b>	Mean (range)	24.7 (2-182)	26.3 (2-186)	47 (7-2285)
	Median	9	10	14
<b>SEQUENTIAL COHORT WITHOUT RNA NGS (N = 90)</b>	Mean (range)	7.2 (2-20)	9.1 (2-59)	16.1 (7-277)
	Median	7	8	9
<b>SEQUENTIAL COHORT WITH RNA NGS (N = 108)</b>	Mean (range)	39.3 (6-182)	40-6 (6-186)	72.8 (7-2285)
	Median	15	15	21

**Table 3:** turnaround time for each cohort. MD time: amount of workdays from the request for DNA NGS or RNA NGS by the pathologist until all the data from molecular diagnostics was available. MD to sign time: amount of workdays from the request for DNA NGS or RNA NGS by the pathologist until the final report is sent to the clinician. Received to sign time: amount of workdays from the arrival of the tissue at the Pathology department until the final report is sent to the clinician. Outliers in the third category are mostly due to late metastasis cases. Outliers in the first and second column are mostly due to late additional RNA NGS in the startup phase of this study.

However, in cases in which additional RNA NGS was required after DNA NGS, the median turnaround time was longer than in the cases in which only DNA NGS was required: 15 working days versus 7 working days.

The never smokers were especially affected. Twenty-four never smokers were enrolled in the sequential approach. In 15 cases, RNA NGS was required, and in five cases, a fusion was identified, whereas RNA NGS failed in two cases. This resulted in a delay in the time-to-driver detection in five of the 24 never smokers (21%), whereas in former- and current smokers, this was the case in only four of 82 cases (4.9%).

### 3.5.6 Immunohistochemistry

When performing IHC, we encountered seven samples that were positive for ALK, four cases positive for ROS1, and one case positive for both ALK and ROS1

(Figure 4). In all cases, we performed RNA NGS to identify the fusion partner and the breakpoint, as these data can provide valuable information regarding the prognosis and resistance to crizotinib. We also aimed to confirm the IHC findings.

ROS1 was strongly positive in one case, in which a ROS1 fusion was found in RNA NGS (Figure 4). Four cases reported ambiguous ROS1 staining, without a fusion detected in RNA NGS. In eight cases that were positive for ALK on the basis of IHC, a fusion was found in RNA NGS in six cases. In the two false-positive IHC results, the staining was weakly positive, whereas the staining was always strongly positive in the true-positive cases.

In the sequential approach, when ALK or ROS1 IHC was positive, RNA NGS was immediately started instead of waiting for the results of DNA NGS. When ALK IHC was strongly positive, the clinician was informed, even before the DNA NGS or RNA NGS results were confirmed to start crizotinib therapy without delay.

In one case, insufficient material was available for IHC, but an ALK fusion was found in RNA NGS performed on cytology slides. In another case, ALK was negative in IHC, and a RPTOR-ALK fusion was found in RNA NGS. However, in this fusion, the ALK breakpoint was in exon 10 instead of in exon 20 or 19, as is usually seen. This fusion resulted in an inactive protein and therefore did not lead to ALK overexpression that can be detected by ALK IHC.

### 3.5.7 NGS challenges and the failure to complete molecular workups

The overall dropout rate of DNA NGS was lower (4%, n = 13) than the overall dropout rate of RNA NGS (18%, n = 54). Of these cases, a driver alteration had already been identified by DNA NGS in 18 cases (33%). Of the remaining cases in which no DNA NGS data with driver mutation and no RNA NGS data could be generated (n = 44 [67%, or 11% of the total cohort]), nine cases were eligible for immunotherapy on the basis of PD-L1 expression. An additional biopsy was recommended owing to RNA NGS failure in 35 cases (9% of the total cohort) (Figure 6).

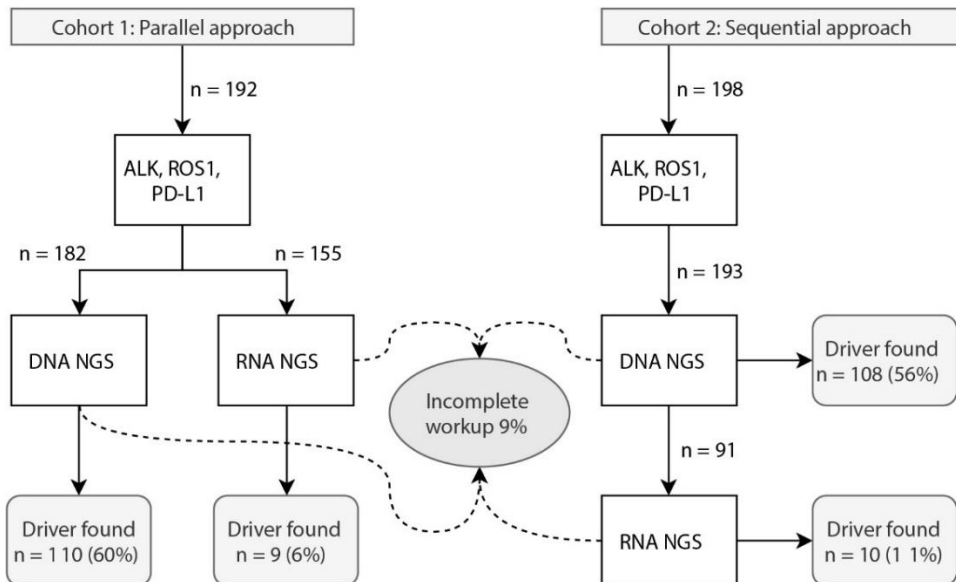


**Figure 6:** Drivers found in the sequential and parallel approaches. The workup was incomplete in 9% of all cases, and a new biopsy was recommended.

### 3.5.8 Cytology

Among all cytology samples ( $n = 150$ ), DNA NGS did not generate reliable data in nine samples (6%). RNA NGS could not be executed in 45 samples (30%), mainly because of the limited number of tumor cells that were available in the specimen. RNA NGS requires 20 ng to 200 ng of nucleic acid, whereas DNA NGS only requires 15 ng.

### 3.5.9 Decalcification

RNA NGS failed in 10 cases (45%) of the decalcified tissues, and six cases (27%) were likewise not suitable for DNA NGS. This was most likely caused by the destruction of nucleic acid by conditions encountered during the decalcification procedure. Fusions detected in small cytology samples were illustrated by the following cases:

#### 3.5.10.1 Case 1

A 70-year-old man presented at the emergency room with cardiac tamponade and pleural effusion. Pericardiocentesis was performed and the drained fluid was analyzed by a pathologist. A thyroid transcription factor-1-positive adenocarcinoma was discovered in the pericardial fluid and in the pleural fluid.

The adenocarcinoma proved to be ALK- and ROS1-negative; the PD-L1 tumor proportion score was 70%. DNA NGS revealed two pathogenic mutations in TP53 and CDKN2A. Subsequent RNA NGS analysis revealed the presence of a MET exon 14 skipping event. The patient was treated with pembrolizumab, initially establishing a progression-free period; but after a few months the disease progressed, and the patient was included in the Drug Rediscovery Protocol trial (NCT02925234) to receive targeted MET exon 14 therapy. Full molecular workup was successfully performed on cytology samples with relatively low tumor cell percentage in this case (Figure 7).

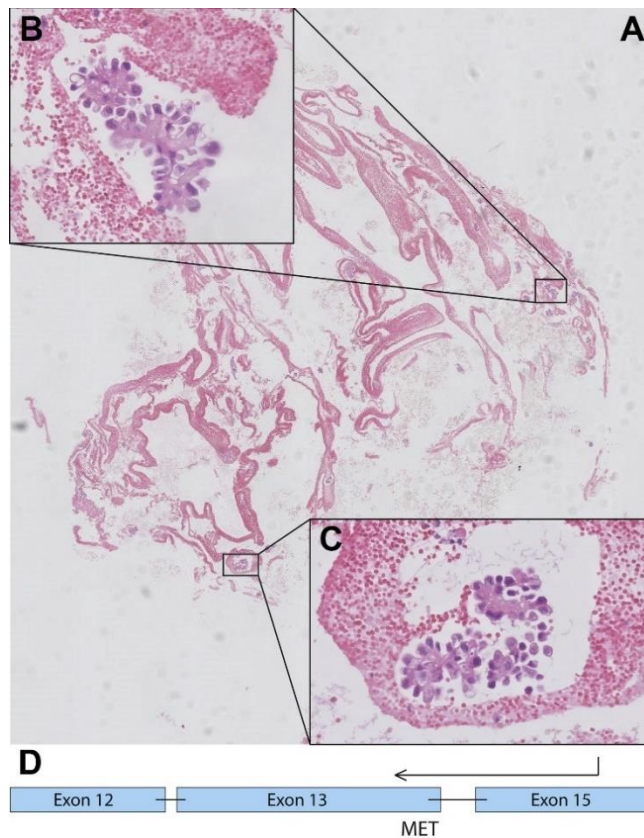


**Figure 7:** Case 1, a 70-year-old man presenting with stage IV NSCLC with positive pleural and pericardial effusions. (A) Hematoxylin and eosin staining of hemorrhagic pericardial fluid with tumor islets that was used for DNA next-generation sequencing (NGS) and RNA NGS; (B, C) enlarged sections of (A); (D) RNA NGS readout showing the MET exon 14 splicing event.

### 3.5.10.2 Case 2

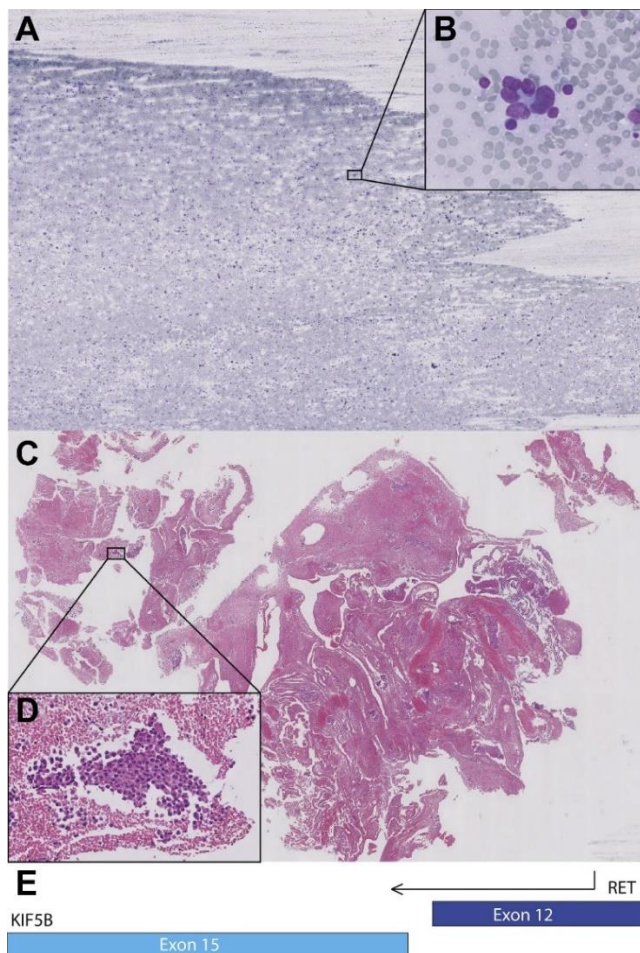


**Figure 8:** Case 2, a 60-year-old man who had never smoked, presenting with multiple nodal, osseous, ocular and subcutaneous metastases of a thyroid transcription factor-1-positive NSCLC. (A) Giemsa staining of a lymph node puncture that was used for the molecular workup, including DNA next-generation sequencing (NGS) and RNA NGS; (B) enlargement of (A); (C) cellblock with hematoxylin and eosin staining of a lymph node puncture that was used for immunohistochemistry; (D) enlargement of (C); (E) RNA NGS readout revealing a KIF5B-RET fusion.

A 60-year-old man presented with loss of vision in his right eye. An ocular tumor of unknown origin was discovered. In the workup, a thoracic computed tomography was performed. Multiple masses in both lungs, the mediastinum,

the kidneys, and subcutis were seen. The patient had never smoked and had no symptoms except mild intermittent back pain. An endobronchial ultrasound-guided lymph node puncture was conducted, and an examination by the pathologist revealed a thyroid transcription factor-1-positive adenocarcinoma. ALK and ROS1 were negative, and PD-L1 was positive in 5% to 10% of the tumor cells. DNA NGS revealed no class 4 or class 5 pathogenic mutations. Fusion analysis by RNA NGS revealed a KIF5B-RET fusion, with the RET breakpoint at exon 12 and the KIF5B breakpoint at exon 15. Initial chemotherapeutic and immunotherapeutic regimens did not lead to stable disease or therapeutic response, and the patient was included in the Dutch Drug Rediscovery Protocol trial (NCT02925234) for RET-targeted treatment. Full molecular workup was successfully performed on a mediastinal lymph node fine-needle aspiration (FNA) sample (Figure 8).

### **3.6 Discussion**

Successful testing for the complex array of molecular targets in metastatic NSCLC demands careful molecular workup and judicious use of diagnostic IHC. For many laboratories, finding a way to navigate the many diagnostic options while not exhausting the tumor tissue of small biopsies or cytology samples remains a challenging task. To be “lean and mean” in molecular diagnostics and to become future-proof, laboratories will have to reduce their number of diagnostic steps in this extensive workup.

In this study, we present our in-house molecular workup for NSCLC that uses both DNA NGS and RNA NGS combined with IHC. To optimize our procedure, we compared a cohort in which we performed parallel DNA NGS and RNA NGS to a cohort in which DNA NGS was followed by RNA NGS only when no driver mutations were detected by DNA NGS in KRAS, BRAF, EGFR, or ERBB2 (including EGFR and ERBB2 amplification), or MET exon 14 skipping. Our results revealed that RNA NGS is a valuable addition to detect fusions for all relevant target sites (ALK, ROS, RET, MET exon 14 skipping, BRAF exon skipping, NTRK, and FGFR), especially in never smokers. We also observed that RNA NGS is able to identify known fusion partners (e.g., EML4-ALK or KIF5B-RET) and novel or unusual partners (e.g., RPTOR-ALK and TACC3-FGFR3).

Additional RNA NGS changed treatment options in 5% of all cases and in 22% for never smokers. These data were in line with the recent study of Benayed et

al. [49] who reported that even in large panels such as MSK-IMPACT, additional RNA NGS is required to identify all fusions and exon-skipping events, especially in cases without a clear driver and with a low tumor mutational burden. Their study reported that in 39.4% of all cases in which the MSK-IMPACT could not identify a driver mutation, sufficient quality and quantity material was left for RNA NGS.

In concordance with the TCGA data, all detected fusions were mutually exclusive with pathogenic driver mutations in EGFR, BRAF, KRAS, MET, and ERBB2, supporting the sequential approach, as presented in Figure 1. [53] This sequential approach reduced the number of RNA NGS analyses by 47.0%.

The sequential approach had a median sample-to-data time of 9 days, which was the same as the parallel approach. However, in cases in which additional RNA NGS was required, the median turnaround time in the sequential approach was 15 days, versus 7 working days in cases in which this was not required. In our laboratory, the alternative of without RNA NGS—that is, DNA NGS with additional FISH and PCR analysis—would take approximately 8 days to 12 days.

When we take into account the cost of the parallel versus the sequential approach, the parallel approach is approximately twice as expensive. DNA NGS costs are estimated at €607, and RNA NGS costs at €500 to €700. Omitting RNA NGS in patients with a clear oncogenic driver in DNA NGS is possible in 47% of all cases, which considerably reduces the average costs of the molecular workup in NSCLC. However, the longer turnaround time is an important disadvantage of the sequential approach.

Moreover, in former and current smokers, the yield of additional RNA NGS is quite low: only seven fusions were found in 313 patients (2%); and because of the IHC screening for ALK, the turnaround time can be reduced in ALK-positive cases. This combination of low RNA NGS yield, high costs, and limited extension of the turnaround time justifies a sequential approach in former and current smokers.

In never smokers, 10 of 46 patients (22%) of all patients harbor a fusion, which can only be detected by RNA NGS. In addition, smokers only represent 12% of all patients presenting with advanced metastatic NSCLC. The higher yield of RNA NGS in this small group of patients asks for a parallel approach, and

greater cost is not a sufficient argument to defer to a sequential approach in these patients. We, therefore, suggest a separate, parallel approach for never smokers, which is outlined in Figure 9.

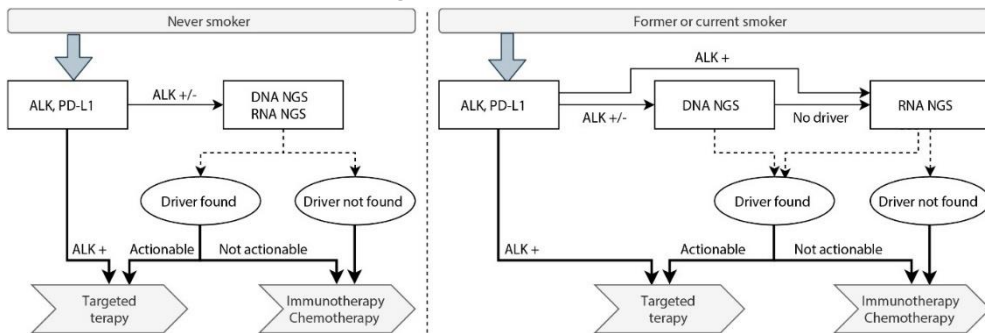


**Figure 9:** Proposed diagnostic process coming from data presented in this article. Left: never smokers; Right: former or current smokers.

More importantly, the combined DNA NGS and RNA NGS workup presented in this study is feasible on small tissue samples and cytology specimens. This is essential for daily clinical practice because in most laboratories, approximately 30% of NSCLC is diagnosed with cytology FNA samples. Our data found that the overall dropout rate was 4% in DNA NGS and 18% in RNA NGS. Cytology samples revealed slightly higher failure rates, with 6% in DNA NGS and 30% in RNA NGS, owing to the higher nucleic acid input required in RNA NGS (20 ng–200 ng) versus DNA NGS (only 15 ng). Overall, in 9% of cases, no driver mutation was found in DNA NGS and insufficient material was left for RNA NGS. In these cases, an additional biopsy was advised.

When comparing our method to large hybrid capture platforms, such as Foundation One, MSK-IMPACT, and MSK-Fusion, our dropout rate is low, especially when taking into account the fact that we made extensive use of cytology samples. [49, 50] The advantages of large panels such as Foundation One can only be harvested for cases with extensive amounts of tissue available. With Foundation One, only 60.9% of all samples of histologic confirmed NSCLC passed the preanalytical quality control check and were evaluable by the NGS assay. [49]

It is important to mention that this workup performs optimally and is most tissue sparing when working with total nucleic acid (isolated in one procedure), so that tissues have to be cut only once. We isolated total nucleic acid in a single procedure using the tissue preparation system Siemens robot. Separate

isolation of DNA and RNA would require more tumor material, possibly resulting in a higher dropout percentage.

As saving tissue is very important in the workup of advanced NSCLC, we should consider omitting ROS1 IHC. This is mainly owing to the fact that the false-positive rate of ROS1 IHC is so high that therapy can never be started without confirmation by RNA NGS. Thus, the only benefit would be that when ROS1 IHC is positive, RNA NGS is started without delay and the ROS1 cases are diagnosed more rapidly. However, the disadvantages are considerable, as the number needed to screen is very high, and in all these cases, valuable tissue is wasted.

A possible disadvantage of our method could be the lower sensitivity of DNA NGS for the detection of copy number variance. Detection of amplifications can be problematic especially in specimens with low tumor cell percentages. This was probably illustrated in the lower number of amplifications compared with TCGA and MSK-IMPACT data, as outlined in Figure 3. In some selected cases, for example, in the workup of post-EGFR-TKI resistance (which was not included in this study), additional ERBB2 or MET FISH might be necessary if no resistance mutations (T790M and C797S) or other resistance mechanisms are detected.

We foresee an increasing need for RNA NGS in the postosimertinib resistance setting, as a wide variety of resistance mechanisms have been described, including fusions. [45] The ability to work with small sample sizes in this clinical setting is even more important, as the diagnostic workup for EGFR-TKI resistance mechanisms is often based on small core needle biopsies or FNA samples of growing metastatic sites. Our method, in which DNA NGS and RNA NGS are combined, could be an ideal and a practical choice for many laboratories dealing with this growing patient category.

In the future, we might further narrow the number of cases in which additional RNA NGS will be required, because tumors harboring pathogenic mutations in oncogenic driver genes such as PIK3CA, HRAS, MAP2K1, MAP2K4, FGFR1, GNAS, or NRAS, do not co-occur with fusion genes or MET exon 14 skipping, as reported in this cohort and the recent article by Benayed et al. [49] However, because both fusions and these somatic driver mutations are quite rare, more experience with molecular diagnostics in NSCLC is needed before we can be certain about the mutual exclusiveness of these rare driver mutations.

In conclusion, we have described our optimization procedure for the molecular workup of advanced-stage NSCLC through a sequential approach for former and current smokers using IHC and DNA NGS followed by RNA NGS in a selected subset of cases without detectable activating mutations in KRAS, BRAF, EGFR, ERBB2, or MET exon 14 skipping.

Switching to a sequential approach drastically reduced the number of unnecessary diagnostic steps and the accompanying costs, as additional RNA NGS was necessary in only 53% of all cases. In never smokers (12% of all patients), we support a parallel approach, because RNA NGS has a much higher yield. More importantly, our method is feasible and successful for small samples, including that of cytologic material, making it an ideal solution for laboratories that want to step away from the classical workup for NSCLC, which combines NGS with multiple FISH analyses, but that do not work with the large sample sizes necessary for large (and more expensive) hybrid capture panels or whole-genome sequencing. In summary, the method presented in this article may drastically reduce the complexity and number of diagnostic steps and can also provide flexibility in the constantly evolving landscape of actionable targets in NSCLC.

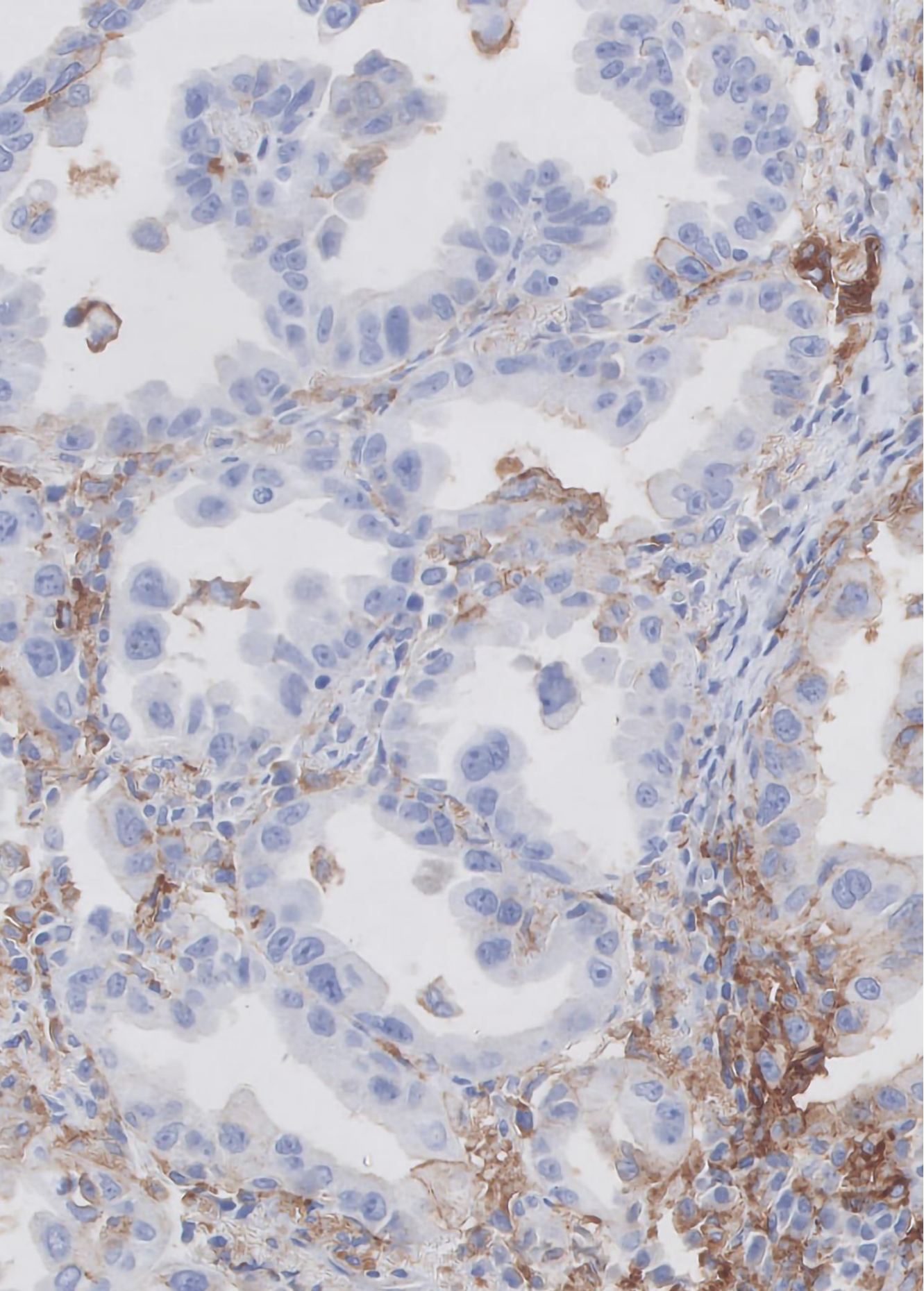
## References

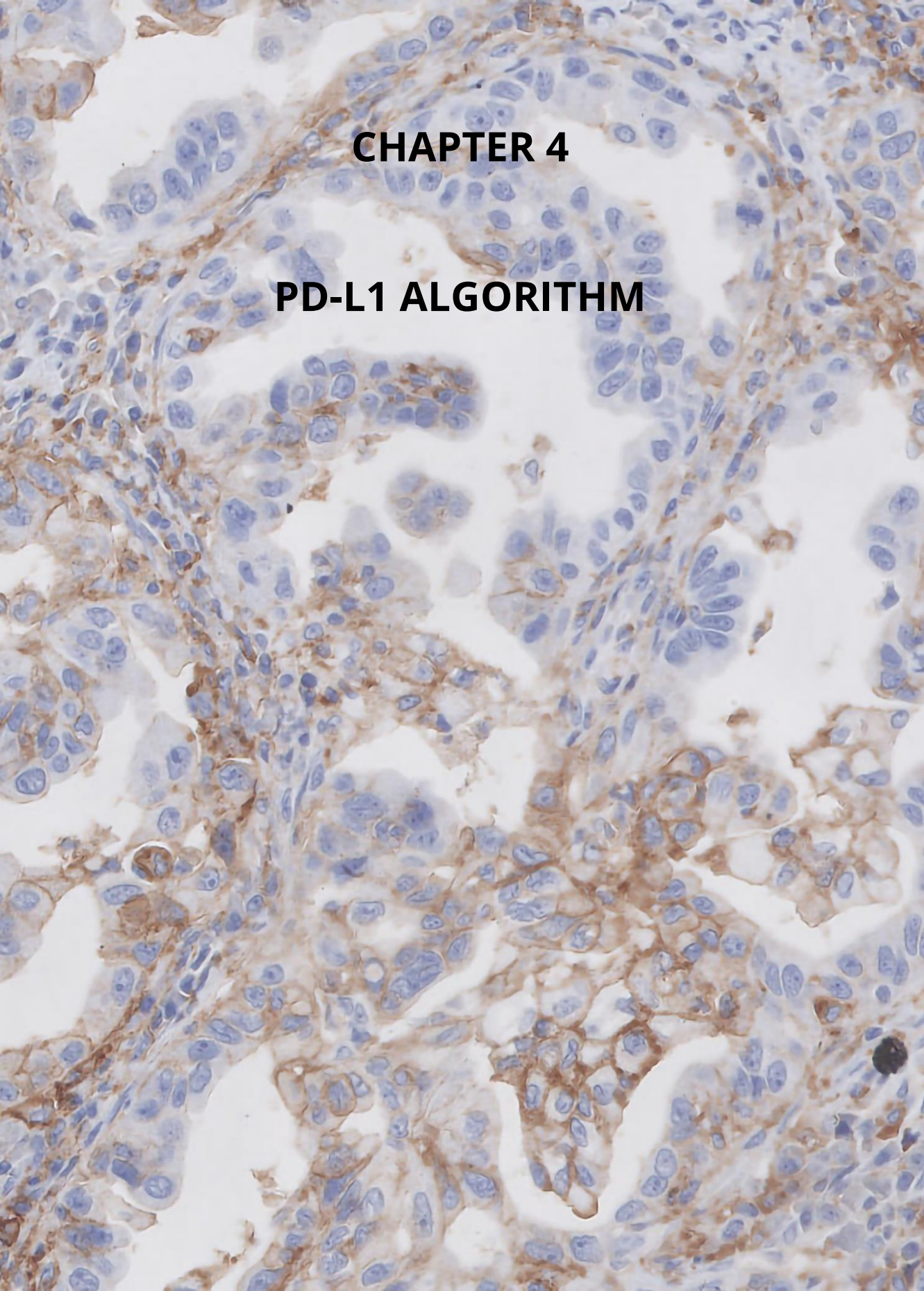
1. Bray F, Ferlay J, Soerjomataram I, et al., *Global cancer statistics 2018: GLOBOCAN estimates of incidence and mortality worldwide for 36 cancers in 185 countries*. *CA Cancer J Clin*. 68:394–424.
2. Howlader N, Noone AM, Krapcho M, et al., *SEER Cancer Statistics Review, 1975-2016*, National Cancer Institute. Bethesda, MD, [https://seer.cancer.gov/csr/1975\\_2016/](https://seer.cancer.gov/csr/1975_2016/), based on November 2018 SEER data submission, posted to the SEER web site, April 2019.
3. Paez JG, Jänne PA, Lee JC, et al. *EGFR mutations in lung cancer: correlation with clinical response to gefitinib therapy*. *Science*, 2004. 304:1497-1500.
4. Lynch TJ, Bell DW, Sordella R, et al., *Activating mutations in the epidermal growth factor receptor underlying responsiveness of non-small-cell lung cancer to gefitinib*. *N Engl J Med*, 2004. 350:2129-2139.
5. Cardarella S, Ogino A, Nishino M, et al., *Clinical, pathologic, and biologic features associated with BRAF mutations in non-small cell lung cancer*. *Clin Cancer Res*, 2013. 19:4532-4540.
6. Planchard D, Kim TM, Mazieres J, et al. *Dabrafenib in patients with BRAF(V600E)-positive advanced non-small-cell lung cancer: a single-arm, multicentre, open-label, phase 2 trial*. *Lancet*, 2016. 17:642-650.
7. Hyman DM, Puzanov I, Subbiah V, et al., *Vemurafenib in multiple nonmelanoma cancers with BRAF V600 mutations*. *N Engl J Med*, 2015. 373:726-736.
8. Stephens P, Hunter C, Bignell G, et al. *Lung cancer: intragenic ERBB2 kinase mutations in tumours*. *Nature*, 2004. 431:525-526.
9. Mazières J, Peters S, Lepage B, et al. *Lung cancer that harbors an HER2 mutation: epidemiologic characteristics and therapeutic perspectives*. *J Clin Oncol*, 2013. 31:1997-2003.
10. Skoulidis F, Byers LA, Diao L, et al., *Co-occurring genomic alterations define major subsets of KRAS-mutant lung adenocarcinoma with distinct biology, immune profiles, and therapeutic vulnerabilities*. *Cancer Discov*, 2015. 5:860-877.
11. Skoulidis F, Goldberg ME, Greenawalt DM, et al., *STK11/LKB1 Mutations and PD-1 Inhibitor Resistance in KRAS-Mutant Lung Adenocarcinoma*. *Cancer Discov*, 2018. 8:822-835.
12. Awad MM, Oxnard GR, Jackman DM, et al., *MET exon 14 mutations in non-small-cell lung cancer are associated with advanced age and stage-dependent MET genomic amplification and c-MET overexpression*. *J Clin Oncol*, 2016. 34:721-730.
13. Frampton GM, Ali SM, Rosenzweig M, et al., *Activation of MET via Diverse Exon 14 Splicing Alterations Occurs in Multiple Tumor Types and Confers Clinical Sensitivity to MET Inhibitors*. *Cancer Discov*, 2015. 5:850-859.
14. Heist RS, Shim HS, Gingipally S, et al., *MET Exon 14 Skipping in Non-Small Cell Lung Cancer*. *Oncologist*, 2016. 21:481-486.
15. Paik PK, Drilon A, Fan PD, et al. *Response to MET inhibitors in patients with stage IV lung adenocarcinomas harboring MET mutations causing exon 14 skipping*. *Cancer Discov*, 2015. 5:842-849.
16. Hirsch FR, Varella-Garcia M, McCoy J, et al., *Increased epidermal growth factor receptor gene copy number detected by fluorescence in situ hybridization*

- associates with increased sensitivity to gefitinib in patients with bronchioloalveolar carcinoma subtypes: a Southwest Oncology Group Study.* J Clin Oncol, 2005. 23:6838-6845.
17. Hirsch FR, Varella-Garcia M, Bunn PA Jr, et al. *Epidermal growth factor receptor in non-small-cell lung carcinomas: correlation between gene copy number and protein expression and impact on prognosis.* J Clin Oncol, 2003. 21:3798-3807.
  18. Gautschi O, Milla J, Filleron T, et al., *Targeting RET in patients with RET-rearranged lung cancers: results from the global, multicenter RET registry.* J Clin Oncol, 2017. 35:1403-1410.
  19. Kohno T, Ichikawa H, Totoki Y, et al., *KIF5B-RET fusions in lung adenocarcinoma.* Nat Med, 2012. 18:375-377.
  20. Sabari JK, Offin MD, Wu SL, et al., *RET-rearranged lung cancers: Immunophenotype and response to immunotherapy.* J Clin Oncol, 2018. 36:9034-9034.
  21. Kwak EL, Bang YJ, Camidge DR, et al., *Anaplastic lymphoma kinase inhibition in non-small-cell lung cancer.* N Engl J Med, 2010. 363:1693-1703.
  22. Shaw AT, Kim DW, Nakagawa K, et al., *Crizotinib versus chemotherapy in advanced ALK-positive lung cancer.* N Engl J Med, 2013. 368:2385-2394.
  23. Soda M, Choi YL, Enomoto M, et al., *Identification of the transforming EML4-ALK fusion gene in non-small-cell lung cancer.* Nature, 2007. 448:561-566.
  24. Hyman DM, Laetsch TW, Kummar S, et al., *The efficacy of larotrectinib (LOXO-101), a selective tropomyosin receptor kinase (TRK) inhibitor, in adult and pediatric TRK fusion cancers.* J Clin Oncol, 2017. 35.
  25. Farago AF, Taylor MS, Doebele RC, et al., *Clinicopathologic Features of Non-Small-Cell Lung Cancer Harboring an NTRK Gene Fusion.* JCO Precis Oncol, 2018.
  26. Bergethon K, Shaw AT, Ou SH, et al., *ROS1 rearrangements define a unique molecular class of lung cancers.* J Clin Oncol, 2012. 30:863-870.
  27. Shaw AT, Ou SH, Bang YJ, et al., *Crizotinib in ROS1-rearranged non-small-cell lung cancer.* N Engl J Med, 2014. 371:1963-1971.
  28. Garon EB, Rizvi NA, Rui R, et al., *Pembrolizumab for the treatment of non-small-cell lung cancer.* N Engl J Med, 2015. 372:2018-2028.
  29. Reck M, Rodríguez-Abreu D, Robinson AG, et al., *Pembrolizumab versus chemotherapy for PD-L1-positive non-small-cell lung cancer.* N Engl J Med, 2016. 375:1823-1833.
  30. Borghaei H, Paz-Ares L, Horn L, et al., *Nivolumab versus docetaxel in advanced nonsquamous non-small-cell lung cancer.* N Engl J Med, 2015. 373:1627-1639.
  31. Brahmer J, Reckamp KL, Baas P, et al., *Nivolumab versus docetaxel in advanced squamous-cell non-small-cell lung cancer.* N Engl J Med, 2015. 373:123-135.
  32. Smolle E and Pichler M. *Non-smoking associated lung cancer: A distinct Entity in Terms of Tumor Biology, Patient Characteristics and Impact of Hereditary Cancer Predisposition.* Cancers (Basel), 2019. 11(2).
  33. National Comprehensive Cancer Network, [Internet], *NCCN Guidelines Version 3.2019 Non-Small Cell Lung Cancer.* 2019. [cited on 1 March 2019]. Available from: [https://www.nccn.org/professionals/physician\\_gls/default.aspx](https://www.nccn.org/professionals/physician_gls/default.aspx)
  34. Herbst RS, Morgensztern D, Boshoff C. *The biology and management of non-small cell lung cancer.* Nature, 2018. 553:446-454.

35. Sabari JK, Santini F, Bergagnini I. *Changing the therapeutic landscape in non-small cell lung cancers: the evolution of comprehensive molecular profiling improves access to therapy*. *Curr Oncol Rep*, 2017. 19:24.
36. Jordan EJ, Kim HR, Arcilla ME, et al., *Prospective comprehensive molecular characterization of lung adenocarcinomas for efficient patient matching to approved and emerging therapies*. *Cancer Discov*, 2017. 7:596-609.
37. Barlesi F, Mazieres J, Merlio JP, et al., *Routine molecular profiling of patients with advanced non-small-cell lung cancer: results of a 1-year nationwide programme of the French Cooperative Thoracic Intergroup (IFCT)*. *Lancet*, 2016. 387:1415-1426.
38. Sholl LM. *Molecular diagnostics of lung cancer in the clinic*. *Transl Lung Cancer Res*, 2017. 6:560-569.
39. Sholl LM, Aisner DL, Varella-Garcia M, et al. *Multi-Institutional Oncogenic Driver Mutation Analysis in Lung Adenocarcinoma: The Lung Cancer Mutation Consortium Experience*. *J Thoracic Oncol*, 2015. 10:768-777.
40. Lam SW, Cleton-Jansen AM, Cleven AHG, et al., *Molecular analysis of gene fusions in bone and soft tissue tumors by Anchored Multiplex PCR-based targeted next-generation sequencing*. *J Mol Diagn*, 2018. 20:653-663.
41. Zheng Z, Liebers M, Zhelyazkova B, et al., *Anchored multiplex PCR for targeted next-generation sequencing*. *Nat Med*, 2014. 20:1479-1484.
42. McLeer-Florin A, Duruisseaux M, Pinsolle J, et al., *ALK fusion variants detection by targeted RNA-next generation sequencing and clinical responses to crizotinib in ALK-positive non-small cell lung cancer*. *Lung Cancer*, 2018. 116:15-24.
43. Yoh K, Seto T, Satouchi M, et al., *Vandetanib in patients with previously treated RET-rearranged advanced non-small-cell lung cancer (LURET): an open-label, multicentre phase 2 trial*. *Lancet Respir Med*, 2017. 5: p. 42-50.
44. Drilon A, Fu S, Patel MR, et al., *A Phase I/Ib Trial of the VEGFR-Sparing Multikinase RET Inhibitor RXDX-105*. *Cancer Discov*, 2018.9:384-395.
45. Oxnard GR, Hu Y, Mileham KF, et al., *Assessment of Resistance Mechanisms and Clinical Implications in Patients With EGFR T790M-Positive Lung Cancer and Acquired Resistance to Osimertinib*. *JAMA Oncology*, 2018. 4:1527-1534.
46. Vendrell JA, Taviaux S, Béganton B, et al., *Detection of known and novel ALK fusion transcripts in lung cancer patients using next-generation sequencing approaches*. *Sci Rep*, 2017. 7:12510.
47. Davies KD, Le AT, Sheren J, et al., *Comparison of Molecular Testing Modalities for Detection of ROS1 Rearrangements in a Cohort of Positive Patient Samples*. *J Thorac Oncol*, 2018. 13:1474-1482.
48. Tafe LJ, de Abreu FB, Peterson JD, et al., *MET Exon 14 Skipping Mutation in Non-Small Cell Lung Cancer Identified by Anchored Multiplex PCR and Next-Generation Sequencing*. *J Cancer Epidemiol Prev*, 2016, 1:1.
49. Benayed R, Offin M, Mullaney K, et al., *High yield of RNA sequencing for targetable kinase fusions in lung adenocarcinomas with no driver alteration detected by DNA sequencing and low tumor mutational burden*. *Clin Can Res*, 2019. 25(15):4712-4722.
50. Marino P, Touzani R, Perrier L, et al., *Cost of cancer diagnosis using next-generation sequencing targeted gene panels in routine practice: a nationwide French study*. *Eur J Hum Genet*, 2018. 26(3):314-323.

51. van Eijk R, Stevens L, Morreau H, et al., *Assessment of a fully automated high-throughput DNA extraction method from formalin-fixed, paraffin-embedded tissue for KRAS, and BRAF somatic mutation analysis*. *Exp Mol Pathol*, 2013. 94:121-125.
52. Thorvaldsdóttir H, Robinson JT, Mesirov JP. *Integrative Genomics Viewer (IGV): high-performance genomics data visualization and exploration*. *Briefings in bioinformatics*, 2013. 14(2): 178-192.
53. Cancer Genome Atlas Research Network, *Comprehensive molecular profiling of lung adenocarcinoma*. *Nature*, 2014. 511:543-550.





**CHAPTER 4**

**PD-L1 ALGORITHM**

## Chapter 4: PD-L1 algorithm

### 4.1 Title page

Title: Development and validation of a supervised deep learning algorithm for automated whole-slide programmed death-ligand 1 tumour proportion score assessment in non-small cell lung cancer

Short running title: PD-L1 algorithm for NSCLC

*Published: Histopathology, 2022. DOI: 10.1111/his.14571*

#### 4.1.1 Authors

LM Hondelink<sup>1</sup>, M Hüyük<sup>1</sup>, PE Postmus<sup>1</sup>, VTHBM Smit<sup>1</sup>, S Blom<sup>2</sup>, JH von der Thüsen<sup>3</sup>, D Cohen<sup>1</sup>

#### 4.1.2 Affiliations

1. Department of Pathology and Department of Pulmonology, Leiden University Medical Centre, Leiden The Netherlands
2. Aiforia Technologies Oy, Helsinki, Finland
3. Department of Pathology, Erasmus Medical Centre, Rotterdam, The Netherlands

#### 4.1.4 Acknowledgements

This study was enrolled in the aiForward project, so the aiForia create software was made available free of charge.

#### 4.1.5 Funding and disclosure

S. Blom is an employee of Aiforia Technologies.

## 4.2 Abstract

### 4.2.1 Aims

Immunohistochemical programmed death-ligand 1 (PD-L1) staining to predict responsiveness to immunotherapy in patients with advanced non-small cell lung cancer (NSCLC) has several drawbacks: a robust gold standard is lacking, and there is substantial interobserver and intraobserver variance, with up to 20% discordance around cutoff points. The aim of this study was to develop a new deep learning-based PD-L1 tumour proportion score (TPS) algorithm, trained and validated on a routine diagnostic dataset of digitised PD-L1 (22C3, laboratory-developed test)-stained samples.

### 4.2.2 Methods and results

We designed a fully supervised deep learning algorithm for whole-slide PD-L1 assessment, consisting of four sequential convolutional neural networks (CNNs), using aiforia create software. We included 199 whole slide images (WSIs) of 'routine diagnostic' histology samples from stage IV NSCLC patients, and trained the algorithm by using a training set of 60 representative cases. We validated the algorithm by comparing the algorithm TPS with the reference score in a held-out validation set. The algorithm had similar concordance with the reference score (79%) as the pathologists had with one another (75%). The intraclass coefficient was 0.96 and Cohen's  $\kappa$  coefficient was 0.69 for the algorithm. Around the 1% and 50% cutoff points, concordance was also similar between pathologists and the algorithm.

### 4.2.3 Conclusions

We designed a new, deep learning-based PD-L1 TPS algorithm that is similarly able to assess PD-L1 expression in daily routine diagnostic cases as pathologists. Successful validation on routine diagnostic WSIs and detailed visual feedback show that this algorithm meets the requirements for functioning as a 'scoring assistant'.

## 4.3 Introduction

The 5-year survival rate of patients with stage IV non-small cell lung cancer (NSCLC) is poor, and this, combined with 2 million new patients annually, makes lung cancer the leading cause of cancer deaths in the world.[1,2]

Immune checkpoint therapy (immunotherapy) targeting the programmed cell death protein 1/programmed death-ligand 1 (PD-L1) pathway [3] has greatly improved survival for NSCLC patients. [4-6] However, response varies greatly between NSCLC patients. Therefore, immunohistochemical PD-L1 expression is currently used as a biomarker to select patients for immunotherapy.

Pathologists measure PD-L1 expression by estimating the percentage of tumour cells with membranous PD-L1 positivity (the tumour proportion score (TPS); see also Formula 1 in Doc. S1). [7,8] The TPS is a continuous score between 0% and 100%, and patients are further divided into three classes, i.e. TPS of <1%, TPS of 1–49%, and TPS of >50%, as outlined in Figure 1. [5] These classes have different treatment options, provided that no targetable mutation (*EGFR*) or fusion (*ALK*; *ROS1*) is detected. [9]

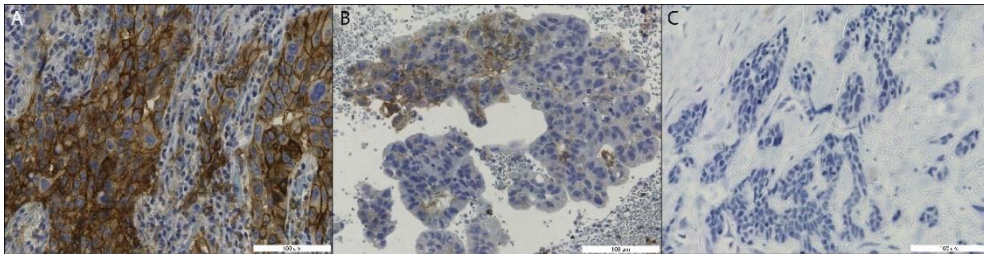


**Figure 1:** Categories of programmed death-ligand 1 (PD-L1) expression, measured as the tumour proportion score (TPS) (Formula 1 in Doc. S1). Blue staining: haematoxylin. Brown staining: PD-L1. A, TPS of 50–100%. B, TPS of 1–49%. C, TPS of <1%.

Unfortunately, this PD-L1 expression scoring system has been proven to be imperfect. The study by Cooper et al. showed that problematic interobserver and intraobserver discordance exists, with disagreement between pathologists in 15.8% of cases around the 1% cutoff point ( $\kappa$  coefficient: 0.68) and disagreement between pathologists in 18.1% of cases around the 50% cutoff point ( $\kappa$  coefficient: 0.58). This study points out that individual pathologists change their assessment in 8–10% of cases and that 1 h of training does not help in improving concordance. [10] These data suggest that patients receive suboptimal treatment due to misclassification, possibly making them suffer from unnecessary side-effects [11, 12] or purposelessly increasing the already substantial costs of advanced NSCLC treatment. PD-L1 TPS assessment could therefore benefit from computational analysis, which eradicates intraobserver

variance and has the potential to eliminate some of the human factors that lead to the high rate of interobserver discordance.

Three computational PD-L1 TPS scoring methods have been proposed in the literature so far, [13] all of which produce high rates of concordance with the reference scores and therefore constitute a relevant proof of concept that computer-aided PD-L1 scoring is possible. However, the proposed algorithms all have similar limitations hampering their performance (and therefore their implementation in clinical practice) beyond the research domain. The limitations include: the use of tissue microarrays (TMAs) [making them not applicable to whole slide images (WSIs) with benign tissue backgrounds], the use of trial material instead of clinical material (resulting in only easy-to-score material being present in the validation set), a limited number of observers for the ground truth score, a lack of precise predictions (undermining the algorithm's explainability for clinicians), requiring manual annotations for each scoring area (resulting in a very labour-intensive process and potential sampling error), and being thresholding-dependent (making them not transferable to a clinical setting, in which staining intensity varies over time). For all of these algorithms, the question is whether they are reliable in a clinical setting. Detailed descriptions of the different study setups and potential limitations are included in Table S1. [14-16]

#### **4.4 Materials and methods**

To summarise, the perfect PD-L1 algorithm does not yet exist. A good, practically usable PD-L1 algorithm should be trained and validated on WSIs that originate from routine diagnostics. In order to correctly assess the PD-L1 TPS within the wide variety of tissue contexts from which NSCLC (stage IV) biopsies originate (benign bronchial epithelium, lymph nodes, adrenal gland, bone and cartilage, skin, liver, kidney, etc.), and also to correctly neglect positive immune cells such as macrophages, a deep learning-based approach is required. Additionally, because of the high interobserver variance in PD-L1 scoring that the algorithm is intended to overcome, the reference scores should be acquired from multiple observers rather than just one. Finally, the algorithm should provide visual feedback at a microscopic level, in order to make algorithm scores interpretable for pathologists and pulmonologists. These criteria are outlined in Table 1. In this article, we therefore present the

first fully supervised deep learning PD-L1 TPS algorithm, based on a cohort from routine diagnostics with robust reference scores generated by three experienced thoracic pathologists.

<b>STUDY SETUP FEATURE</b>	<b>CRITERION FOR APPLICABILITY TO CLINICAL DIAGNOSTICS</b>
CASE SELECTION	Routine diagnostic cases, including 'difficult' features, e.g. metastasis tissue background or artefacts
GROUND TRUTH	As robust as possible: multiple expert observers or response data
VALIDATION	Validation at the whole slide level
ALGORITHM FEEDBACK	Easily interpretable, detailed visual feedback

**Table 1:** *Criteria for algorithm applicability to clinical diagnostics*

#### 4.4.1 Case selection

One hundred and ninety-nine consecutive NSCLC specimens from routine diagnostics at the Leiden University Medical Centre, for which PD-L1 staining had been performed for routine diagnostics and the TPS was registered in the pathology report, were included. Cases were excluded if the patient (at the time of the biopsy) did not give permission for the use of leftover tissue for research purposes, if a small-cell or neuroendocrine morphology was described, or if the biopsy contained <100 tumour cells.

The samples originated from both in-house and referral cases. Three cytology cases with large tumour islands resembling histology specimens were included; all other cytology cases (including all endobronchial ultrasound-guided transbronchial needle aspiration specimens) were excluded. Patients with a second primary NSCLC on which PD-L1 staining had also been performed were included twice (both tumours once). Both metastasis biopsies and primary tumours were included. All samples were irreversibly anonymised after inclusion, by use of a unique four-digit random number.

#### 4.4.2 PD-L1 staining methods

Slides were stained for routine diagnostics, over a period of several years. Formalin-fixed paraffin-embedded blocks were cut into 3-µm sections with a Leica RM2255 Automated Microtome (Leica Biosystems B.V., Amsterdam, the Netherlands). Sections were placed on microscope slides and dried at either 60°C for 30 min to 16 h, or at 37°C for 72 h. After being dried, the slides were

deparaffinised, and antigen retrieval was performed in citrate buffer (Target Retrieval Solution, pH 6) for 40 min. Immunohistochemistry (IHC) was performed according to a laboratory-developed test protocol. Slides were stained with the Dako Omnis immunostainer and Dako EnVision Flex+ reagents and 1:20 dilution of PD-L1 clone 22C3 (Dako Omnis, Dako Agilent Technologies, Leuven, Belgium). The IHC slides were then counterstained with haematoxylin, and coverslips were applied. Tonsil and placental tissue were used as positive controls for PD-L1 expression.

#### 4.4.3 Scoring

All of the 199 included samples were independently scored (TPS; Doc. S1, Formula 1) by three trained pulmonary pathologists (D.C., J.T., and V.S.). The pathologists were blinded to each other's scores. The continuous TPS was divided into three categories (<1%, 1–49%, and 50–100%) for part of the analyses. The level of concordance between the pathologists was calculated by making 597 pairwise comparisons from the 199 scored cases. If the paired pathologists scored in the same category (<1%, 1–49%, and 50–100%), the case was considered to be 'concordant'. For comparison with algorithm performance, we calculated the mean of the three pathologists' continuous TPSs and used that as the reference score for the algorithm (Formula 2 in Doc. S1).

#### 4.4.4 Scanning

We anonymised glass slides before scanning, by generating random barcodes for each slide. Digital WSIs were acquired with Nanozoomer 2.0-HT (Hamamatsu Photonics, Hamamatsu City, Japan) scanners at a resolution of 0.23  $\mu\text{m}/\text{pixel}$ . The WSI metadata did not contain any personal data. WSIs were uploaded to the Aiforia Hub platform (Aiforia Technologies, Helsinki, Finland) as .ndpi files without additional processing.

#### 4.4.5 Training and validation set

A training set of 60 samples was selected from the 199 included cases. In the training set, there was variance in tumour type, biopsy site, tissue size (tumour resection or small core needle biopsy), and the TPS. We included extra lymph node biopsies and squamous cell carcinomas in the training set, because only a handful of these cases were included in the training set when we selected

randomly. All remaining samples were included in the validation set, which resulted in a held-out validation set of 139 cases.

#### 4.4.6 Algorithm setup

The algorithm consists of four separate convolutional neural networks (CNNs) (Figure 2) and is programmed in C++. The first three CNNs are binary semantic segmentation models. The first CNN segments high-quality tissue versus background or low-quality tissue. The class 'low-quality tissue' includes white background, out-of-focus tissue, folding artefacts, air bubbles, glass edges, and other tissue that is of too low quality to be used for scoring. As the PD-L1 TPS score must score only tumour cells and neglect immune cells, such as macrophages, the second and third CNNs both segment neoplastic tissue versus all other high-quality tissues. Both CNNs use precisely the same annotations, but the second CNN utilises a larger tile size (200  $\mu\text{m}$ )—which results in coarse segmentation—whereas the third model uses smaller tiles (50  $\mu\text{m}$ ) and is used to refine the predictions of the second CNN. This method of refining segmentation predictions enabled more precise prediction of neoplastic cells and islets, and has not been described before for pathology image analysis. The fourth CNN is an object detection model with two classes: PD-L1-positive cells and PD-L1-negative cells. Each CNN is used only within the segmented area of the previous CNN, which, for example, results in the ignoring of PD-L1-positive and PD-L1-negative immune cells outside of the neoplastic areas. The four-CNN setup was chosen in order to mimic human scoring, and to enhance explainability to clinicians and patients.

#### 4.4.7 Annotations

All annotations were placed by the same trained annotator (L.H.), under the supervision of thoracic pathologists D.C. and J.T., in regions of interest (ROIs) in the training set (60 WSIs). Examples of annotations are shown in Figure 2 and

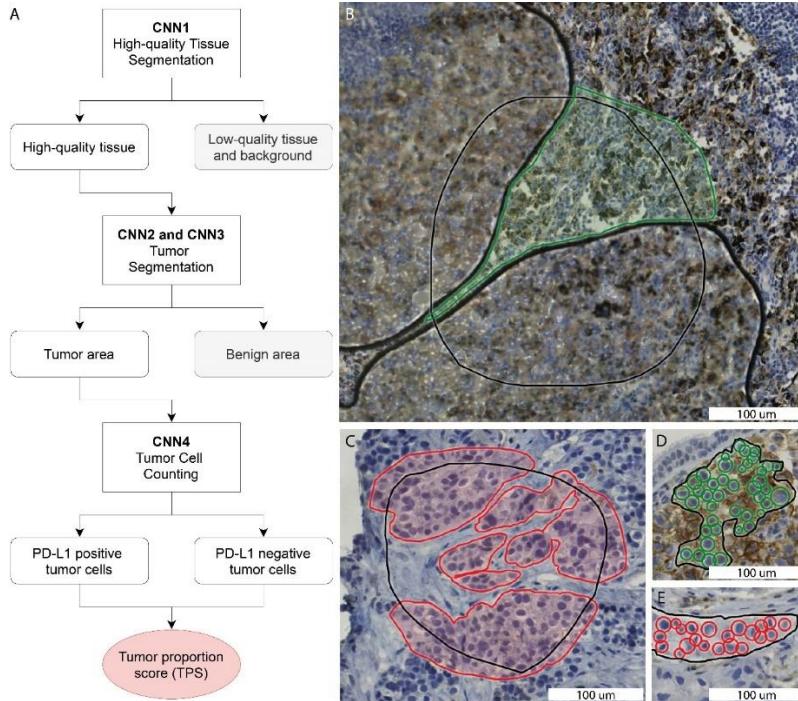


**Figure 2:** Algorithm setup and annotations. A, Schematic algorithm setup with four convolutional neural networks (CNNs) to calculate the programmed death-ligand 1 (PD-L1) tumour proportion score (TPS). B, Annotations for high-quality tissue segmentation (CNN1). Green annotated: high-quality tissue that is in focus and does not contain artefacts. Black: annotated region of interest (ROI), and non-annotated area within the ROI: the tissue is of low quality in this example, because of air bubbles. C, Annotations for tumour segmentation (CNN2 and CNN3). Red annotated: tumour. Black: annotated ROI, and non-annotated area within the ROI: non-neoplastic tissue. D,E, Annotations for tumour cell counting (CNN4). Green: annotated PD-L1-positive nuclei. Red: annotated PD-L1-negative nuclei. Black: annotated ROI. The TPS can be calculated from the number of PD-L1-positive tumour cells and the number of PD-L1-negative tumour cells (Formula 1 in Doc. S1). All annotations were placed in the training set ( $n = 60$ ), which was withheld from validation.

Figure S1. In order to speed up the last part of the annotation process, we used an adaptation of the human in the artificial intelligence (AI) loop (HAIL) method, as outlined in Figure 3. [17] In this method, the preliminary AI model proposes annotations that can be approved, edited or rejected by the annotator. This

process substantially speeds up annotating, as previously described in the literature, [17] and enables screening for 'difficult' features early in the algorithm development process. All annotations were placed in the training set ( $n = 60$ ), which was not used for validation.

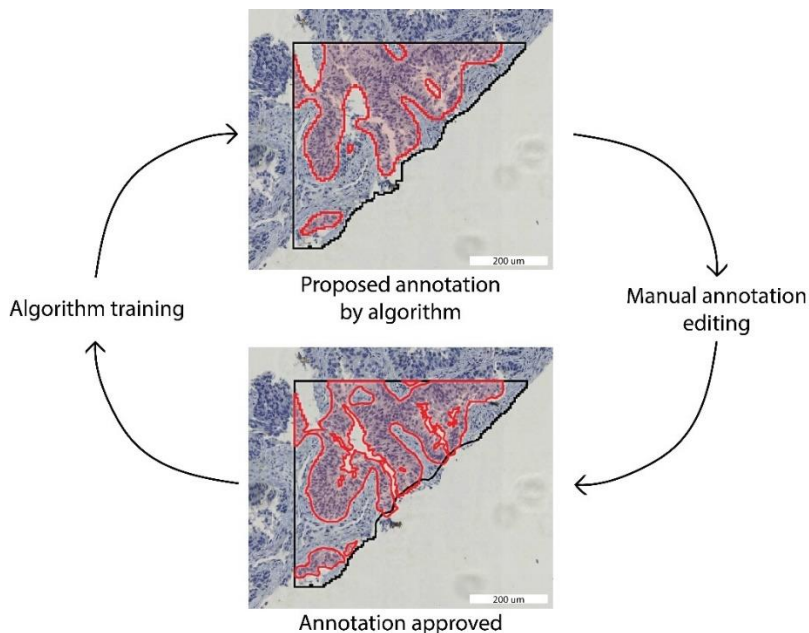


**Figure 3:** Human in the artificial intelligence loop (HAIL) annotation method. Red: neoplastic tissue. Black: region of interest. The preliminary algorithm proposes annotations, which can be approved, edited or rejected by the annotator. This process speeds up annotating and enables screening for 'difficult' features early in the algorithm development process. In each HAIL cycle, multiple annotations are proposed, edited, and accepted.

#### 4.4.8 Algorithm training and validation

Algorithm training and validation were performed with aiforia v4.6, as previously published. [18-19] The error against annotated training data was used as an evaluation metric for each CNN separately. The loss function for semantic segmentation networks was multiclass logistic regression. For the object detection network, a custom-built loss function was used within the aiforia panel. For each CNN, augmented tiles (the augmentation settings are outlined in Figure S2) were used: CNN1, 8 052 800 tiles; CNN2, 5 860 000 tiles; CNN3, 6 472 800 tiles; and CNN4, 58 201 600 tiles.

For validation, the algorithm was applied to all WSIs in the validation set. The algorithm TPS for each WSI was acquired and compared with the whole-slide reference score from the pathologists. Cases were considered to be 'concordant' when the algorithm score and the reference score were in the same category: TPS of <1%, 1–49%, or ≥50%. Cases were considered to be 'not scorable' when the algorithm detected <100 neoplastic cells in the WSI. Cases were considered to be either 'around the 1% cutoff point' (reference score of <25%) or 'around the 50% cutoff point' (reference score of ≥25%).

#### 4.4.9 Ethics

Cases were anonymised by use of a unique and anonymous research number. Specimens were handled according to the Code for Proper Secondary Use of Human Tissue in The Netherlands (Dutch Federation of Medical Scientific Societies). This study was approved by the local Medical Ethical Committee (B20.008).

## 4.5 Results

One hundred and ninety-nine NSCLC histology cases were included in the study. We compared our algorithm-derived PD-L1 TPS (algorithm score) with the mean of three scores of specialised pathologists (reference score).

#### 4.5.1 Patients and cases

The characteristics of the training and validation set are shown in Table 2. The two groups are slightly different, which is a result of enriching the training set for lymph node biopsies and squamous cell carcinomas, as only a handful of those cases were included in the training set by random selection.

CHARACTERISTIC	TRAINING SET (N = 60)	VALIDATION SET (N = 139)	P-VALUE
<b>AGE (YEARS) (RANGE)</b>	69 (45–86)	68 (48–90)	0.7*
<b>SEX, N (%)</b>			1.0†
MALE	35 (58)	81 (58)	
FEMALE	25 (42)	58 (42)	
<b>TUMOUR TYPE, N (%)</b>			0.03‡
ADENOCARCINOMA	44 (73)	117 (84)	
SQUAMOUS CELL CARCINOMA	16 (27)	18 (13)	

ADENOSQUAMOUS CARCINOMA	0	4 (3)	
<b>BIOPSY SITE, N (%)</b>			0.01‡
LUNG	30 (50)	89 (64)	
LYMPH NODE	14 (23)	11 (8)	
DISTANT METASTASIS	16 (27)	39 (28)	
<b>PD-L1 IN REPORT, N (%)</b>			0.53‡
NEGATIVE (<1%)	28 (47)	69 (50)	
LOW POSITIVE (1–49%)	20 (33)	36 (26)	
HIGH POSITIVE (50–100%)	12 (20)	34 (24)	

**Table 2:** Case characteristics. Significant difference are due to enriching the training set for lymph node biopsies and squamous cell morphology, as only a few of those were included when we selected the training set randomly. \*Unpaired t-test. †Fisher’s exact test. ‡Chi-squared test.

#### 4.5.2 Interobserver variability between pathologists

The three pathologists were in complete agreement in 124 of 199 cases (62%). In pairwise comparisons ( $n = 597$ ; Figure 4), the overall concordance between any two pathologists was 75%. Around the 1% cutoff (136 cases), all three pathologists agreed in 83 cases (61%). There were 408 pairwise comparisons around 1%, resulting in an overall concordance of 74%. Around the 50% cutoff (63 cases), all three pathologists agreed in 41 cases (65%). Between any two pathologists in the 189 pairwise comparisons around 50%, the concordance was 77%. The Fleiss  $\kappa$  coefficient was 0.61 overall (substantial agreement; 95% confidence interval 0.612–0.616). The mean absolute difference between the pathologists’ assessments was 8%. These data are similar to the concordance rates described in the literature. [10, 20-26]

#### 4.5.3 Algorithm training and metrics

We trained the four CNNs separately. For each CNN, the training settings and output (tile size, amount of training data annotated, epochs trained, and error against training data) are summarised in Table 3. Error against training data was calculated with Formula 1 for semantic CNNs (CNN1, CNN2, and CNN3), and with Formula 2 for object detection CNN (CNN4). We used an early

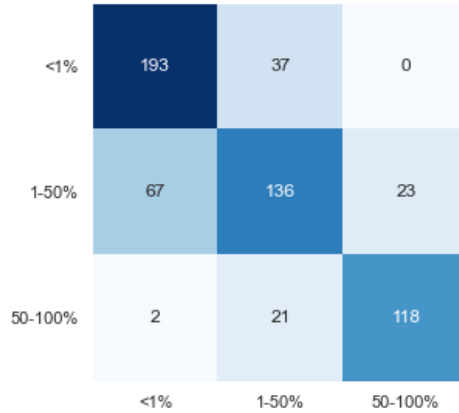


**Figure 4:** Confusion matrix for interobserver variance between pathologists. The confusion matrix is based on three observers and 199 cases, constituting 597 pairwise comparisons. One of the paired observers is plotted on the x-axis and the other observer is plotted on the y-axis.

stopping mechanism, which ended the training after ~18 h when there was no progress in the loss function output over a set amount of epochs.

$$error = \frac{false\ positive\ area\ (mm^2) + false\ negative\ area\ (mm^2)}{Region\ of\ interest\ (ROI)\ area\ total\ (mm^2)}$$

**Formula 1:** Error formula for segmentation CNNs (CNN1, CNN2, and CNN3).

$$error = 1 - \frac{true\ positive\ area}{true\ positive\ area + false\ positive\ area + false\ negative\ area}$$

**Formula 2:** Error formula for the object detection CNN (CNN4).

#### 4.5.4 Algorithm validation

In the validation set, as outlined in Figure 5, the concordance between the reference score and the algorithm score was 79% overall, whereas any two pathologists agreed with each other in only 75% of the cases. The algorithm concordance was also 79% around the 1% and 50% cutoff points, whereas any two pathologists agreed with each other in 74% and 77% of the cases around these cutoff points. The average difference between any two pathologists was 8%, and the average difference between the algorithm score and the reference score was 5%, which is significantly lower ( $P = 0.01$ , unpaired  $t$ -test). The intraclass coefficient (with a consistency definition) was 0.96 [95% confidence

interval (CI) 0.94–0.97], when the continuous algorithm score was compared with the continuous reference score. The algorithm identified 39 359 neoplastic cells per slide on average (range, 188–749 558 cells). Cohen’s  $\kappa$  coefficient for the algorithm was 0.68. This is similar to the Fleiss  $\kappa$  coefficient calculated for the pathologists (0.61).

CNN	TILE SIZE ( $\mu\text{M}$ )	RESOLUTION ( $\mu\text{M}/\text{PIXEL}$ )	ANNOTATED DATA	NO. OF CNN LAYERS	EPOCHS TRAINED	ERROR AGAINST TRAINING DATA (%)
CNN1: HIGH-QUALITY TISSUE	50	1.61	517 mm <sup>2</sup>	8	5033	0.12
CNN2: NEOPLASTIC TISSUE (COARSE)	200	1.57	960 mm <sup>2</sup>	12	14 650	0.49
CNN3: NEOPLASTIC TISSUE (REFINEMENT)	50	0.39	960 mm <sup>2</sup>	12	16 182	0.15
CNN4: CELL DETECTION	86	0.44	5159 objects	6	18188	9.1

**Table 3:** Training parameters per convolutional neural network (CNN). Training parameters for each CNN included tile size, resolution, the amount of annotated training data, the number of convolutional layers per CNN, epochs trained, and error against the training data. Error formulas are provided in Formulas 1 and 2.

Nineteen cases were registered as ‘unscorable’ by the algorithm. In 11 cases, this was due to poor scanning quality and the WSI being out of focus (partly or completely). In five cases, there were severe artefacts, which had not been included in the training set and made the WSI difficult to score for the algorithm (Figure S3A) In both of the two remaining slides, the tumour was strongly dis cohesive, falling apart in such small parts that it resembled cytology, which was not included in the training set. In these cases, the algorithm did not correctly identify all of the tumour cells and counted <100 tumour cells (Figure S3B). One hundred and twenty cases remained for algorithm validation.

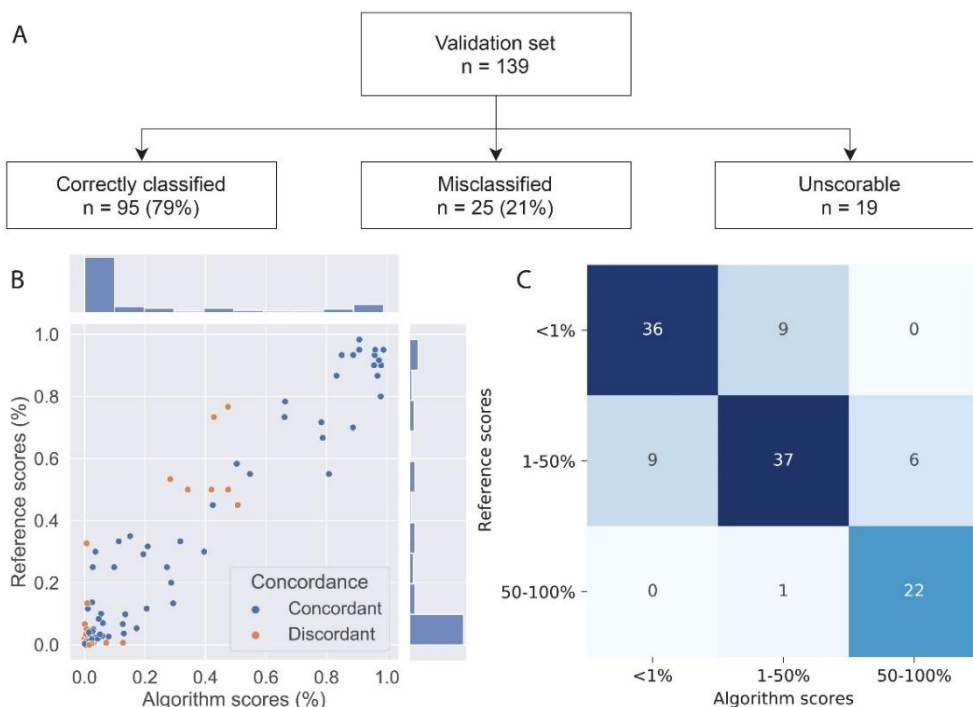


**Figure 5:** Algorithm validation set results. *A*, Flowchart for the validation process. *B*, Scatterplot for the mean of the three pathologists' continuous tumour proportion scores (TPSs): the reference score (Formula 2 in Doc. S1) is on the y-axis, and the continuous algorithm score is on the x-axis. *C*, Confusion matrix for categorical TPSs (<1%, 1–49%, and 50–100%): the reference score categories are on the y-axis, and the algorithm score categories are on the x-axis.

For cases scored <0.5% by the algorithm ( $n = 32$ ), the concordance with the reference score was 94%. For cases scored >60% by the algorithm ( $n = 20$ ), the concordance with the reference score was 100%. The cases with scores of <0.5% and >60% constituted 43% of the validation set ( $n = 52$ ). Examples of algorithm applicability for both the 'difficult' cases (TPS of 0.5–60%) and the 'easy' cases are provided in Figure 7 and Figures S4–S6.

#### 4.5.5 Explaining discordance

On closer examination of the cases that were misclassified by the algorithm (orange dots; Figure 5B), it is clear that, in 20 of 25 misclassified cases (80%), the pathologists were also in disagreement, meaning that one of the pathologists scored the case in a different treatment category. This occurred

significantly more frequently than in the cases that were correctly classified by the algorithm (27%,  $P = 0.000003$ , Fisher's exact test), which suggests that these cases were more difficult to score for both human and machine. Common features in the misclassified cases included the following:

1. The reference score was close to the 1% or 50% cutoff point.
2. Neoplastic tissue was surrounded or infiltrated by PD-L1-positive immune cells (Figure 6A,D.)
3. Neoplastic cells stained for PD-L1, but the staining was non-membranous (Figure 6B).
4. Neoplastic cells stained for PD-L1, but the entire membrane did not stain positively (incomplete staining) (Figure 6C).
5. Neoplastic cells stained for PD-L1, but with low intensity (Figure 6C).
6. There were severe artefacts, including anthracosis, folds, ink, degeneration, preservation-related issues, and scanning-related issues (Figure 6B).
7. A small number (<250) of neoplastic cells were available for scoring.

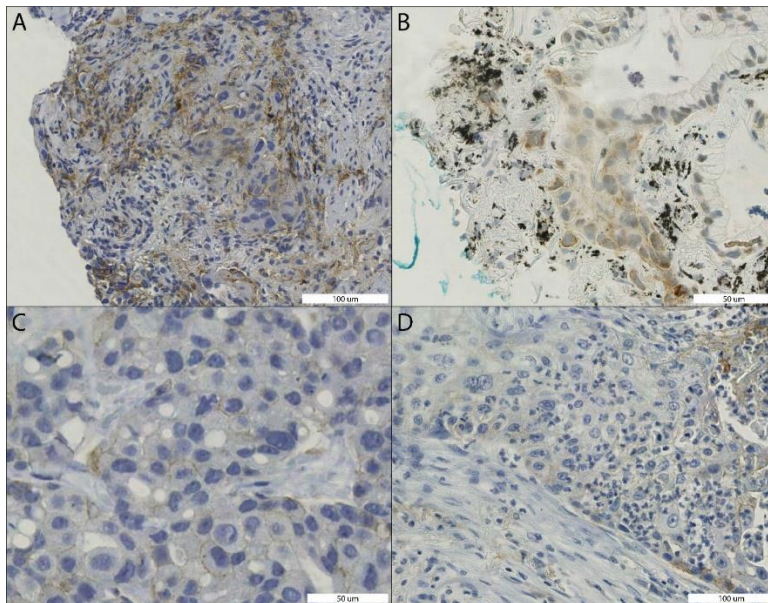


**Figure 6:** Difficult-to-score features. A, Neoplastic tissue surrounded by benign programmed death-ligand 1 (PD-L1)-positive cells. B, PD-L1 staining in neoplastic cells: partly nuclear, partly cytoplasmic, and partly membranous (anthracosis and

ink). C, Low-intensity PD-L1 staining. D, PD-L1-positive immune cells infiltrating neoplastic tissue.

The misclassified cases were not significantly different from the correctly classified cases with regard to tumour type ( $P = 0.5$ , chi-squared test), biopsy site ( $P = 0.4$ , chi-squared test), or PD-L1 TPS category ( $P = 1.0$ , chi-squared test).

#### 4.5.6 Visual algorithm feedback

The algorithm provides detailed visual feedback of predictions, at both the whole slide level and the microscopic level. The cell counting aspect of the algorithm enables exact approximation of the TPS, whereas, obviously, pathologists can only give a rough estimate. A case example is shown in Figure 7. Additional case examples are shown in Figures S4–S6.

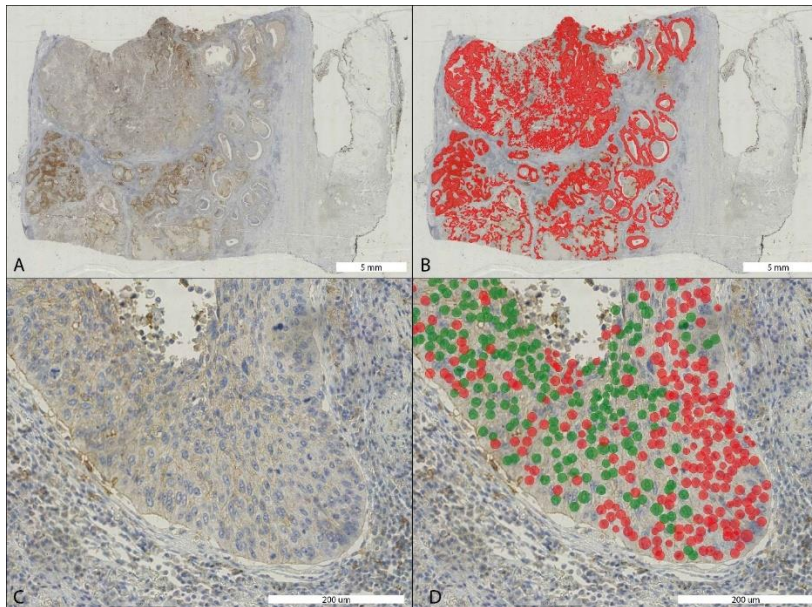


**Figure 7:** Case example algorithm scoring of a 'difficult' case close to the 50% cutoff. A, A programmed death-ligand 1 (PD-L1)-stained lobectomy slide overview of a squamous cell carcinoma. B, Prediction from convolutional neural network (CNN) 3 (neoplastic area segmentation). Red: neoplastic tissue. C, Representative close-up. D, Prediction from CNN4 (cell detection). Red: PD-L1-negative cell. Green: PD-L1-positive cell. In total, the algorithm counted 98 235 PD-L1-positive cells and 118 604 PD-L1-negative cells in this whole slide image, resulting in a tumour proportion

score of 45.3%. The pathologists scored this case at 30%, 60%, and 45%, respectively. The reference score was therefore 45%.

#### 4.5.7 Segmentation refinement

Our algorithm utilises two sequential segmentation CNNs for neoplastic tissue detection. The first CNN (coarse CNN) has a tile size of 200  $\mu\text{m}$ , whereas the subsequent CNN (refinement CNN) has a tile size of 50  $\mu\text{m}$ . An example of this setup is outlined in Figure 8. Adding the refinement CNN reduces the error against the training data from 0.49% to 0.15%, which constitutes a 3.3-fold decrease (Table 3). This approach therefore improves the predictions and decreases the required amount of annotations, as both segmentation CNNs utilise the same set of annotations. The added benefit of this approach was especially clear in cases with small patches of neoplastic tissue, as shown in Figure 8.

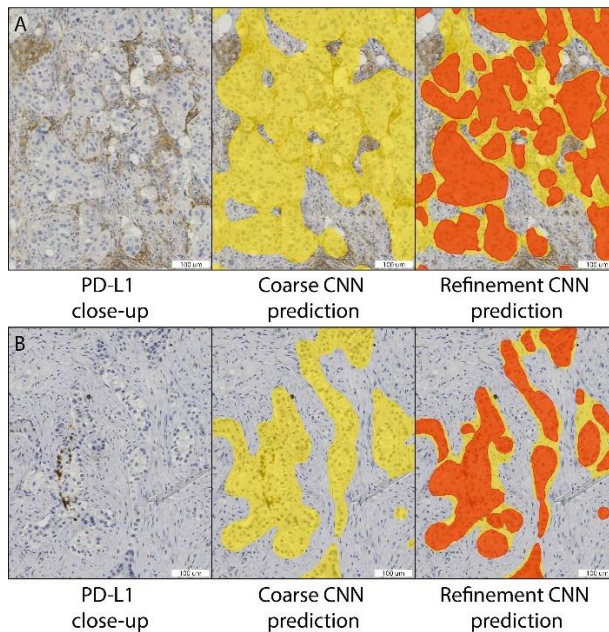


**Figure 8:** Segmentation refinement examples. Left: programmed death-ligand 1 (PD-L1)-stained tissue. Middle: overlay predictions (yellow) from the first neoplastic segmentation convolutional neural network (CNN) (coarse CNN). Right: overlay predictions from the first (yellow) and second (red) neoplastic segmentation CNNs (refinement CNNs). In case A (negative tumour cells with closely associated positive immune cells), use of only the coarse CNN would have resulted in falsely counting

*more PD-L1-positive cells, and potentially a higher tumour proportion score (TPS) (false-positive). In case B (negative cells in negative stroma), using only the coarse CNN would have resulted in falsely counting more PD-L1-negative cells, and potentially a lower TPS (false-negative).*

## **4.6 Discussion**

The PD-L1 TPS is an established biomarker, with direct treatment consequences for late-stage NSCLC patients. However, PD-L1 as a biomarker for response to immunotherapy has several drawbacks, the most important being the high interobserver and intraobserver variance around rigid cutoff points (at 1% and 50%), and the fact that negative patients may also respond (and vice versa). Although a more definitive solution for a more accurate prediction of response to immunotherapy is still a subject of research, some of the human factors leading to high interobserver and intraobserver variance may be solved by the use of computational PD-L1 scoring. Several attempts have been made to create PD-L1 scoring algorithms, but all have specific limitations that hamper robust translation into clinical practice.

We therefore developed and validated a fully supervised deep learning algorithm for computational PD-L1 scoring, which gives scores concordant with the reference score in 79% of cases, whereas any two pathologists agree with each other in 75% of cases. Cohen's  $\kappa$  coefficient for the algorithm is 0.68 and the intraclass coefficient is 0.96; respectively, these constitute 'substantial' to 'almost perfect' agreement, and are close to the agreement rates between the three experienced thoracic pathologists in this study.

An additional strength of our algorithm is that it provides detailed visual whole-slide predictions at a microscopic level, owing to the fully supervised setup of the model. This feedback increases interpretability and explainability, which is an important criterion for algorithms that will be used by pathologists in a clinical setting.

We believe that—in order to be of value in daily clinical practice—any algorithm should be designed with cases derived from routine diagnostic WSIs, as opposed to 'perfect' trial material [14, 15] or TMAs. [16] Our algorithm is trained and validated on routine diagnostic whole slide histological material, including a wide range of metastatic sites and tissue artefacts. Because of its deep learning-based nature, the algorithm performs well in the highly

heterogeneous tissue backgrounds in WSIs (artefacts, lymph nodes, bronchial epithelium, adrenal gland, skin, brain, bone, kidney, etc.), which requires extensive annotations and is not easily achieved with simpler machine learning approaches. [16] For validation, algorithm scores were compared with the scores of multiple observers, which is essential because the reference score needs to be as robust as possible. It must be noted that our  $\kappa$  coefficient for pathologist agreement is relatively low as compared with those in some PD-L1 interobserver studies using trial material or TMAs, [14, 15] but is in line with those in other studies with similar broad inclusion criteria. [10]

Given the described accuracy and clinical applicability of our model, one may think of two different areas of usage: (i) PD-L1 scoring in a (case-by-case) diagnostic setting; and (ii) PD-L1 scoring of trial material and/or large series in a research environment. In a diagnostic setting, we see this algorithm as a potential 'scoring assistant' or second-opinion tool, aiding and saving time for pathologists, especially in difficult cases. In a situation in which scoring of large series or trial material is required, this algorithm may stand alone in the scoring of 'easy' cases with  $<0.5\%$  or  $>60\%$  PD-L1 positivity, as the algorithm reaches an accuracy of 96%. A pathologist could then focus on the subset of difficult cases with PD-L1 scores between 0.5% and 60%. A second observer pathologist may be replaced by our algorithm. Overall, our PD-L1 algorithm will function mostly as a scoring assistant or second observer, thereby saving time and human effort, while remaining equally accurate.

Although the implementation of this and other algorithms in daily clinical practice is imminent, the applicability of this algorithm is likely to be hampered by domain divergence (different scanners, different antibodies, different stainings, etc.). When this algorithm is used in a new laboratory, or when laboratory circumstances change, 'domain adaptation' (adapting the algorithm to the same task but in a new dataset) is required.

The difficulty of the domain adaptation process and the choice of a method of adapting is heavily dependent on the domain relatedness (or the measure of domain divergence), which is a subject of ongoing research in the field of computer vision. Domain adaptation can be performed in many different ways (shallow adaptation, deep supervised adaptation, adversarial adaptation, semisupervised adaptation, domain matching, etc.). [27, 28]

Histopathology articles describing the process of domain adaptation in computational pathology are mostly lacking. We consider this to be a potential drawback. Clear guidelines for 'domain adaptation' and 'post-implementation monitoring' will need to be established in the near future. This issue will therefore be the subject of future research, in which we will use this PD-L1 algorithm for a nationwide PD-L1 domain adaptation study.

Another future research challenge for the field of PD-L1 assessment and digital pathology is its application in cytology. In cytology specimens, there is substantially less tissue context, and the task of PD-L1 TPS assessment is therefore different and perhaps more difficult. Despite these challenges, it is often necessary to use cytology material for PD-L1 analysis in clinical practice when no histology material is available, which is the case in up to 40% of cases.<sup>9</sup> Our algorithm is not applicable to, and is not easily transferrable to, cytology specimens; a separate algorithm would have to be developed for this purpose. This algorithm would need to take the different cytological backgrounds and common cell types such as mesothelial cells, macrophages and (fragments of) lymphoid tissue into account.

In conclusion, we have developed a deep learning PD-L1 TPS algorithm that is truly applicable to daily routine whole slide specimens. State-of-the-art computational techniques such as the double segmentation CNN and the HAIL annotations worked synergistically with the clinical perspective of highly experienced thoracic pathologists in this study, and resulted in the first PD-L1 algorithm that is accurate on routine diagnostic material, in all tissue contexts, and on WSIs. In order to create smart pathology-based deep learning algorithms that are actually meaningful for the patients and clinicians of tomorrow, a true alliance of both clinical and computational experts is crucial.

## References

1. Bray F, Ferlay J, Soerjomataram I, et al., Global cancer statistics 2018: GLOBOCAN estimates of incidence and mortality worldwide for 36 cancers in 185 countries. *CA Cancer J Clin* 2018; **68**; 394–424.
2. Howlader N, Noone AM, Krapcho M, et al., *SEER Cancer Statistics Review, 1975–2016*. Bethesda, MD: National Cancer Institute, 2019.
3. Dong H, Strome SE, Salomao DR, et al., *Tumor-associated B7-H1 promotes T-cell apoptosis: a potential mechanism of immune evasion*. *Nat Med* 2002; **8**; 793–800.
4. Gettinger S, Rizvi NA, Chow LQ, et al., *Nivolumab monotherapy for first-line treatment of advanced non-small-cell lung cancer*. *J Clin Oncol* 2016; **34**; 2980–2987.
5. Gandhi L, Rodriguez-Abreu D, Gadgeel S, et al., *Pembrolizumab plus chemotherapy in metastatic non-small-cell lung cancer*. *N Engl J Med* 2018; **378**; 2078–2092.
6. Garon EB, Rizvi NA, Hui R, et al., *Pembrolizumab for the treatment of non-small-cell lung cancer*. *N Engl J Med* 2015; **372**; 2018–2028.
7. Doroshov DB, Bhalla S, Beasley MB, et al., *PD-L1 as a biomarker of response to immune-checkpoint inhibitors*. *Nat Rev Clin Oncol* 2021; **18**; 3345–362.
8. Langer CJ, Gadgeel SM, Borghaei H, et al., *Carboplatin and pemetrexed with or without pembrolizumab for advanced, non-squamous non-small-cell lung cancer: a randomised, phase 2 cohort of the open-label KEYNOTE-021 study*. *Lancet Oncol*. 2016; **17**; 1497–1508.
9. Cohen D, Hondelink LM, Solleveld-Westerink N, et al., *Optimizing mutation and fusion detection in NSCLC by sequential DNA and RNA sequencing*. *J Thorac Oncol* 2020; **15**; 1000–1014.
10. Cooper WA, Russell PA, Cherian M, et al., *Intra- and interobserver reproducibility assessment of PD-L1 biomarker in non-small cell lung cancer*. *Clin Cancer Res* 2017; **23**; 4569–4577.
11. Simons KH, de Jong A, Jukema JW, et al., *T cell co-stimulation and co-inhibition in cardiovascular disease: a double-edged sword*. *Nat Rev Cardiol* 2019; **16**; 325–343.
12. Chen R, Hou X, Yang L, et al., *Comparative efficacy and safety of first-line treatments for advanced non-small cell lung cancer with immune checkpoint inhibitors: a systematic review and meta-analysis*. *Thorac Cancer* 2019; **10**; 607–623.
13. Inge LJ, Dennis E, *Development and applications of computer image analysis algorithms for scoring of PD-L1 immunohistochemistry*. *IOTECH* 2020; **6**; 2–8.
14. Widmaier M, Wiestler T, Walker J, et al., *Comparison of continuous measures across diagnostic PD-L1 assays in non-small cell lung cancer using automated image analysis*. *Mod Pathol* 2020; **33**; 380–390.

15. Kapil A, Meier A, Zuraw A, et al., *Deep semi supervised generative learning for automated tumor proportion scoring on NSCLC tissue needle biopsies*. Sci Rep 2018; **8**; 17343.
16. Taylor CR, Jadhav AP, Gholap A, et al., *A multi-institutional study to evaluate automated whole slide scoring of immunohistochemistry for assessment of programmed death-ligand 1 (PD-L1) expression in non-small cell lung cancer*. Appl Immunohistochem Mol Morphol 2019; **27**; 263–269.
17. Lutnick B, Ginley B, Govind D, et al., *An integrated iterative annotation technique for easing neural network training in medical image analysis*. Nat Mach Intell 2019; **1**; 112–119.
18. Smith MA, Westerling-Bui T, Wilcox A, et al., *Screening for bone marrow cellularity changes in cynomolgus macaques in toxicology safety studies using artificial intelligence models*. Toxicol Pathol 2021; **49**; 905–911.
19. Bédard A, Westerling-Bui T, Zuraw A. *Proof of concept for a deep learning algorithm for identification and quantification of key microscopic features in the murine model of DSS-induced colitis*. Toxicol Pathol 2021; **49**; 897–904.
20. Butter R, Hart NA, Hooijer GKJ, et al., *Multicentre study on the consistency of PD-L1 immunohistochemistry as predictive test for immunotherapy in non-small cell lung cancer*. J Clin Pathol 2020; **73**; 423.
21. Chang S, Park HK, Choi Y-L, et al., *Interobserver reproducibility of PD-L1 biomarker in non-small cell lung cancer: a multi-institutional study by 27 pathologists*. J Pathol Transl Med 2019; **53**; 347–353.
22. Ratcliffe MJ, Sharpe A, Midha A, et al., *Agreement between programmed cell death ligand-1 diagnostic assays across multiple protein expression cutoffs in non-small cell lung cancer*. Clin Cancer Res 2017; **23**; 3585–3591.
23. Rimm DL, Han G, Taube JM, et al., *A prospective, multi-institutional, pathologist-based assessment of 4 immunohistochemistry assays for PD-L1 expression in non-small cell lung cancer*. JAMA Oncol 2017; **3**; 1051–1058.
24. Scheel AH, Dietel M, Heukamp LC, et al., *Harmonized PD-L1 immunohistochemistry for pulmonary squamous-cell and adenocarcinomas*. Mod Pathol 2016; **29**; 1165–1172.
25. Williams GH, Nicholson AG, Snead DRJ, et al., *Interobserver reliability of programmed cell death ligand-1 scoring using the VENTANA PD-L1 (SP263) assay in NSCLC*. J Thorac Oncol 2020; **15**; 550–555.
26. Brunnström H, Johansson A, Westbom-Fremer S, et al., *PD-L1 immunohistochemistry in clinical diagnostics of lung cancer: inter-pathologist variability is higher than assay variability*. Mod Pathol 2017; **30**; 1411–1421.
27. Wilson G, and Cook DJ. *A survey of unsupervised deep domain adaptation*. ACM Trans Intell Syst Technol 2020; **11**; 51.

28. Wang M, Deng W. *Deep visual domain adaptation: a survey*. Neurocomputing 2018; **312**; 135–153.







**CHAPTER 5**

**NTRK IMMUNOHISTOCHEMISTRY**

## Chapter 5: NTRK immunohistochemistry

### 5.1 Title page

Title: The sensitivity of pan-TRK immunohistochemistry in solid tumors: a meta-analysis.

Short running title: Sensitivity of pan-TRK immunohistochemistry

*Published in: European Journal of Cancer, 2022. DOI: 10.1016/j.ejca.2022.06.030*

### 5.1.1 Authors

Liesbeth M. Hondelink, Anne M.R. Schrader, Golzar Asri Aghmuni, Nienke Solleveld-Westerink, Anne-Marie Cleton-Jansen, Demi van Egmond, Arnoud Boot, Sarah Ouahoud, Midia N. Khalifa, Suk Wai Lam, Hans Morreau, Judith V.M.G. Bovee, Tom van Wezel\* & Danielle Cohen\*

### 5.1.2 Affiliations

Department of Pathology, Leiden University Medical Center (LUMC), the Netherlands

\*: both authors contributed equally

### 5.1.4 Acknowledgement:

We thank Inge Briaire-De Bruijn and Marinka Verhoeven for their sharing their expertise in immunohistochemistry with us and assisting us with performing pan-TRK immunohistochemical staining. We thank professor Vincent Smit for enabling this research and the molecular diagnostics at the department of Pathology.

## 5.2 Abstract

### 5.2.1 Introduction

Since the approval of neurotrophic tropomyosin receptor kinase (NTRK) tyrosine kinase inhibitors for first-line advanced stage pan-cancer therapy, pathologists and molecular biologists have been facing a complex question: how should the large volume of specimens be screened for NTRK fusions? Immunohistochemistry is fast and cheap, but the sensitivity compared to RNA NGS is unclear.

### 5.2.2 Methods

We performed RNA-based next-generation sequencing on 1,329 cases and stained 24 NTRK-rearranged cases immunohistochemically with pan-TRK (ERP17341). Additionally, we performed a meta-analysis of the literature. After screening 580 studies, 200 additional NTRK-rearranged cases from 13 studies, analysed with sensitive molecular diagnostics as well as pan-TRK IHC, were included.

### 5.2.3 Results

In the included 224 NTRK-rearranged solid tumours, the sensitivity for pan-TRK IHC was 82% and the false-negative rate was 18%. NTRK3 fusions had more false negatives (27%) compared to NTRK1 (6%) and NTRK2 (14%) ( $p = 0.0006$ ). Membranous, nuclear and peri-nuclear staining patterns strongly correlated with different fusion products, with membranous staining being more prevalent in NTRK1 and NTRK2, nuclear in NTRK3, and perinuclear in NTRK1.

### 5.2.4 Conclusion

Despite a reduction in the number of molecular analysis, using pan-TRK immunohistochemistry as a prescreening method to detect NTRK fusions in solid tumours will miss 18% of all NTRK-fused cases (especially involving NTRK3). Therefore, the most comprehensive and optimal option to detect NTRK fusions is to perform molecular testing on all eligible cases. However, in case of financial or logistical limitations, an immunohistochemistry-first approach is defensible in tumours with a low prevalence of NTRK fusions.

## 5.3 Introduction

Neurotrophic tropomyosin receptor kinase (NTRK) fusions are powerful oncogenic drivers, which are common in rare tumour types, e.g., infantile fibrosarcoma and secretory breast cancer, but rare (with prevalence estimates below 1%) in some common tumours, e.g., lung adenocarcinoma and colorectal carcinoma. [1, 2]

In recent clinical trials, a remarkable survival benefit of NTRK tyrosine kinase inhibitors (TKIs) was observed, with high response rates and durable, long-term progression-free survival in patients with NTRK-rearranged cancers. [3-6] Therefore, NTRK TKIs have been approved for first-line treatment in all NTRK-rearranged advanced stage cancers. This approval is independent of cancer type, making NTRK one of the first tumour-agnostic targets. [7, 8]

In addition, several tumour types, such as Spitz tumours and secretory carcinoma, are (in part) characterised by the presence of NTRK fusions. Without the ability to sensitively detect NTRK fusions in diagnostics, patients with these tumour types could end up with the wrong diagnosis and – in selected cases – even suboptimal treatment.

The gold standard for fusion detection is targeted RNA-based next-generation sequencing (RNA NGS) or whole genome sequencing (WGS), but these molecular techniques are expensive and time-consuming and have limited worldwide accessibility. [9] As an alternative, pan-TRK immunohistochemistry (IHC) with the ERP17341 antibody (Abcam) has been investigated as a potential screening tool, as it is much faster, has lower costs, and is more widely available than molecular diagnostics. [10]

Several recent studies report that pan-TRK IHC screening is a reliable alternative for molecular analysis. [11-13] However, other studies report a problematic false-negative rate over 15%, [14-18] potentially leading to underdetection. However, due to the overall low prevalence of NTRK fusions in solid tumours, most studies included only a limited number of NTRK-rearranged cases, which makes that robust recommendations for using pan-TRK IHC as a screening method for the detection of NTRK fusions are lacking. [11-24]

In this study, we describe a cohort of 1329 solid tumours that were analysed for NTRK fusions with anchored multiplex PCR (AMP)-based targeted RNA NGS in routine diagnostics in our institution. In addition, we performed a meta-analysis for studies comparing pan-TRK IHC with molecular analysis for the detection of NTRK fusions. The aim of our study was to robustly describe the sensitivity and false-negative rate of pan-TRK IHC, in order to make a well-considered choice on the use of pan-TRK IHC as a screening tool for NTRK fusions in solid tumours in the clinical setting.

## **5.4 Materials and methods**

### 5.4.1 Case selection

We retrospectively analysed all solid tumours that routinely underwent anchored multiplex (AMP)-based targeted RNA NGS among others for NTRK1, NTRK2, and NTRK3 gene fusions in the Leiden University Medical Center (LUMC), Leiden, the Netherlands, between 2008 and 2021. All solid tumour types were eligible for inclusion, irrespective of malignant, borderline malignant, or benign diagnosis. Cases in which RNA NGS analyses were incomplete or failed, e.g., due to insufficient tissue, were excluded. There is an overrepresentation of radioactive iodine-insensitive thyroid carcinomas and driver-negative lung and colorectal carcinomas, since these cases were more frequently submitted for RNA NGS, due to a high quantity of referrals of these cancers to the LUMC. Cases were screened for therapeutic reasons (NTRK TKI treatment), diagnostic reasons (e.g. differential diagnosis of Spitz tumours with spitzoid melanoma), or both.

The study was performed according to the Dutch FEDERA Code for Proper Use of Human Tissue. A waiver of consent was given by the Leiden-the Hague-Delft Medical Ethical Committee (B20.017). Cases were anonymised completely before processing, omitting the need to obtain informed consent from the included patients.

### 5.4.2 Fusion analysis

For NTRK fusion analysis, RNA was isolated from formalin-fixed paraffin-embedded (FFPE) tissue by microdissection using five 10 µm slides and extracted using a tissue preparation system robot (Siemens). AMP-based-targeted RNA NGS was performed with the ArcherDx assay, with either the

Comprehensive Thyroid and Lung panel, the Solid Tumors panel, or the Sarcoma v2 panel, which all cover the complete NTRK1, NTRK2, and NTRK3 genes and are validated according to the NEN-EN-ISO15189 guidelines. This method is capable of detecting fusions with either a novel or unknown fusion partner by using gene-specific primers in conjunction with molecular barcoded adapters. The generated libraries were sequenced on the IonTorrent S5 platform (Thermo Fisher Scientific, Canada). Analysis was performed using a local installation of the Archer Analysis software. Different versions (ranging from version 5.1.7 to version 6.2.3) were used. NGS library generation, analysis, and reporting were performed under ISO15189 accreditation in the molecular diagnostics section of the pathology department (LUMC).

#### 5.4.3 Immunohistochemistry

For the purpose of this study, pan-TRK IHC was performed on cases with a confirmed NTRK fusion by RNA NGS. For IHC, 4- $\mu$ m-thick slides were cut from the FFPE tissue blocks of histological biopsies or resection specimens and automatically stained with the pan-TRK monoclonal antibody clone EPR17341 (Abcam, Cambridge, MA) on the Dako Omnis stainer, in a 1:50 dilution. [4] A subset of cases was stained manually, with the same antibody in a 1:150 dilution. Cases with insufficient FFPE tissue were excluded.

The pan-TRK IHC was independently scored by two pathologist (DC and AS) and discordant cases were discussed until consensus was reached. Cases were considered positive when staining of any pattern and intensity was seen in more than 1% of the tumour cells. In addition, for each positive case, the staining pattern was determined: cytoplasmatic, nuclear, membranous, or a combination of  $\geq 2$  patterns. In case of multiple staining patterns in the same slide, the case was included in both staining categories.

#### 5.4.4 Meta-analysis

In addition, we performed a meta-analysis of the literature to evaluate the sensitivity and false-negative rate of pan-TRK IHC as a screening method for NTRK fusions, using the PRISMA criteria. [25] We searched PubMed on June 19, 2021, with the search term included in Supplement 1. First selection existed of title and abstract screening by LH. Second selection existed of full text screening of the resulting articles by LH.

All studies comprising five or more unique cases of solid tumours that were evaluated with pan-TRK IHC with the monoclonal antibody clone EPR17341 as well as a molecular diagnostics test with high sensitivity for the detection of NTRK fusions were included in our analysis. Suitable molecular techniques included targeted RNA NGS, whole genome sequencing (WGS), DNA-based NGS panels with good coverage of the NTRK1, NTRK2, and NTRK3 introns and fluorescence in situ hybridisation (FISH) for the NTRK1, NTRK2, and NTRK3 genes, as these molecular tests are known to have high sensitivity and specificity. [26, 27] Additionally, studies in which cases were prescreened with Nanostring and, when positive, confirmed with one of the aforementioned molecular techniques, were also included. Studies in which pan-TRK IHC was used as a screening tool to select cases for molecular analysis were excluded, as these studies might introduce a selection bias with regard to the sensitivity and false-negative rate. Studies written in another language than English and harmonisation studies were excluded.

Based on the included studies, we constructed a database for each case listing the diagnosis, type of molecular analysis used, molecular analysis results, fused NTRK gene and breakpoint (when available), fusion partner and breakpoint (when available), and pan-TRK IHC result and staining pattern (when available). Our own cohort of NTRK-fused cases was added to this database.

#### 5.4.5 Statistics

Statistical analysis was performed using IBM SPSS Statistical software, version 26. Statistical significance was set at a P-value of <0.05.

## 5.5 Results

### 5.5.1 Case characteristics

In total, we included 1329 cases on which RNA NGS was routinely performed. This cohort included 738 lung and thoracic tumours, 190 thyroid carcinomas, 82 digestive tract tumours, 68 bone and soft tissue tumours, 65 carcinomas of unknown primary, 66 head and neck tumours, 52 central nerve system tumours, 32 melanocytic tumours, 18 urogenital tumours, nine breast cancers, and nine other lesions (Table 1). RNA NGS was performed for diagnostic purposes in 69 cases, therapeutic purposes in 960 cases, and for both

diagnostic and therapeutic purposes in 300 cases. In 751 cases that were analysed for therapeutic purposes, mainly colorectal carcinomas and lung adenocarcinomas, previous DNA NGS was performed without identification of a driver mutation. In 347 cases, a strong driver mutation, such as KRAS or EGFR, was identified in DNA NGS. In all other cases, DNA NGS was not performed.

DIAGNOSIS GROUP OR TRACTUS	INCLUDED CASES	NTRK FUSIONS	NTRK1	NTRK2	NTRK3	SENSITIVITY
LUNG AND THORAX	738	2 (0.3%)	0	0	2	50%
THYROID	190	12 (6.3%)	2	0	10	75%
DIGESTIVE TRACT	82	2 (2.4%)	1	0	1	100%
SARCOMA	68	2 (2.9%)	1	0	1	100%
CARCINOMA OF UNKNOWN PRIMARY	65	0	0	0	0	-
HEAD AND NECK	66	4 (6.1%)	0	0	4	100%
CENTRAL NERVE SYSTEM	52	0	0	0	0	-
SKIN	32	4 (12.5%)	0	1	3	75%
UROGENITAL TRACT	18	0	0	0	0	-
BREAST	9	1 (11.1%)	0	0	1	100%
OTHER	9	0	0	0	0	-
<b>TOTAL</b>	<b>1329</b>	<b>27 (2.0%)</b>	<b>4</b>	<b>1</b>	<b>22</b>	<b>79%</b>

**Table 1:** Overview of all included solid tumor types including the NTRK-fusion prevalence.

### 5.5.2 Fusion analysis

Using RNA NGS, 27 of the 1329 (2%) cases demonstrated an NTRK gene fusion. These cases comprised the NTRK1 gene in four (15%) cases, the NTRK2 gene in one (4%) case, and the NTRK3 gene in 22 (81%) cases (Figure 1). NTRK1 was fused with TPM3 in three cases (mismatch repair deficient colorectal carcinoma, spindle cell sarcoma, and thyroid carcinoma) and with TPR in one case (thyroid carcinoma). The NTRK2 fusion occurred in a Spitz nevus with SQSTM1 as the fusion partner. The NTRK3 fusions most frequently involved ETV6 (17 cases: nine thyroid cancers, four secretory carcinomas, one breast

cancer NST, one inflammatory myofibroblastic tumour, one lung adenocarcinoma, and one Spitz nevus). Additionally, we observed two MYO5A:NTRK3 fusions (Spitz nevi), two EML4:NTRK3 fusions (mismatch repair proficient colorectal carcinoma and thyroid carcinoma), and one SYNJ1:NTRK3 fusion (lung adenocarcinoma).

A	B			C
Colorectal carcinoma	TPM3	e6	e10 NTRK1	membranous
Spindle cell sarcoma	TPM3	e8	e10 NTRK1	cytoplasmic
Thyroid carcinoma (pap)	TPM3	e8	e12 NTRK1	cytoplasmic and membranous
Thyroid carcinoma (foll)	TPR	e21	e10 NTRK1	negative
Spitz nevus	SQSTM1	e5	e16 NTRK2	cytoplasmic
Thyroid carcinoma (pd)	ETV6	e4	e13 NTRK3	cytoplasmic
Thyroid carcinoma (pap)	ETV6	e4	e13 NTRK3	cytoplasmic
Thyroid carcinoma (pap)	ETV6	e4	e13 NTRK3	cytoplasmic
Thyroid carcinoma (pap)	ETV6	e4	e13 NTRK3	negative
Thyroid carcinoma (pap)	ETV6	e4	e14 NTRK3	cytoplasmic
Thyroid carcinoma (pap)	ETV6	e4	e14 NTRK3	cytoplasmic
Thyroid carcinoma (pap)	ETV6	e4	e14 NTRK3	cytoplasmic
Thyroid carcinoma (pap)	ETV6	e4	e14 NTRK3	cytoplasmic
Thyroid carcinoma (pap)	ETV6	e4	e14 NTRK3	cytoplasmic
Thyroid carcinoma (foll)	ETV6	e4	e14 NTRK3	negative
Secretory carcinoma	ETV6	e5	e15 NTRK3	cytoplasmic and nuclear
Secretory carcinoma	ETV6	e5	e15 NTRK3	nuclear
Secretory carcinoma	ETV6	e5	e15 NTRK3	cytoplasmic and nuclear
Secretory carcinoma	ETV6	e5	e15 NTRK3	cytoplasmic and nuclear
Breast cancer NST	ETV6	e5	e15 NTRK3	nuclear
IMT	ETV6	e5	e15 NTRK3	
Lung adenocarcinoma	ETV6	e4	e14 NTRK3	
Spitz nevus	ETV6	e4	e14 NTRK3	cytoplasmic
Spitz nevus	MYO5A	e32	e13 NTRK3	negative
Spitz nevus	MYO5A	e23	e14 NTRK3	cytoplasmic
Colorectal carcinoma	EML4	e2	e13 NTRK3	cytoplasmic
Thyroid carcinoma (foll)	EML4	e2	e14 NTRK3	
Lung adenocarcinoma	SYNJ1	e4	e16 NTRK3	negative

**Figure 1:** Overview of all NTRK-fused cases in our cohort, arranged by diagnosis (A), fusion product including breakpoints (B), and pan-TRK immunohistochemical staining pattern (C). In three cases, immunohistochemistry was not performed due to tissue unavailability. Breast cancer NST: breast cancer no special type, IMT:

*inflammatory myofibroblastic tumor, pap: papillary type, foll: follicular type, pd: poorly differentiated type.*

### 5.5.3 Immunohistochemistry

In 24 of the 27 (89%) NTRK-fused cases, pan-TRK IHC was successfully performed. In three cases, insufficient tissue was available for pan-TRK IHC. Nineteen (79%) of the successfully stained cases scored positive. Positive staining consisted of cytoplasmatic staining in 12 (63%) cases, nuclear staining in two (11%) cases, membranous staining in one (5%) case, combined cytoplasmatic and nuclear staining in three (16%) cases, and combined cytoplasmatic and membranous staining in one (6%) case (Figure 2). The two observers were concordant in 100% of the cases. Benign neural tissue stained positive for pan-TRK as well as some macrophages.

Five (21%) of the 24 NTRK-fused cases were completely negative with pan-TRK IHC (Figure 2). This false negativity was observed in 4 of 19 (21%) NTRK3-fused cases and in one of four (25%) NTRK1-fused cases. The negative cases included a lung carcinoma with a SYNJ1:NTRK3 fusion, a Spitz nevus with a MYO5A:NTRK3 fusion, and three thyroid carcinomas, two with ETV6:NTRK3 fusions, and one with a TPR:NTRK1 fusion. Overall, the sensitivity of pan-TRK IHC in our cohort was 79%, and the false-negative rate was 21%. This indicates that when using pan-TRK IHC as a screening method, 21% of NTRK-fused cases in our cohort would have been missed.

### 5.5.4 Meta-analysis

A literature search in PubMed on June 19th 2021 (search strategy in Supplement 1) yielded 580 articles. After first selection, which included removal of duplicates and screening of the title and abstract, 54 articles remained. After second selection, which included assessment of the full-texts of the 54 potentially relevant articles, a total of 13 eligible studies were included in our analysis. [11-21, 23, 28] A flow chart of the selection process of the meta-analysis is presented in Figure 3. An overview of the characteristics of the included studies is provided in Supplement 2. The complete dataset is provided in Supplement 3.

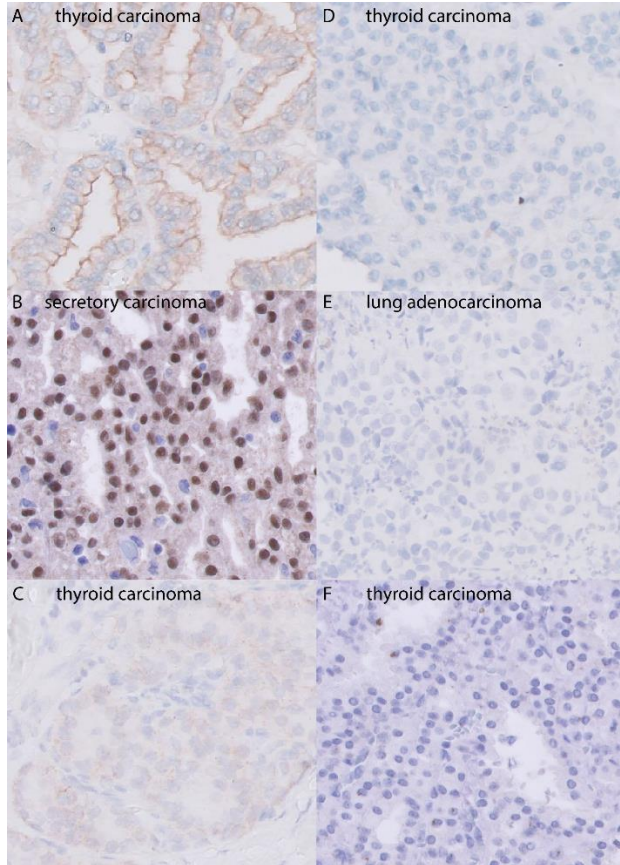


**Figure 2:** Pan-TRK immunohistochemistry with positive (A, B, C) and negative staining (D, E, F). Membranous positivity in thyroid carcinoma with NTRK1 fusion (A), nuclear positivity in a secretory carcinoma in the parotid gland with NTRK3 fusion (B), cytoplasmic positivity in a thyroid carcinoma with NTRK3 fusion (C), pan-TRK negative thyroid carcinoma with NTRK3 fusion (D), pan-TRK negative lung adenocarcinoma with NTRK3 fusion (E), and pan-TRK negative thyroid carcinoma with NTRK1 fusion (F).

The 13 included studies describe the NTRK fusion status of 6609 solid tumours. In 200 (3%) of these cases, an NTRK fusion was detected. When combining these 200 cases with our cohort, the total number of NTRK-fused cases is 224, including 83 (37%) NTRK1 fusions, 21 (9%) NTRK2 fusions, and 120 (54%) NTRK3 fusions. Overall, pan-TRK IHC was positive in 184 of 224 (82%) cases, resulting in a sensitivity of pan-TRK IHC for the detection of NTRK fusions of 82% (Table 2). In 40 of 224 (18%) of the NTRK-fused cases, however, pan-TRK IHC was false

negative. The highest percentage of false negativity with pan-TRK IHC was seen in NTRK3 fusions (27%) compared with NTRK1 (6%) and NTRK2 (14%), which is statistically significant ( $\chi^2$  test, p-value <0.001).

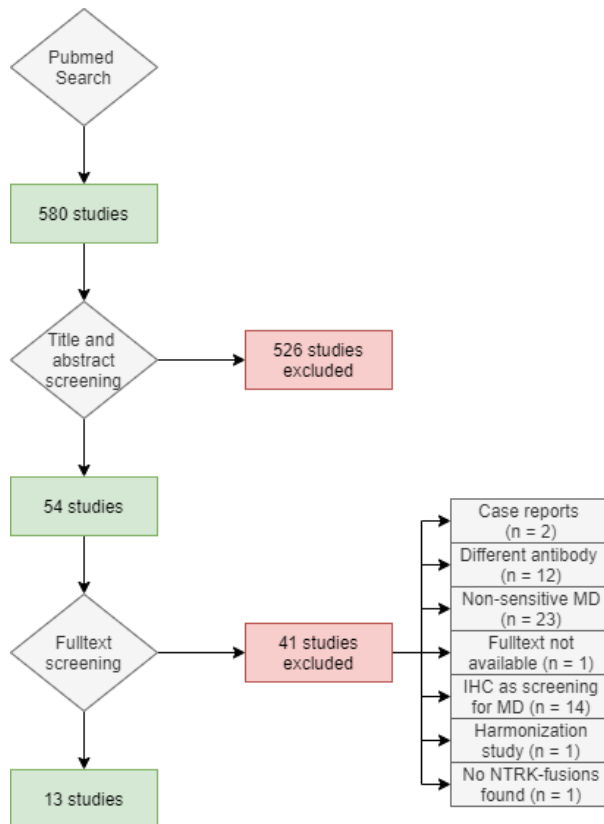


**Figure 3:** Meta-analysis workflow and results.

In the meta-analysis and our own cohort, NTRK fusions did not co-occur with other driver mutations (such as BRAF V600E, KRAS G12C, etc.). The mutual exclusivity of driver mutations in TKI-treatment naive tumours is in line with the literature. [29]

Regarding the staining patterns of pan-TRK IHC, membranous staining was significantly more common in NTRK2-fused cases ( $\chi^2$  test, P-value <0.001), while nuclear staining was associated with NTRK3 fusions ( $\chi^2$  test, P-value <0.001), and perinuclear staining was only seen in NTRK1 fusions ( $\chi^2$  test, P-value <0.001). An overview of the staining patterns is provided in Table 2.

	<i>NTRK1</i> FUSION (N = 83)	<i>NTRK2</i> FUSION (N = 21)	<i>NTRK3</i> FUSION (N = 120)	P-VALUE	ALL <i>NTRK</i> FUSIONS (N = 224)
PAN-TRK IHC	0.0006				
NEGATIVE	5 (6%)	3 (14%)	32 (27%)		40 (18%)
POSITIVE	78 (94%)	18 (86%)	88 (73%)		184 (82%)
STAINING PATTERNS					
CYTOPLASMIC (N = 100)	32 (80%)	5 (71%)	37 (70%)	0.53	74 (74%)
MEMBRANOUS (N = 131)	14 (29%)	4 (44%)	4 (5%)	0.0002	22 (17%)
NUCLEAR (N = 168)	8 (12%)	1 (8%)	45 (51%)	0.0000004	54 (32%)
PERINUCLEAR (N = 122)	12 (24%)	0	0	0.0001	12 (10%)

**Table 2:** Immunohistochemistry results versus molecular diagnostics for 224 *NTRK*-rearranged cases. Pan-TRK IHC had an overall sensitivity of 82% and a false-negative rate of 18%. Staining patterns were significantly different across *NTRK* genes. Studies that did not address the scoring patterns outlined in this table were excluded from part of this table. Some cases displayed multiple staining patterns in the same slide and were scored in both staining categories. P-values are calculated with  $\chi^2$  test.

## 5.6 Discussion

This study describes the sensitivity and false-negative rate of pan-TRK IHC for the detection of *NTRK* fusions in solid tumours, based on our cohort of 24 *NTRK*-fused cases combined with a meta-analysis of literature comprising another 200 *NTRK*-fused cases, in order to make a well-considered choice on the use of pan-TRK IHC as a screening tool for *NTRK* fusions in solid tumours the clinical setting.

This study demonstrates a sensitivity of 82% and a false-negative rate of 18% for pan-TRK IHC with the monoclonal antibody clone EPR17341 (Abcam) to detect *NTRK* fusions in solid tumours. Therefore, using IHC as a screening method and confirming IHC-positive cases with molecular methods (the IHC-first approach) will result in missing 18% of the *NTRK*-fused cases. In the authors opinion, a 'miss rate' of 18% is high, especially in the clinical setting of

NTRK as a therapeutic target, considering the substantial clinical benefit of treatment with NTRK TKIs. The molecular-only approach (omitting IHC) is more sensitive and comprehensive, but will result in a substantial logistical and financial burden for most laboratories, especially in tumour types with a low a priori chance of finding NTRK fusions. Pathologists and molecular biologists will need to consider the 18% miss rate and weigh it against the chance of finding an NTRK fusion and the burden of broad molecular testing in their specific laboratory circumstances, to come to the most optimal NTRK fusion testing for their patient population. The IHC-first approach does miss 18% of targetable fusions but might be a defensible alternative in specific circumstances. Testing is not useful for cases with a known driver mutation, such as KRAS G12C or BRAF V600E, as those are mutually exclusive with NTRK fusions.

False negativity for pan-TRK IHC was correlated to the fused NTRK gene, as it was significantly more common in NTRK3-fused cases (27%) compared with NTRK1 (6%) and NTRK2 (14%) ( $\chi^2$  test, P-value < 0.001). The reason for these significant differences between the NTRK genes is unknown and might be a subject for further research. In order to rule out false negativity in our cohort because of the pan-TRK antibody titration (1:150), we performed a titration experiment on one of the two false-negative ETV6:NTRK3-fused thyroid carcinomas. The neoplastic cells finally stained positive at a dilution of 1:10 but so did the surrounding normal tissue (Supplement 4).

The clinical relevance of pan-TRK IHC-negative NTRK-fused solid tumours with regard to NTRK TKIs is currently unknown. Patients with NTRK-fused tumours who lack IHC expression might have a diminished response compared with IHC-positive patients as a result of limited NTRK gene expression. In our cohort and meta-analysis, follow-up and response data were not available. Therefore, this study is unable to determine whether IHC-negative patients have the same benefit of TKI treatment as IHC-positive patients and this should be a topic of future research.

Despite the analysis of the world-wide literature, a limitation of this study is the relatively small number of confirmed NTRK-fused cases, reducing the power of the meta-analysis. In total, 224 of 7938 (3%) solid tumours with an NTRK fusion were identified in literature and our cohort, demonstrating the overall rarity of this genetic alteration in solid tumours. As several cohorts in this meta-analysis, including our own, might be enriched for NTRK-fused cases, e.g. due

to selection of cases based on the absence of a driver mutation by DNA NGS, specific morphology of the tumour, or the inclusion of therapy-resistant tumours, our study might already overrepresent NTRK-fused cases. Another limitation is heterogeneity of the included studies for inclusion criteria and techniques used for pan-TRK IHC and molecular diagnostics for NTRK fusions. Despite the fact that all studies used a cut-off of 1% staining with pan-TRK IHC for a case to be considered positive, there was substantial variation in the dilution used for pan-TRK IHC.

Currently, NTRK is the only pan-cancer treatment target, but this is likely to change in the near future. Novel therapies for alternative targets are discovered each year, and several of these treatments are already available in experimental settings, via early access, or compassionate use programs, greatly increasing the number of treatment options of late stage cancer patients. In addition, the diagnostic setting not only requires screening of the NTRK genes but also of other fusion genes, e.g. RET, ROS1, and ALK. Therefore, for both therapeutic and diagnostic purposes, a multi-target analysis of NTRK in combination with other genes of interest will become more and more clinically relevant, preferring comprehensive molecular analysis, such as RNA NGS and WGS, over single-target assays, such as IHC and FISH. [30]

In conclusion, our study demonstrates a sensitivity of 82% and a false-negative rate of 18% for pan-TRK IHC as a screening method for the detection of NTRK fusions in solid tumours. These data should be considered when choosing a strategy to screen for NTRK fusions in the clinical setting.

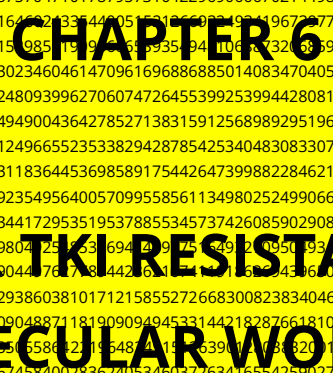
## References

1. Westphalen CB, Krebs MG, Le Tourneau C, et al., *Genomic context of NTRK1/2/3 fusion-positive tumours from a large real-world population*. NPJ Precis Oncol, 2021. **5**(1): p. 69.
2. Hsiao SJ, Zehir A, Sireci AN, et al., *Detection of Tumor NTRK Gene Fusions to Identify Patients Who May Benefit from Tyrosine Kinase (TRK) Inhibitor Therapy*. J Mol Diagn, 2019. **21**(4): p. 553-571.
3. Drilon A, Laetsch TW, Kummar S, et al., *Efficacy of Larotrectinib in TRK Fusion-Positive Cancers in Adults and Children*. N Engl J Med, 2018. **378**(8): p. 731-739.
4. Cocco E, Scaltriti M and Drilon A, *NTRK fusion-positive cancers and TRK inhibitor therapy*. Nat Rev Clin Oncol, 2018. **15**(12): p. 731-747.
5. Huang FW and Feng FY, *A Tumor-Agnostic NTRK (TRK) Inhibitor*. Cell, 2019. **177**(1): p. 8.
6. Hong DS, DuBois SG, Kummar S, et al., *Larotrectinib in patients with TRK fusion-positive solid tumours: a pooled analysis of three phase 1/2 clinical trials*. Lancet Oncol, 2020. **21**(4): p. 531-540.
7. Delgado J, Pean E, Melchiorri D, et al., *The European Medicines Agency review of entrectinib for the treatment of adult or paediatric patients with solid tumours who have a neurotrophic tyrosine receptor kinase gene fusions and adult patients with non-small-cell lung cancer harbouring ROS1 rearrangements*. ESMO Open, 2021. **6**(2): p. 100087.
8. Garber K, *In a major shift, cancer drugs go 'tissue-agnostic'*. Science, 2017. **356**(6343): p. 1111-1112.
9. Marchiò C, Scaltriti M, Ladanyi M, et al., *ESMO recommendations on the standard methods to detect NTRK fusions in daily practice and clinical research*. Annals of Oncology, 2019. **30**(9): p. 1417-1427.
10. Demetri GD, Antonescu CR, Bjerkeheggen B, et al., *Diagnosis and management of tropomyosin receptor kinase (TRK) fusion sarcomas: expert recommendations from the World Sarcoma Network*. Ann Oncol, 2020. **31**(11): p. 1506-1517.
11. Rudzinski ER, Lockwood CM, Stohr BA, et al., *Pan-Trk Immunohistochemistry Identifies NTRK Rearrangements in Pediatric Mesenchymal Tumors*. The American Journal of Surgical Pathology, 2018. **42**(7).
12. Gatalica Z, Xiu J, Swensen J, et al., *Molecular characterization of cancers with NTRK gene fusions*. Modern Pathology, 2019. **32**(1): p. 147-153.
13. Hechtman JF, Benayed R, Hyman DM, et al., *Pan-Trk Immunohistochemistry Is an Efficient and Reliable Screen for the Detection of NTRK Fusions*. Am J Surg Pathol, 2017. **41**(11): p. 1547-1551.
14. Kong Y, By R, Parvathareddy SK, et al., *NTRK fusion analysis reveals enrichment in Middle Eastern BRAF wild-type PTC*. Eur J Endocrinol, 2021. **184**(4): p. 503-511.
15. Castillon M, Kammerer-Jacquet S, Cariou M, et al., *Fluorescent In Situ Hybridization Must be Preferred to pan-TRK Immunohistochemistry to Diagnose NTRK3-rearranged Gastrointestinal Stromal Tumors (GIST)*. Appl Immunohistochem Mol Morphol, 2021.
16. Bocciarelli C, Caumont C, Samaison L, et al., *MSI-High RAS-BRAF wild-type colorectal adenocarcinomas with MLH1 loss have a high frequency of targetable*

- oncogenic gene fusions whose diagnoses are feasible using methods easy-to-implement in pathology laboratories.* Hum Pathol, 2021. **114**: p. 99-109.
17. Fu Y, Li Z, Gao F, et al., *MLH1/PMS2 Expression Could Tell Classical NTRK Fusion in Fluorescence In Situ Hybridization Positive Colorectal Carcinomas.* Front Oncol, 2021. **11**: p. 669197.
  18. Solomon JP, Linkov I, Rosado A, et al., *NTRK fusion detection across multiple assays and 33,997 cases: diagnostic implications and pitfalls.* Mod Pathol, 2020. **33**(1): p. 38-46.
  19. Chiang S, Cotzia P, Hyman DM, et al., *NTRK Fusions Define a Novel Uterine Sarcoma Subtype With Features of Fibrosarcoma.* Am J Surg Pathol, 2018. **42**(6): p. 791-798.
  20. Chang JC, Zhang L, Drilon AE, et al., *Expanding the Molecular Characterization of Thoracic Inflammatory Myofibroblastic Tumors beyond ALK Gene Rearrangements.* J Thorac Oncol, 2019. **14**(5): p. 825-834.
  21. Sasaki E, Masago K, Fujita S, et al., *Salivary Secretory Carcinoma Harboring a Novel ALK Fusion: Expanding the Molecular Characterization of Carcinomas Beyond the ETV6 Gene.* Am J Surg Pathol, 2020. **44**(7): p. 962-969.
  22. De Winne K, Sorber L, Lambin S, et al., *Immunohistochemistry as a screening tool for NTRK gene fusions: results of a first Belgian ring trial.* Virchows Arch, 2021. **478**(2): p. 283-291.
  23. Remoué A, Cohan-Charlet V, Bourhis A, et al., *Non-secretory breast carcinomas lack NTRK rearrangements and TRK protein expression.* Pathol Int, 2019. **69**(2): p. 94-96.
  24. Strohmeier S, Brcic I, Popper H, et al., *Applicability of pan-TRK immunohistochemistry for identification of NTRK fusions in lung carcinoma.* Scientific Reports, 2021. **11**(1): p. 9785.
  25. Moher D, Liberati A, Tetzlaff J, et al., *Preferred Reporting Items for Systematic Reviews and Meta-Analyses: The PRISMA Statement.* Journal of Clinical Epidemiology, 2009. **62**(10): p. 1006-1012.
  26. Bruno R and Fontanini G, *Next Generation Sequencing for Gene Fusion Analysis in Lung Cancer: A Literature Review.* Diagnostics, 2020. **10**(8): p. 521.
  27. Tachon G, Cortes U, Richard S, et al., *Targeted RNA-sequencing assays: a step forward compared to FISH and IHC techniques?* Cancer Medicine, 2019. **8**(18): p. 7556-7566.
  28. Wong DD, Vargast AC, Bonar F, et al., *NTRK-rearranged mesenchymal tumours: diagnostic challenges, morphological patterns and proposed testing algorithm.* Pathology, 2020. **52**(4): p. 401-409.
  29. Cohen D, Hondelink LM, Solleveld-Westerink N, et al., *Optimizing Mutation and Fusion Detection in NSCLC by Sequential DNA and RNA Sequencing.* J Thorac Oncol, 2020. **15**(6): p. 1000-1014.
  30. Radonic T, Geurts-Giele WRR, Samsom KG, et al., *RET Fluorescence In Situ Hybridization Analysis Is a Sensitive but Highly Unspecific Screening Method for RET Fusions in Lung Cancer.* J Thorac Oncol, 2021. **16**(5): p. 798-806.

3.14159265358979323846264338327950288419716939937510582097494459230781640628620899862803482534211706798214808651328230664709384460955058  
22317253594812848111745028410270193852110555964462294895493038196442881097566593344612847564823378678316527120190914564856692346034861  
04543266482133936072602914127372458700660315588174881520926682925409171536436789259036001133053054882046652138414695194151160943305  
7270365795919530921861713819326117931051185480744623799627495967351885572428941327938183011949129833673362440656643086021394946352922473  
71907021798609437027705392171762931767523846748184676694051320056812714526356082778577134275778960917363717872146844090122495343014654  
958537105079227968925892354201995611212902196086403441815981362977477130996051870721134999999837297804995105973173281609631859502445945  
53469083026425230825334468053526193118817101000313783875288658753320838142061717766914730359825349042875546873115956286388235378759375  
1957781857780532171226806130019278766111959092164201989389558201056485863278865936153381827968230301920330185296899577362259941389  
1294721725783479131515574857244541056995808295331168617278955790598381754637464939319255604009277011513090984882401285836106356370  
766010471018194295559619894676783744944825537977472684710404753464620804668425906949129331367702898915210475216205696602405803815019351  
125338243003558764024749647326391419927260426992279678235478163600934172164121992458631503028618297455570674983850549458858692699569092  
72107975093295321165344987202755960236480665499119881834797753566369807426542527865518481754672890977729798008164706001615424949  
217321721477235014414917356854816136115732525123347574184946843852339073941433345477624168625189835694856985629192221482725504525688  
767179049460165346680498862723279178608578438382796797668145410095388378636095068006422512520511739298489608412848862694560424196528502  
221066118630674427862203919494504712371378696095636437191728746776465757396241389086583264599581339047802759009946576407895126946839835  
2595709825822620522489407726719478268482601476990902640136394437455305068203496252451749399651431429809190659250937221696461151570985838  
741059788599772975498930161753928681382686838694274155991855925249539594301409972524680845987273644690584637622262609912460805  
124388439045124413654972678079771569143599770129616089441694868558480635342207225282848864815845602850618827394526274676789525213  
852254995466672782398645659611635488623057745649803559363456817432411251507606947945109659609402522887971089314566913686722874894056010  
150330861792868092087476091782493858900971490967598526136554978189312978482168299894872626880485756401427047755513237964145152374623436  
454285844479526586782105114135473573952311342716610213596953623144295248493718711014576540359027993440374200731057853960219838744780847  
849868332144571368675194350642021845319104848100537061468067491927819119793995206141966342875444063475123718192179989839101591956181467  
5142691239748994007186494231961567945208095146550225231603881930142093762137855956638937780830906979207734672218256259661501421250306  
803844773454920260541466592520149744285073251866600213243408819071048633173464965145390579626856100550810665879699816357473638405257145  
91028970641401109712062804390397595156771570042033786993600723055876317635942173132514712053292819182618612586732157919841484882916447  
060957527069572209176571167229109816999152801520067127485832228718352095339657251210835791513698820914442100675103346711031412671113699  
08655163983150197016511516851714376576183515565088490989898983734552832316355076479185358979185449632132933089587064206752597091  
548141654985946163718027098199430992448895757128289059232332609729971208443357326548938239119325974636673058360414281388303203824903758  
98524374417029132765618093773444030707469211201913020330801976211011004492932151608424448596376698389522868478312355265821314495768572  
62433441893039686426243410772296780280731891544110104468232527162010526522721116603966655730925471105578537634668206531098965269186205  
64769312570586356020185881007239360598764861179105334885046611365768675324944166803962659798771855608445529641266540853061434441385867  
69751456614068006023787765913440171249447010562230538994561310571127004078547323269939081454664645880797278668306343285878569830523  
580893306575740679545716377525420211495576158140025012622859413021647155097925923099079654737612551765675135751782966645477917450112996  
14890304639947132962170340437518957359614589019389713117904297828564750320318969151402878085990480109412172213179476477262241425485  
45403321571853061422881375804306332175182979862273172159160771669254728738986654949450114540628433663937900397626567214638530673609  
65731209180738327166416274888800786925602902284721040317118608204190044296617119637921337551149595015660496318629472654736425230817  
7036751590673502350728354056704038674351362224771589150495309844893330963408780769325993978054193414473774418426312986080998886874132  
604721569516239658645730216315981931951673538129741677294786724229246543668009806769282382806899640048243540370141631496589794092432378  
9690706979422362508221688957383798623001593776471651228935786015881617557829735234460428151262720373431465319777741603199066554187639  
7929334419521541341899485444734567383162499341913181480927771038638773417207545654322077092120190516609628049092636019759888216133  
231666365286193266863360627356795405077235547105895948027908143562401451718062446436267945612753181340783033625423278394  
497538243720583531147711992606381334677687969597030983391307710987040859133746414428227726346594704745878477872019277152807317679077071  
572134447306057007334924369311383504931631284042512192565179806941135280131470130478164378851852909285452011658393419656213491434159562  
58658655705526904652098580338507224648293972858478316305777560688876446248246857926039535277348030480290058760758251047470916434396136  
2676044925762420420832085661196625545337213153595845068772460290161876679524061634252577195429162991306455377991403734043287526288896  
39958794757291746426357455254079091451357111369410911939325101076028252026187985318877058429725916778131496990090192116971737278476847  
268608490033770242429165130050051683233643503895170298939223345172201381280696501178440874519601212285993716231301711444846409038906449  
5444006198690754851606263275052983491874078668088183385102283345085048608250393021332197155184306325545007668282943041377655219375717546  
11395398463396383047641199665385815384205685338621867252334028308711232827892125077126294632659398989893582167456021012839646220134  
9671518819097303811980049973407239610368540663319395097901906969395245300540580685501956730229219139391858603449039020595510022635353  
619204199474553859381023439554495977837790237421617271117236434354394782218185286240851400666044332588856986705431547069657474585503323  
233421073015459405165537906866273337995851156257843229882737231989875714159578111963583300594087306812160287649628674460477464915995054  
9737425626901049037781986835938146574126804925648798556145372347863730309046883834363465573949864192705638729317487233208376011230299107  
67938627089438799362016295154133714248928307201269014754668476535761647737946752004907571555278419653621302460461601363581559074220202  
031827760527712900556148425551879253034351398442532234157623361064250639047597008656271095359194658975141313942627693062474353632569160  
7815478181152843667957061108615331504452127473924544945423682886061340841486377670096120715124914043027253860764822363414334623518975766  
4521641376796903149501910857598442391986291642193994907362346468441173940326591840443780513338945257423995082965912285085582157250310  
7125701266830204929525201187267675262501454205168416348475651699981161410102996078386909291603028840026910414079288621507882425167090  
870069928212066041837180653556752525323286129104248776182758297651579598470356222629348600341587228805349896502262917487882027342092  
222453398562647669149055628425039127577102840279980663658254889264880254566101729670266407655904290994568150652653053718294127033693137  
851786090407086671149655834343476933857817113864558736781230145876871266034891390956200993936103102916161528813843790990423174733639480  
45759314931405297634757481193567091101377512100803155902485309066920376119220332290943346768514221447737939375170344366199104033751117  
354719185046449026365512816228824462575916333039107225383747182104888308657391771509682887429656995995744906617583441375212039709683400  
00535984917541738188999446974867626551682765848358845314277589700290951703835297163445621186066510124120065975585127617  
858382920419748442360800719304576189323492292796501987518721272675079812554709589045563579212210333466974992356302549478024901141951232  
82815309114079073860251522742995818072471625916684551333123948049470919115132673430282441860414263639548000480026704962482017928964766  
92581832713142517029652348896276684403232609275249603579964692565049368183609032380929345958897069536534906304216654473575890456328  
878505525564054482465158754711962184439685253375438856909411303150952617937800297412076651479942590298695946995567612186561967337  
862362561252163208628692221032748892186543648022967807057656151446320469297068212073883778142335628236089632080682224680122482611771858  
963814091839036736722208883215137556003727983940041529700287830766709444745601345564172543709069793961225714298946715435784687886144458  
1231459357198492252847160504922124247014124780573455105080019086996033027634780810817545011930714122339086639383395294257869050763410

063835198343893415961318543475464955697810382930971646514384070070736041123735998434522516105070270562352660127648483084076118301305279  
320542746286540360367453286510570658748822569815793678976697422057505968344086973502014102067235850200724522563265134105592401902742162  
484391403599895353945909440704691209140938700126456001623742880210927645793106579229552498872758461012648369998822569596881592056001016  
55256375678566272966198857827948883343975187445551296536344380396642055798293680435220779842942325302257634180703964769941597915  
945300697521482933665556615678736400536665641654732170439035213295352916941459904160875320186839793702348886894791510716378529023452924  
407736594956305100742108714261349745956151384987137570471017879573104229690666702144986374645952808243694457897723300487647652413390759  
20434019634039114732023380715095222010682563427471647523354400515710507191496777070415956837353551667302739007497297363549645332888  
69844061196496162773449518273695588220757355176651598510994561993594106473263899075407923242003009259007017319603622547564789406  
4754834664776041146323905651343068449539790709030234604614709616968889501408347040546049258699138296682468185710318879065287036508  
3243197444074718556789348230894310682870272289073624809396670607472645538225399442808113736943388729406372615959946026246297070625948  
455690347119729964090894180595343932512362355081349490043642785271383159125689892951964272875739469142725343669415323610045373048819855  
17065941217352462589548730167600298865925786628561249665523538294287854253404830833070165372285635591525347844598183134112900199920598  
135220511733658564078268494276441137639386692480311836445369858917544264739988228462184490007769776776312795722672655562596285427653183  
00240709223436657791601280931794017185985999338423549564005705955561134980252499066984230017350358040811685526531170995708994273287  
09258487894436600504108922669178352587078595129834417295351953788553457374260859029081765155780309094640873506123226112009373108048548  
52635722825768203416050484662775041093620180179804253536940970549209509339829227385159740547021482897111777923761225  
7887347718819682546298126868581705170053552638004476178442161517115524346061117592654823993917604260176338704549901761  
436412046921823706488784196896861181558158736062938603810171215855272668300823834046564758004513808016363688742163714064354955618689  
6112282140753026551004241048967835285882902436709048871181909094945331442182826618103100733547705498159680720094746961343609286148494  
178501718077930681085469000944589192444338992560558422195484435639121953201017076866887239718014613432445726400973742570  
073592100315415089367930081699805365202760072774967458400283624053460372634165542590276018348403068113818551059797056640075094260878857  
3579603732451447687603688098806097164258497595138069309449401515422221943291302173912538355915031003303251117491569691745021749433151  
55885403922164097229101129035521815762823281823425483261119128009282525619020526301639114772473314857391077758744253876117465786711694  
1774624144111126358353871361011023267987756102468240322648346417663698066378576813492045302240819727856471983963087815432211669122464  
159117767322532643356861461865452226812688726844596844241610785401676814208088502800541436131462308210259417375623899420757136275167457  
318918945628352570441335437585753426986994725470316566139919998626282472706413362217892390317608542894373393561889165125042440400809527  
198378738648058472689546243882343751788520143956007510481194988423960601369573423155907967034614914344788636401031823507365027785908975  
78272731305048989909092291350337325085598265560708924261242947360701939077271302068917092465484234407865050366801360466895118400936  
6860954632500214585293095000907151058236272932645373821049387249966993394246855164832611341461106802674466373343753407642940266829738  
652209357016263846485285149036293201991996882851718395366913452224447080459239660281715655156566611135982311225062890585491450971575539  
00243931535190902107119457300243880176615035270862602537878179514478061013715004489917210022201335013106016391541589578037117792752259  
787428919179155224171895853616805947142319339842021874564925644346239253193135103311476394911995072858436581361953693296992898397149  
419394069572486396883690326556436421664425276079147108998843157337496488352927693282207629472832815374099615455987982598910937171262182  
830258481123890119682214294576675807186538065064870261338928229949725745303238389638184394477077940228435988341003583854238973542439564  
755568409522484455413923941000162076936368467764301781965937997155746854196633489374843912942391433659360410035234377065888677811394  
98616478741740793268587386247328896456435987746676384796650476111825658378878454858148962961273998413442726086061872455623606431537  
101127468097780704464091582803487697589483282417392929605820486191966709189580893320121031843034012849511620353428041442751672858302435  
59830032042024512072872535581195840149180969253395075778400067465526031446167050827682722235341911026341631571474061238504254859884199  
076112872580591139356896014316682831763235673254170734208173322304629879928049085140947903688786878949305469557030726190095020764334933  
591060245450864536289354568629585313153371838682656178622736371697577418302398600659148161640494965011732131389547062088474802365071  
31150898427992754268532779743113951435741722197597993596852528574526379628612691572359866205734083757668738842664059099350300183133  
754324546359675048442352848747014435454195762584716198134073468541117668831186544893769795665172796623267148103386439137518659467  
300244345005449953997423723287124948347060440634716063258306498297955101095418362350303094530973358344628394763047756450150085075789495  
4893139394489921612552559770143685894358587752637962559708167764380012543650237141278346792610199558524717220177237004178084194239487  
2504680155603598939054898572354674564239005850216719031395262645543913166313453089390602046784387785054239305247313620129476918749751  
9101147231258932677253918146607300088207768863114810902209724507591672970078505807171863810549679731001678708506942070922329080703832  
6345345030802786099055690013413718236837099194951648960075504934126787643674638490206396401976685952326546391383631857456981471962108  
410809618846054560390384553437291414465134749407848844237721751543342603066988317683310011331086904219390310801437843341513709243503136  
7763108491351615642269847507430329716746960466653152703532546711266752246055119958183196376707617991919203579582007596503023462677579  
4393644076065690108011494274110093913691381072581378135789400559500183542511841721360557275210352680373572652792241737360575112788721  
819084890617813897107708239100279695938387589093568814895026322439372656247277603789081445883785501970284377936240782507048758  
164703245812908783952324532378960298416692254896497156069811921865849267704039564812781021799132174163058105545988013004845629976511212  
41536374515005635070127815926714241342103301566165356024733807843028655252722753049998837015348793008062601809623815161366903341113865  
3851091936739383523945888322505887064507539473952043968079067088064450969865488016828743437861264538158342807530618454859037982179945  
9968115441974253263493602902510015888271647450068207041937615845721231834600728933955054829357137256840232268213012476794522648209  
1023564772723082081063518899152692889108455517126603965034768467825001611015323516051965590211844949907789992007329476905868577887  
209829013529566139788848605097860859570177312981553149516814671769597609942100361835591387778176984587581044662839988060061622984861693  
533738657877359833616133841338536842119789389001852956919678045548285848370117096721253533875862158231031038776682721157269495181795  
897546939926421991552338576623167625475703546994148929041301856861194391962838870543677743222768091313654488453667680000010652624854  
730558615899991401170798385483188750142938908995068545307651168033732226511600337222651799144225280816517166776672793534851542002381  
746089232839170327542575086765511785939500279338959205766827896776445312840401855401043513483895312013263783692835808271937831265496174  
59970567450718332065034556644034490453627560011250184335607361222765949278393706478426456763881880756561216896050416113903906396016202  
21536849410926053876887148379895999911209916464644119185682770045742434304216727264455893301277815868695250694993646101756850601671453  
5431581480105458860564501332037586454858403326977170934809105562116715468484778039447569798042631809917564228098739987669732376957370  
1580806822904599212366168902596273040679316531149401764737693873514093361833216142802149763399189354884875625987542873077559559554  
651963944018218409984124898262367377146722606163364329640633572810707887581640438148501884114318859882769449011932129682715888413386943  
468285900666408063140775727505630729400492940302420498416565479736705485504458657202276378404668233798528271057843197353417950113472  
736251740207346282604502285157979559764760472284099956160156910890384984520679265942055503958792298185264800706837650418365620945543  
46135134150210679974881916341359556719649654032187216026480390409358748259096612725079482827693893525173662180507962977851461884327192  
23223810158744450528665238022532843891375273845892384442547265309817157844783421252327020690287232300538621634798850946954720047952  
31120150432932662827276321779088400878614802214753765781058197022263097174950721272484794781695729614236585957820908307332335603484653



## Chapter 6: EGFR TKI resistance molecular workup

### 6.1 Title page

Title: Real-world approach for molecular analysis of acquired EGFR tyrosine kinase inhibitor resistance mechanisms in NSCLC

*Published in: Journal of Thoracic Oncology Clinical Research Reports 2021. DOI: 10.1016/j.jtocrr.2021.100252*

#### 6.1.1 Authors

L.M. Hondelink<sup>1</sup>, M. Jebbink<sup>2</sup>, J.H. von der Thüsen<sup>3</sup>, D. Cohen<sup>1</sup>, H.J. Dubbink<sup>3</sup>, M. Paats<sup>4</sup>, A. Dingemans<sup>4</sup>, A.J. de Langen<sup>2</sup>, M.C. Boelens<sup>5</sup>, E.F. Smit<sup>2,6</sup>, P.E. Postmus<sup>6</sup>, T. van Wezel<sup>\*1,5</sup> & K. Monkhorst<sup>\*5</sup>

#### 6.1.2 Affiliations

1: Department of Pathology, Leiden University Medical Center (LUMC), Leiden, the Netherlands

2: Department of Thoracic Oncology, The Netherlands Cancer Institute (NKI), Amsterdam, the Netherlands

3: Department of Pathology, Erasmus Medical Center (EMC), Rotterdam, the Netherlands

4: Department of Pulmonology, Erasmus Medical Center (EMC), Rotterdam, the Netherlands

5: Department of Pathology, The Netherlands Cancer Institute (NKI), Amsterdam, the Netherlands

6: Department of Pulmonology, Leiden University Medical Center (LUMC), Leiden, the Netherlands

\*: both authors contributed equally.

#### 6.1.4 Acknowledgement

The authors thank the molecular diagnostics teams at the departments of Pathology in Leiden University Medical Center, Erasmus Medical Center and the Netherlands Cancer Institute.

## 6.2 Abstract

### 6.2.1 Background

With the approval of first-line osimertinib treatment in stage IV EGFR-mutated NSCLC, detection of resistance mechanisms will become increasingly important-and complex. Clear guidelines for analyses of these resistance mechanisms are currently lacking. Here, we provide our recommendations for optimal molecular diagnostics in the post-EGFR tyrosine kinase inhibitor (TKI) resistance setting.

### 6.2.2 Methods

We compared molecular workup strategies from three hospitals of 161 first- or second-generation EGFR TKI-treated cases and 159 osimertinib-treated cases. Laboratories used combinations of DNA next-generation sequencing (NGS), RNA NGS, in situ hybridization (ISH), and immunohistochemistry (IHC).

### 6.2.3 Results

Resistance mechanisms were identified in 72 first-generation TKI cases (51%) and 85 osimertinib cases (57%). RNA NGS, when performed, revealed fusions or exon-skipping events in 4% of early TKI cases and 10% of osimertinib cases. Of the 30 MET and HER2 amplifications, 10 were exclusively detected by ISH or IHC, and not detected by DNA NGS, mostly owing to low tumor cell percentage (<30%) and possibly tumor heterogeneity.

### 6.2.4 Conclusions

Our real-world data support a method for molecular diagnostics, consisting of a parallel combination of DNA NGS, RNA NGS, MET ISH, and either HER2 ISH or IHC. Combining RNA and DNA isolation into one step limits dropout rates. In case of financial or tissue limitations, a sequential approach is justifiable, in which RNA NGS is only performed in case no resistance mechanisms are identified. Yet, this is suboptimal as-although rare-multiple acquired resistance mechanisms may occur.

## 6.3 Introduction

Approximately 11% of all lung adenocarcinomas harbor a driver mutation in the EGFR gene. [1] Most of these EGFR mutations have been targeted with first-

and second-generation tyrosine kinase inhibitors (TKIs) for several years, resulting in a substantial improvement of both overall and progression-free survival for these patients. [2, 3] In 2017, osimertinib, a third-generation TKI, was approved by the Food and Drug Administration and European Medicines Agency as second line [4] and more recently as first line for the treatment of metastatic EGFR-mutated NSCLC, which further improved survival.

Although targeted treatment with selective TKIs has been found to improve overall survival substantially, all tumors eventually acquire resistance, inevitably resulting in death. [5] In first- and second-generation TKI resistance (such as erlotinib, gefitinib, afatinib), acquired resistance mechanisms predominantly consist of on-target mutations in EGFR, mainly T790M, [6-9], but also D761Y [10], L747S [11], and T854A point mutations and EGFR amplification. [6-9], [12] Off-target resistance mechanisms include mutations in BRAF, PIK3CA, and KRAS, amplifications of HER2 and MET, oncogenic fusions in RET, FGFR3, ROS1, and NTRK, and MET- and EGFR-exon skipping and transformation into SCLC. [6-9, 13-18] Squamous transformation has so far only been described in case reports after first- and second-generation TKIs. [19]

For osimertinib treatment (both first line and later lines), the most frequent on-target resistance mutation is C797S, [20-22] although G724S, G796, L792, L718, G719, L844, and V834 have also been reported. In contrast to first- and second-generation TKIs, off-target mechanisms occur more frequently and are more heterogeneous. Off-target resistance mechanisms after osimertinib include not only all resistance mechanisms after earlier TKIs but also amplifications of FGFR1 and transformation to a squamous phenotype. [20, 21, 23-25] Off-target resistance mechanisms are more prevalent after osimertinib compared with the first- and second-generation TKI-treated cases. [16]

The volume of patients who are referred to a tertiary referral hospital for EGFR TKI resistance mechanism screening is increasing. This number will likely continue to rise even more in the years to come, owing to improved access to TKIs, sequential use of different TKIs, and adjuvant TKI treatment for earlier stages of NSCLC. Several of these acquired resistance mechanisms are currently or will soon become treatable [24, 26] through regular reimbursed treatment or in an experimental, off-label, early access, or compassionate-use setting, which makes adequate screening for acquired resistance essential.

Although single-assay screening (with whole-genome sequencing [WGS] or large hybrid capture panel) is the most elegant method of screening owing to its completeness, currently this is not yet feasible in most laboratories worldwide. Small biopsies and cytology specimens still are the mainstay of tissue procurement during EGFR TKI therapy, which limits the potential broad applicability of large panel strategies, for which larger amounts of tumor material are necessary. Moreover, even large hybrid capture panels sometimes miss exon-skipping events, oncogenic fusions, and copy number variation owing to the length of introns, blind spots within the targeted areas, and large deletions, which cannot be captured.

In practice, a consensus on how to screen for these resistance mechanisms is currently lacking. This results in substantial differences between laboratories. This disagreement is largely explained by the broad spectrum of possible acquired resistance mechanisms, with potential co-occurrence, and the broad range of potential screening modalities, each with their own advantages and limitations. Thus, although DNA next-generation sequencing (NGS) panels detect point mutations, deletions, and insertions, they fail to detect most fusions and exon-skipping events and occasionally miss copy number variation as well, especially if the tumor cell percentage is low. In situ hybridization (ISH) or immunohistochemistry (IHC) for fusion targets and amplifications is a single-target assay that constitutes a time- and tissue-consuming challenge. RNA NGS is the preferred technique to detect both exon-skipping events and fusions, including their fusion partners, but current RNA NGS panels do not detect all point mutations, deletions, and insertions that DNA NGS can detect. In conclusion, the multitude of potential resistance mechanisms combined with a multitude of potential techniques to detect them presents to both thoracic pathologists and molecular biologists the complex challenge of choosing the optimal workup for tumor biopsies from patients progressing on EGFR TKI therapy.

This multicenter study therefore aims to provide recommendations on the most efficient and effective resistance analysis after EGFR TKI treatment, by evaluating the existing workflow in a retrospective “real world” cohort analysis that includes 320 routinely acquired resistance biopsy specimens analyzed in three specialized hospitals in The Netherlands. We aimed to address five “challenges” in effective screening after EGFR TKI resistance, which are as

follows: somatic mutation detection, fusion detection, amplification detection, tissue scarcity, and comparison to the pretreatment biopsy. By addressing these challenges step by step, we will propose a workup that takes into account the added value and effectivity of each test modality and is specifically tailored to deal with specific EGFR TKI resistance issues, such as (non)mutual exclusivity and tissue scarcity.

## **6.4 Material and Methods**

### 6.4.1 Study setup

We included 320 EGFR-mutated NSCLC biopsy specimens from 248 patients (317 adenocarcinomas and three squamous cell carcinomas) from three hospitals in The Netherlands, which were submitted to the pathology department for EGFR TKI resistance analysis between January 2018 and February 2020. The biopsy specimens were included in the early TKI group when the patient had acquired resistance to a first- or second-generation TKI, such as erlotinib, gefitinib, and afatinib. The biopsy specimens were included in the osimertinib group when the patient had acquired resistance to osimertinib.

Tumors (n = 3) that originally presented with neuroendocrine differentiation were excluded, owing to the morphologic and molecular differences with NSCLC. Cytology and non-cytology materials were both included. Patients receiving first-line TKI treatment were included and later therapy lines. Patients harboring tumors that became resistant to multiple TKI lines were included twice: once in the early TKI group after the first resistance to the first- or second-generation TKI and once in the osimertinib group after resistance to osimertinib. Some patients were treated with first-line osimertinib, but most received multiple TKI lines (Supplementary Figure 1). In addition, in some patients, the first resistance biopsy specimen did not yield a resistance mechanism, so it was repeated. Those biopsy specimens were included as well. These “double inclusions” occurred in 60 patients and reflects the “real world” TKI resistance setting, in which pathologists are required to perform resistance analysis multiple times for the same patient.

The laboratories performed RNA NGS, MET ISH, DNA NGS, HER2 IHC, or HER2 ISH to varying degrees. The laboratories were all NEN-EN-ISO 15189 accredited, which includes regular evaluations, audits, and quality checks. Due to the

retrospective, anonymized nature of this study, informed consent was not required.

#### 6.4.2 DNA NGS

DNA NGS was performed with laboratory-specific customized oncogene panels that cover hotspots in relevant genes, including EGFR, MET, HER2, KRAS, BRAF, PIK3CA, FGFR1, FGFR2, and FGFR3, and several other mutations. Copy number analysis was performed with the DNA NGS data by locally validated pipelines. Details on all other genes included in the customized NGS panels and copy number analysis pipelines are available in the Supplementary Methods. The panels vary slightly, but relevant resistance mechanisms, which are recited in the Introduction section, are covered in each panel.

#### 6.4.3 RNA NGS

All laboratories used anchored multiplex polymerase chain reaction-based NGS (RNA NGS) technology from Archer DX. Either the FusionPlex Comprehensive Thyroid and Lung Panel or the FusionPlex Lung Panel was used. Reads were analyzed with vendor-supplied software on an IonTorrent platform. The panels used included fusions and exon-skipping events in ALK, BRAF, EGFR, FGFR1, FGFR2, FGFR3, MET, NRG1, NTRK1, NTRK2, NTRK3, RET, and ROS1. A comprehensive overview of the methods used for RNA NGS is included in the Supplementary Methods.

#### 6.4.4 RNA/DNA isolation

All analyses were performed with formalin-fixed, paraffin-embedded (FFPE) tissue, including cell blocks from cytology specimens. DNA and RNA were isolated differently in each laboratory. At the Erasmus Medical Center, DNA was isolated with Chelex or Maxwell, as previously described, whereas RNA was isolated with the Qiagen method. At the Leiden University Medical Center, total nucleic acid was isolated with a Siemens tissue preparation robot and used for both DNA NGS and RNA NGS as previously described. [27] At the Netherlands Cancer Institute, DNA and RNA were isolated separately with a Qiagen FFPE preparation kit.

If DNA and RNA were isolated separately, DNA was stored at  $-20^{\circ}\text{C}$  and RNA at  $-80^{\circ}\text{C}$ . If total nucleic acid was isolated, the isolate was stored at  $-20^{\circ}\text{C}$  short

term and  $-70^{\circ}\text{C}$  long term. A more detailed description of the RNA and DNA isolation process is supplied in the Supplementary Methods. Tumor cell percentage was considered “low” if it was below 30%.

#### 6.4.5 In situ hybridization (MET- and HER2 ISH)

HER2 ISH was either performed with Ventana Dual ISH and stained on the Ventana Benchmark Ultra or with Dual SISH from Roche Diagnostics. MET ISH was performed with Dual Color MET-Cen7 probe either from Leica Kreotech, Zytolight Spec, or Roche Diagnostics. Additional information regarding the ISH is available in the Supplementary Methods.

#### 6.4.6 HER2 IHC

Slides were either stained for HER2 with the Dako A0485 antibody on the Dako Omnis immunostainer using Dako EnVision Flex+ in a laboratory developed test with citrate and a 1:100 dilution or stained on the Benchmark Ultra with Ventana 4B5 antibody. A more comprehensive explanation on the protocol for IHC is in the Supplementary Methods.

#### 6.4.7 Morphologic examination and typing

All cases were evaluated by one expert thoracic pathologist per center (DC, KM, JT) and classified according to the 2015 WHO classification.

Immunohistochemical staining was used for typing when indicated. In case of suspected morphologic transformation to squamous or small-cell phenotype, this was confirmed by IHC (synaptophysin, CD56, and chromogranin for small-cell, P40 for squamous).

#### 6.4.8 Molecular comparison to pre-treatment biopsy

All molecular profiles of resistance biopsies were compared with the molecular profile of the pretreatment biopsy where possible. We considered a molecular alteration in the resistance biopsy an “acquired resistance mechanism” if (1) the alteration was absent in the pretreatment biopsy and (2) the molecular alteration was considered to be a class 4 or 5 pathogenic mutation, reported to be associated with an acquired EGFR TKI resistance phenotype in previous literature, such as EGFR T790M, KRAS G12C, and BRAF V600E. On the basis of the literature, we assumed that treatment naive, EGFR-mutated tumors do not harbor oncogenic fusions. Owing to this assumption, first-line TKI resistance

biopsy specimens could be compared with treatment-naive specimens without pretreatment RNA NGS.

We considered molecular alterations “acquired driver mutations” if (1) the alteration was considered to be a class 4 or 5 pathogenic alteration, but not reported to be associated with an acquired EGFR TKI resistance phenotype, such as TP53, CDKN2A, and CTNNB1, and (2) the alteration was absent in the pretreatment biopsy.

There were several situations in which molecular comparison of the resistance biopsy and the pretreatment biopsy was suboptimal or impossible, for instance in case of incomplete molecular workup of the pretreatment biopsy owing to scarce material, with liquid biopsy as the only pretreatment material. In the setting of suboptimal comparability of molecular profiles, cases were excluded from the analyses of resistance mechanism prevalence, as illustrated in Figure 1. We used the Alamut, CKB, OncoKB, Franlinn, and Cosmic databases for pathogenicity assessment.

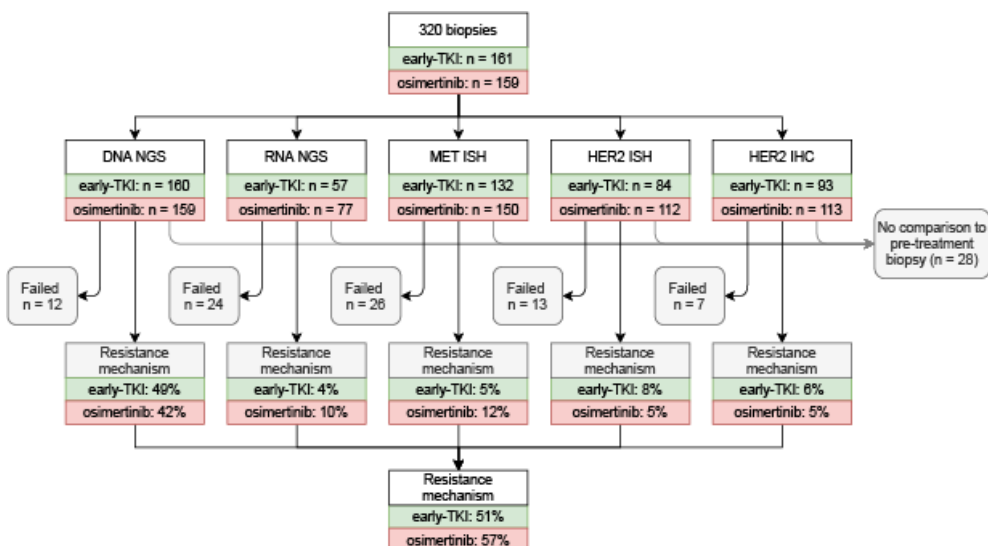
#### 6.4.9 Amplifications

Amplifications for all genes, except MET and HER2, were considered amplifications if the estimated copy number was 10 or more. For MET and HER2, an estimated copy number between six and 10 was considered “low amplification,” and an estimated copy number of more than 10 “high amplification,” as MET and HER2 amplifications with six to 10 copies can be clinically relevant. [28, 29]

HER2 IHC scoring was performed by a customized scoring system. The percentage of tumor cells with “no staining,” “low intensity staining,” “moderate intensity staining,” and “high intensity staining” was estimated by histopathologic examination. Cases were considered to have a score of 0 if 90% or more tumor cells had no or low-intensity staining. Cases were considered to have a score of 1+ if more than 50% but less than 90% of the tumor cells had low-intensity staining. Cases were considered to have a score of 2+ if more than 50% but less than 90% of the tumor cells had moderate- or high-intensity staining. Cases were considered to have a score of 3+ if 90% or more tumor cells had high-intensity staining. Staining was based on

membranous HER2 staining. Cells with incomplete membranous staining were considered positive.

**Figure 1:** Performed DNA NGS, RNA NGS, ISH, and IHC in this study for each treatment group. Percentages for each test are based on successful analyses, and total percentage of resistance mechanisms (51% and 57%) is based on all attempted analyses that could be compared with the pre-TKI biopsy, including



analyses which returned no result owing to insufficient tissue. IHC, immunohistochemistry; ISH, in situ hybridization; NGS, next-generation sequencing; TKI, tyrosine kinase inhibitor.

#### 6.4.10 Smoking

Patients were considered to be never smokers if they did not smoke at least 1 month before the NSCLC diagnosis and had accumulated fewer than two pack-years in their lifetime. Patients were considered to be former smokers if they had stopped smoking more than 1 month before they were first diagnosed with NSCLC and had accumulated two pack-years or more. Patients were considered to be current smokers if they had smoked in the month before being diagnosed with NSCLC, regardless of pack-years.

#### 6.4.11 Statistics

Statistical analysis was performed using IBM SPSS Statistics software, version 25. OncoPrints were visualized with cBioPortal version 3.5.4 OncoPrinter. [30, 31]

#### 6.4.12 Ethics

The data were obtained from routine diagnostic reports and anonymized before processing. This study was approved by the institutional review board at the Netherlands Cancer Institute.

### 6.5 Results

#### 6.5.1 Specimen collection

We included 320 biopsy specimens from 248 patients in this study. Characteristics are outlined in Table 1. Most of the patients were of female sex or never smoker (Table 1 and Supplementary Table 1), more frequent than has been described in the treatment-naïve advanced-stage NSCLC population in The Netherlands. [32]

The early TKI group included significantly more cytology specimens than the osimertinib group ( $p = 0.004$ , Fisher's exact test). This is likely due to the more frequent use of endobronchial or endoesophageal ultrasound-guided lymph node aspiration in the referring hospitals. Several patients were included in both the early TKI group and the osimertinib group, reflecting use of second-line osimertinib after resistance to the first- or second-generation TKI. The timeline of this patient group is outlined in Supplementary Figure 1.

#### 6.5.2 Challenge #1 Somatic mutation detection

DNA NGS was used to screen for somatic mutations, including point mutations and small deletions and insertions. DNA NGS was performed in 319 of 320 cases and was successful in 307 cases, as outlined in Figure 1. In the early TKI group, DNA NGS detected a resistance mechanism in 66 early TKI cases (49% of successful tests) and in 62 osimertinib cases (42% of successful tests). The identified somatic mutations are summarized in Figure 2A–C and are often, but not always, mutually exclusive with other resistance mechanisms. We used the definition for “acquired resistance mechanisms” as described in the Material and Methods section.

	FIRST AND SECOND GENERATION TKI RESISTANCE (N = 161)	OSIMERTINIB RESISTANCE (N = 159)	P-VALUE
<b>SEX</b>			0.55 <sup>a</sup>
FEMALE	105 (65%)	109 (69%)	
MALE	56 (35%)	50 (31%)	
<b>AGE</b>	65 (31 – 89)	63 (32 – 86)	0.09 <sup>b</sup>
<b>BIOPSY SITE</b>			0.73 <sup>c</sup>
PRIMARY TUMOR	58 (36%)	53 (33%)	
LYMPH NODE	23 (14%)	20 (13%)	
DISTANT METASTASIS	80 (50%)	86 (54%)	
<b>TUMOR TYPE</b>			0.12 <sup>a</sup>
ADENOCARCINOMA	161 (100%)	156 (98%)	
SQUAMOUS CELL CARCINOMA	0	3 (2%)	
<b>SPECIMEN TYPE</b>			0.004 <sup>a</sup>
CYTOLOGY	64 (40%)	39 (25%)	
HISTOLOGY	97 (60%)	120 (75%)	

**Table 1:** specimen characteristics for each treatment group, registered per specimen (n = 320). P-values were calculated with Fisher's exact test (a), unpaired t-test (b) or Pearson's chi square test (c).

Mutual exclusivity is outlined in Figure 3A–C, where we reveal that in 23 cases overall (7% of all cases), multiple new resistance mechanisms are present in the resistance biopsy. In the early TKI group, multiple resistance mechanisms were detected in 14 cases (9% of all early TKI cases), and in the osimertinib group in nine cases (6% of all osimertinib cases). The prevalence of co-occurring mutations in resistance biopsies is substantial, especially considering not all biopsies underwent RNA NGS and ISH, as found in Figure 1. Nevertheless, when we look closer at which resistance mechanisms co-occur, we observe that it is frequently (in 16 of 23 cases, 70%) PIK3CA or EGFR amplification in concurrence with another mutation. Co-occurrence of “strong” resistance mechanisms, such as T790M, HER2 amp, KRAS, or MET amp, is rare and occurs only in seven cases in this cohort (2%).

Acquired resistance EGFR mutations in the early TKI group include the following: A298V, I706T (variant of unknown significance), K754E, S768I, T790M, C797S, and EGFR-exon skipping (exons 21–27 or exons 2–7). EGFR mutations in the osimertinib group include the following: L62R, A298T, L718Q (variant of unknown significance), G724S, I744M, G796S, C797S, L972H, and EGFR-exon skipping. We conclude that the identified on-target and off-target resistance

mechanisms are similar to those identified in the literature, for both treatment groups.

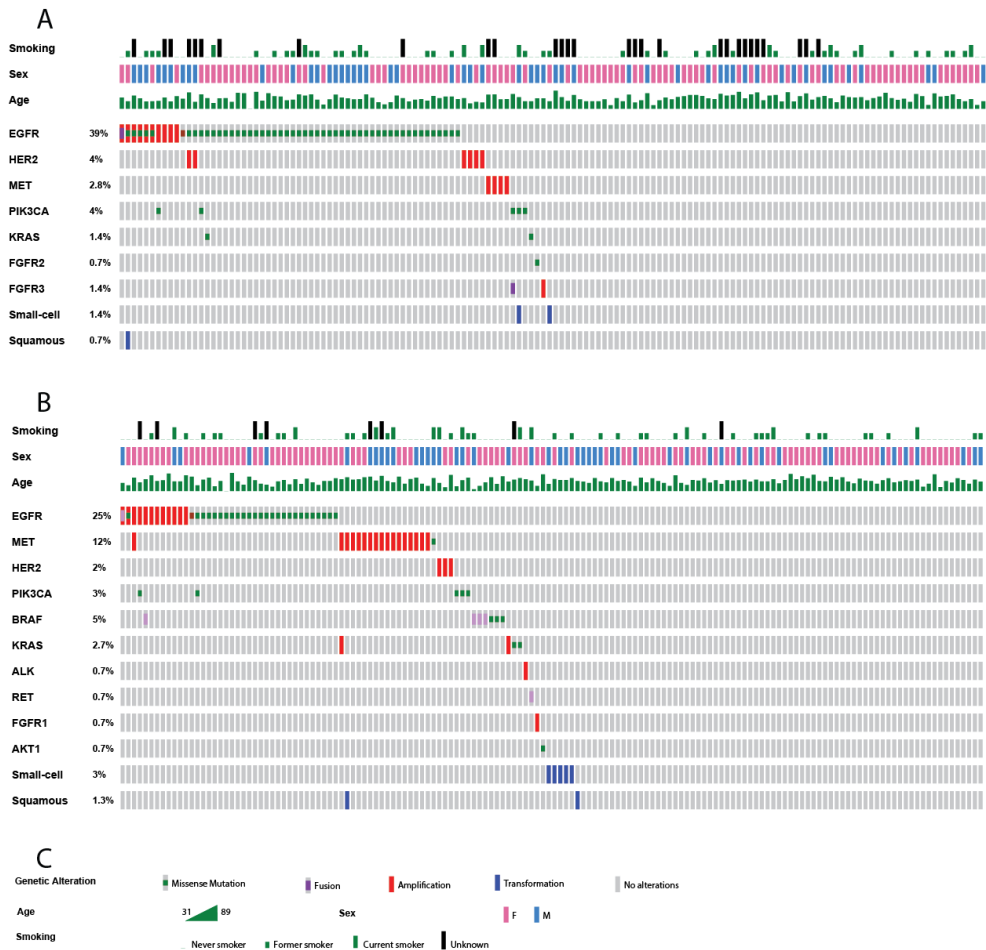


**Figure 2:** (A) OncoPrint for the first- and second-generation TKI resistance cohort (early TKI group). EGFR mutations include the following: A298V, I706T (VUS), K754E, S768I, T790M, C797S, and exon skipping. (B) OncoPrint for the third-generation TKI resistance cohort (osimertinib group). EGFR mutations include the following: L62R, A298T, L718Q (VUS), G724S, I744M, G796S, C797S, L972H, and exon skipping. (C) Legends. All listed mutations are pathogenic driver mutations, which were not present in the pretreatment biopsy. This includes the listed EGFR mutations: the original EGFR mutation is not included in this figure. F, female; M, male; TKI,

tyrosine kinase inhibitor; VUS, variant of unknown significance.

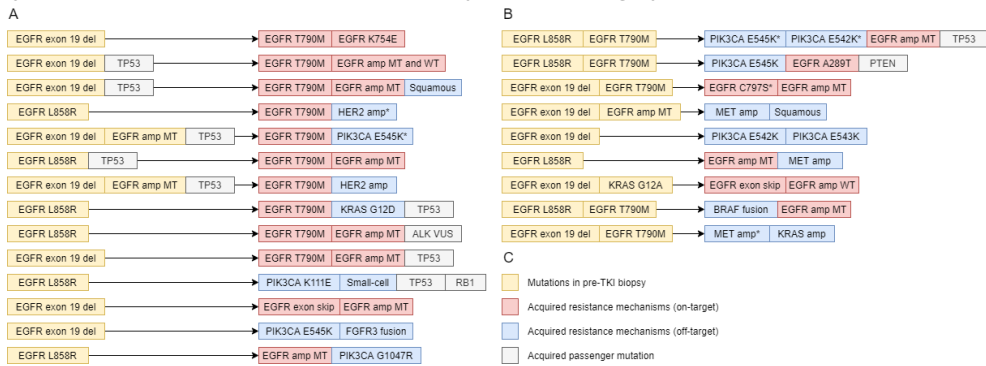


**Figure 3:** Cases harboring multiple resistance mechanisms. (A) First- and second-generation TKI resistance cohort (early TKI group). (B) Third-generation TKI resistance cohort (osimertinib group). (C) Legend. Mutations marked with \* are present in only part of the tumor cells, indicating clonal heterogeneity. amp, amplification; del, deletion; MT, mutant; TKI, tyrosine kinase inhibitor; WT, wild-type.

### 6.5.3 Challenge #2 Fusion and exon skipping detection

RNA NGS was performed in 134 cases. It was successful in 110 cases (82%), whereas in 24 cases (18%), insufficient RNA was available for the analysis. In eight cases overall (7% of all successful analyses), an exon-skipping or fusion event was found by RNA NGS, all of which are visualized in Figure 4. These events occurred twice in the early TKI group (4% of successfully tested cases) and six times in the osimertinib group (10%,  $p = 0.46$ , Fisher's exact test). The identified fusions and exon-skipping events were not mutually exclusive with other resistance mechanisms, as outlined in Figures 2 and 3; instead they co-occurred with other resistance mechanisms in four cases. In the early TKI group, both rearrangements co-occurred with other resistance mechanisms, being PIK3CA mutation and EGFR amplification, respectively. In the osimertinib group, two of six fusions or exon-skipping events overlapped with other mechanism (33%), both with an EGFR amplification. This is in line with the literature, where co-occurrence of a fusion or exon-skipping event with a stronger resistance mechanism, such as BRAF, KRAS, EGFR T790M, or MET amplification, has not been found often.

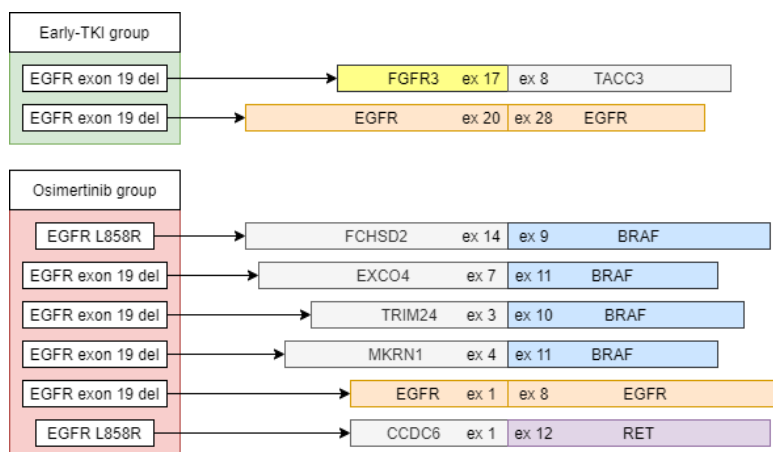


**Figure 4:** Fusions and exon-skipping events identified in RNA NGS. del, deletion; ex, exon; NGS, next-generation sequencing.

Several of the identified fusions and exon-skipping events (FGFR3, BRAF, RET) are potentially treatable by clinical trials or early access, off-label, or compassionate-use programs. Excluding RNA NGS from the standard EGFR TKI resistance workup completely will therefore result in missing potentially treatable resistance mechanisms in 4% of patients in the early TKI group and 10% of osimertinib patients, 8% overall. This percentage may be even higher in patients treated with first-line osimertinib because fusions have been found to be more prevalent in that group. [16]

#### 6.5.4 Challenge #3 Amplification detection

In this study, we screened for relevant amplifications with MET ISH and HER2 ISH and IHC, including DNA NGS copy number variation. MET ISH was performed in 282 cases, 88% of all cases overall. In 22 cases (7%), there was not enough tissue to complete the analysis, and in four cases (1%), the result was invalid. In the remaining 256 cases, MET amplification was identified in six cases (5%) in the early TKI group and in 17 cases (12%) in the osimertinib group. HER2 ISH was performed in 196 cases overall (62%). In 11 cases (3%), there was not enough tissue available and twice the ISH result was invalid (1%). In the 183 other cases, HER2 amplification was identified six times (8% of successful analyses) in the early TKI group and five times (5% of successful analyses) in the osimertinib group. ISH results for both MET and HER2 are summarized in Table 2.

<b>MET ISH</b>	<b>EARLY-TKI GROUP (N = 114)</b>	<b>OSIMERTINIB GROUP (N = 142)</b>	<b>P-VALUE</b>
NOT AMPLIFIED	108 (95%)	125 (88%)	0.12
LOW AMPLIFICATION (6-10 COPIES)	1 (1%)	2 (1%)	
HIGH AMPLIFICATION (>10 COPIES)	4 (4%)	11 (8%)	
HIGH AMPLIFICATION IN PART OF THE TUMOR CELLS (CLONAL HETEROGENEITY)	1 (1%)	4 (3%)	
<b>HER2 ISH</b>	<b>EARLY-TKI GROUP (N = 76)</b>	<b>OSIMERTINIB GROUP (N = 142)</b>	<b>P-VALUE</b>
NOT AMPLIFIED	70 (92%)	102 (95%)	0.53
LOW AMPLIFICATION (6-10 COPIES)	1 (1%)	3 (3%)	
HIGH AMPLIFICATION (>10 COPIES)	5 (7%)	2 (2%)	
HIGH AMPLIFICATION IN PART OF THE TUMOR CELLS (CLONAL HETEROGENEITY)	0	0	

**Table 2:** MET and HER2 in situ hybridization results per TKI treatment group. P-values are calculated by pooling all amplified cases and performing Fisher's exact test. Cases in which MET or HER2 ISH was not performed or was unsuccessful, were not included in this table.

Most MET and HER2 amplifications were identified with both ISH and DNA NGS. Nevertheless, several amplifications were exclusively detected with ISH. The results from cases that underwent both DNA NGS and ISH are outlined in Table 3. In the three cases in which DNA NGS detected copy number variation for MET, but ISH reported no amplifications, these were all due to polysomy, which was described in the MET ISH report. In the eight cases in which MET amplification was detected by ISH but missed in DNA NGS, this was due to one of the following four reasons: (1) the amplification was present only in part of the tumor cells (an example of which is provided in Fig. 5A–C) in three cases; (2) low tumor cell percentage or low DNA input in three cases; (3) low amplification (5–10 copies) in one case; and (4) decreased accuracy of the copy number analysis owing to a very high amplification in another gene in one case. Omitting MET ISH from the EGFR resistance workup would therefore have resulted in misdiagnosing (missing and overdiagnosing) MET amplifications in 4% of resistance biopsies.

<b>MET ISH</b>	<b>DNA NGS: NO AMPLIFICATION</b>	<b>DNA NGS: AMPLIFICATION</b>
----------------	----------------------------------	-------------------------------

NO AMPLIFICATION	224	3
AMPLIFICATION	8	13
<b>HER2 ISH</b>	<b>DNA NGS: NO AMPLIFICATION</b>	<b>DNA NGS: AMPLIFICATION</b>
NO AMPLIFICATION	167	0
AMPLIFICATION	2	7

**Table 3:** ISH and DNA NGS copy number analysis comparison. Several amplifications, both in HER2 and MET were exclusively identified via ISH, usually due to low tumor cell percentage, low amplification (fewer copies) or the amplification being present only in part of the tumor cells (clonal heterogeneity). Only cases with sufficient tissue for DNA NGS and MET ISH were included.

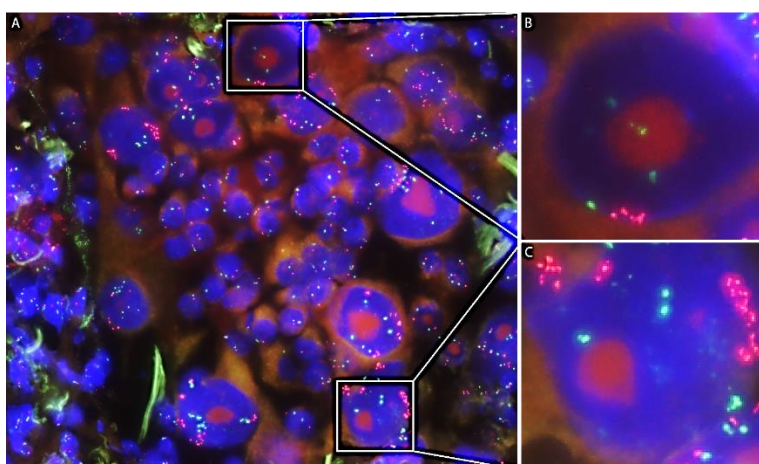


**Figure 5:** MET amplification ISH, cytology specimen. Red dots: MET probes; green dots: centromere 7 probes. In several tumor cells, the MET:centromere 7 ratio is greater than 10, but in other tumor cells, this ratio is 1. Overall, the MET-amplified tumor cells were a minority in this slide (approximately 25% of tumor cells), and the MET amplification was therefore not detected with NGS. (A) ISH overview. (B) Tumor cell without MET amplification, close-up. (C) Tumor cell with high (>10 copies) MET amplification, close-up. ISH, in situ hybridization; NGS, next-generation sequencing.

For HER2, all amplifications detected with DNA NGS were also detected with ISH, but two amplifications (22%) were exclusively found by ISH. In both cases, a low amplification (6–10 copies) was identified in ISH, which was missed in DNA NGS, even though the tumor cell percentage was adequate (50% and 80%). Omitting HER2 ISH from the EGFR resistance workup would therefore have resulted in missing HER2 amplification in 1% of the cases, which constitutes 22% of all HER2 amplifications.

Several amplifications, both in HER2 and MET, were exclusively identified by ISH, usually owing to low tumor cell percentage, low amplification (fewer copies), or the amplification being present only in part of the tumor cells (clonal heterogeneity). Only cases with sufficient tissue for DNA NGS and MET ISH were included.

HER2 IHC and HER2 ISH were both performed in 180 cases. The results for these cases are outlined in Table 4. All cases in which ISH identified an amplification had high HER2 expression (3+). Omitting either HER2 ISH or HER2 IHC therefore would not have resulted in misdiagnosing any HER2 amplifications.

	IHC: 0	IHC: 1+	IHC: 2+	IHC: 3+
ISH: 0-5 COPIES	105	52	13	0
ISH: 6-10 COPIES	0	0	0	4
ISH: >10 COPIES	0	0	0	6

**Table 4:** HER2 *in situ* hybridization (ISH) versus HER2 immunohistochemistry (IHC).

#### 6.5.5 Challenge #4 Tissue scarcity

In DNA NGS, 12 cases were of insufficient quality for a complete analysis (4%). This was true for 24 cases (18%) of all attempted RNA NGS analyses. MET ISH was not possible in 26 cases (9% of all attempts); for HER2 ISH, this was 13 cases (7% of all attempted HER2 ISH); and for HER2 IHC, seven cases (3% of all attempts). This is a relatively low dropout, compared with the results from hybrid capture NSCLC studies in literature [33] or WGS. There was no clear correlation between dropout and specimen type or biopsy site.

#### 6.5.6 Challenge #5 Comparison with pre-treatment biopsy

All resistance biopsies underwent morphologic examination by pulmonary pathologists. In several cases, transformation to another morphologic phenotype was observed. In the early TKI group, small-cell transformation was observed twice (1%) and squamous transformation once (1%). In the osimertinib group, five cases transformed to a small-cell phenotype (3%) and two to a squamous phenotype (1%).

In 28 cases (9%), molecular comparison to the pretreatment biopsy was not optimal. This was often due to the use of small (circulating tumor)DNA NGS

panels on the pretreatment biopsy, which do not cover amplifications and fusions. In this setting, it is difficult to determine which molecular alterations were novel compared with the pretreatment biopsy, especially in second-line osimertinib cases. These 28 cases were therefore excluded from the mutation prevalence analyses in this study.

#### 6.5.7 Loss of T790M after osimertinib

A total of 84 cases harbored a T790M mutation on start of osimertinib treatment. In 47 of those cases, the T790M mutation was not identified anymore in the post-osimertinib resistance biopsy (54%). The T790M mutation was lost significantly more often ( $p = 0.045$ ) in cases without a new resistance mechanism, as illustrated in Table 5.

	LOSS OF T790M	T790M NOT LOST	P-VALUE
TREATMENT TIME	452	595	0.07 <sup>b</sup>
AGE	66	59	0.002 <sup>b</sup>
SMOKING PACKYEARS	5.5	3.5	0.43 <sup>b</sup>
<b>SMOKING HISTORY</b>			0.11 <sup>a</sup>
NEVER-SMOKER	27	28	
EVER-SMOKER	20	9	
<b>NEW RESISTANCE MECHANISM</b>			0.045 <sup>a</sup>
NO RESISTANCE MECHANISM	25	11	
NEW RESISTANCE MECHANISM	22	26	

**Table 5:** loss of T790M and detection of new resistance mechanisms. P-values were calculated with Fisher's exact test (a) and independent t-test (b).

#### 6.5.8 Acquired driver mutations

In 110 cases (36% of successful analyses), new driver mutations (which were not present in the pre-TKI biopsy) were discovered in the resistance biopsy, whereas in 14 cases (5%), a previously present driver mutation was not identified anymore. The meaning of this remains unknown. Patients with new driver mutations were not different in age, treatment time, smoking status, pack-years, or TKI treatment group.

## 6.6 Discussion

In this study, we analyzed the molecular findings of 320 biopsy specimens submitted for EGFR TKI resistance in three different hospitals. Acquired resistance mechanisms were identified in 54% of all cases by DNA NGS, RNA NGS, MET ISH, HER2 ISH, and HER2 IHC. Each additional molecular test had a substantial yield: omitting RNA NGS would lead to misdiagnosis in 8% of cases, MET ISH in 4%, and HER2 ISH and IHC in 1%.

By comparing the results from these assays, we illustrated how clonal heterogeneity can decrease the sensitivity of DNA NGS, especially for amplifications and in cases with a low tumor cell percentage. We revealed that clonal heterogeneity frequently occurs in EGFR TKI-resistant NSCLC, and that it may lead to problematic discrepancies between DNA NGS and ISH. Furthermore, we proved that acquired resistance mechanisms for EGFR TKIs are not always mutually exclusive, both in the early TKI group (co-occurring mechanisms in 9%) and in the osimertinib group (co-occurring mechanisms in 6%).

Owing to clonal heterogeneity and the co-occurrence of acquired resistance mechanisms, performing a parallel workup that includes DNA NGS, RNA NGS, MET ISH, and HER2 ISH or IHC is the most sensitive and most comprehensive option for molecular diagnostics in the setting of a routine EGFR TKI resistance biopsy (Figure 6A). Nevertheless, the added benefit of RNA NGS is limited for cases in which a “strong” resistance mechanism has already been identified with DNA NGS, MET ISH, and HER2 ISH or IHC: in this study, 0 case harbored an additional fusion or exon-skipping event, and observations in the literature are limited. In practice, however, there are several arguments that favor a parallel approach. First, with different types of tissue (FFPE blocks, cytology smears, cytology blocks, and combinations thereof) that are presented, logistics are challenging not only for requesting pathologists but also for the laboratory. Second, a parallel workup is tissue efficient, and third, when the tumor progresses, you can compare results of the analysis of that biopsy with a full analysis. Nevertheless, if substantial concerns exist with regard to tissue exhaustion (when DNA and RNA are isolated in separate steps), financial feasibility, or lack of capacity to perform the tests, it is justifiable to opt for a sequential approach, in which DNA NGS, MET ISH, HER2 ISH, or IHC is

performed, and additional RNA NGS is performed in case no resistance mechanisms or only PIK3CA or EGFR amplification is identified (Figure 6B). Nevertheless, it should be noted that this sequential approach takes longer, which can be problematic for patients, and the risk of missing relevant fusions—however small—is likely not 0%, as resistance mechanisms may co-occur.

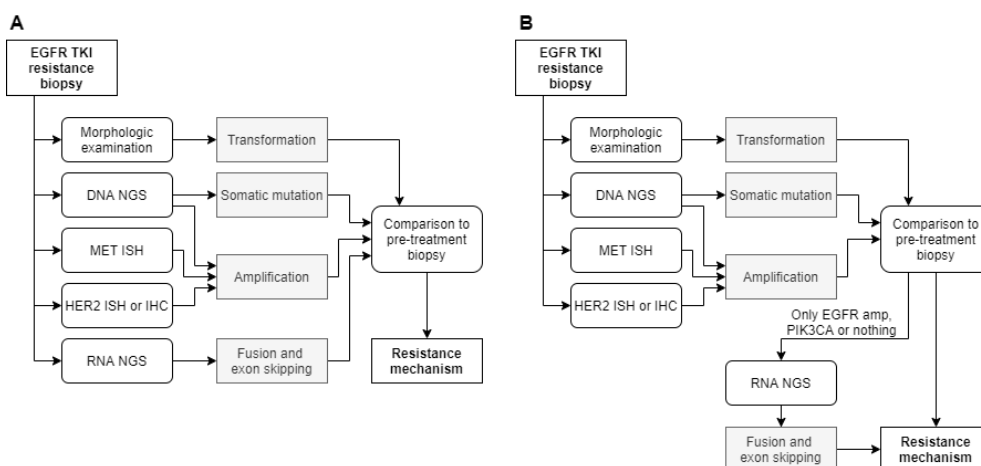


**Figure 6:** Summary of recommendations for EGFR TKI resistance screening. (A) Parallel approach, safest option. (B) Sequential approach, preferred when limited tissue or financial feasibility is an issue. amp, amplification; IHC, immunohistochemistry; ISH, in situ hybridization; NGS, next-generation sequencing; TKI, tyrosine kinase inhibitor.

Either HER2 ISH or IHC can be used; they are equally accurate for detecting HER2 amplifications. The dropout of this approach is relatively low, especially compared with large hybrid capture panels<sup>33</sup> and WGS, which might become the preferred method in the future, when technological advancements reduce the dropout rates, which are especially high when using small biopsies and cytology material. The low dropout rate in this study is in part due to the isolation method: isolating total nucleic acid and splitting in RNA and DNA later is a meaningful step in the EGFR resistance workup, as described. [32]

A potential limitation of this study, owing to the retrospective and “real world” nature, is that most patients in the osimertinib group were treated with osimertinib as a second, third, or even fourth treatment line. Nevertheless, because osimertinib is now approved for first-line treatment, most patients in the future will present with first-line osimertinib resistance. Literature suggests

that the mutations found in first-line osimertinib resistance are comparable with those in second-line osimertinib resistance, but with more fusions and exon-skipping events. [20] If that is true, our recommendations for a diagnostic sequence will still be applicable, and the yield of RNA NGS will even be higher. In addition, owing to the “real world” nature of our research, our cohort is different from previously described registration-trial cohorts with regard to inclusion criteria and resistance mechanism prevalence. [4, 34]

Another potential limitation is the variation between laboratories. Although each laboratory in this study had a similar NEN-EN-ISO 15189 accreditation and approach, and panels overlapped substantially, there might still have been subtle differences. We believe that a more uniform approach could benefit future patients with cancer and streamline communication between laboratories.

Owing to the retrospective nature of this study and currently lacking of robust recommendations for molecular diagnostics after EGFR TKI resistance, not all molecular tests were performed for all cases in this study. Especially the number of cases tested for RNA NGS was limited.

Another caveat is the clinical benefit of screening for acquired resistance mechanisms after EGFR TKI resistance. Robust proof that screening for these mutations actually improves survival is still lacking. Nevertheless, owing to the rapidly changing landscape of targeted treatment options and swift accessibility by trials, compassionate-use, and early access programs, we assume that screening for these acquired resistance mechanisms will become an important requirement. In our cohort, patients were frequently included in a clinical trial when a resistance mechanism was identified.

Many biopsy specimens in this study revealed a loss of T790M or had acquired a new driver mutation during the TKI treatment. The clinical consequences of these findings are unknown and should be investigated further. Ultimately, we like to discover whether this is a sign of tumor dedifferentiation or therapy-induced selection and has any (progression-free) survival consequences.

The aim of this study was to recommend the most optimal molecular diagnostic sequence for the EGFR TKI resistance setting. In 54% of all EGFR resistance biopsies, we were able to identify a resistance mechanism with our molecular diagnostics sequence. Although mechanisms of acquired resistance

might be discovered in the future, our approach (combining DNA NGS, RNA NGS, MET ISH, HER2 ISH, or HER2 IHC) is currently the most comprehensive and safest option for patients with acquired resistance to EGFR TKIs.

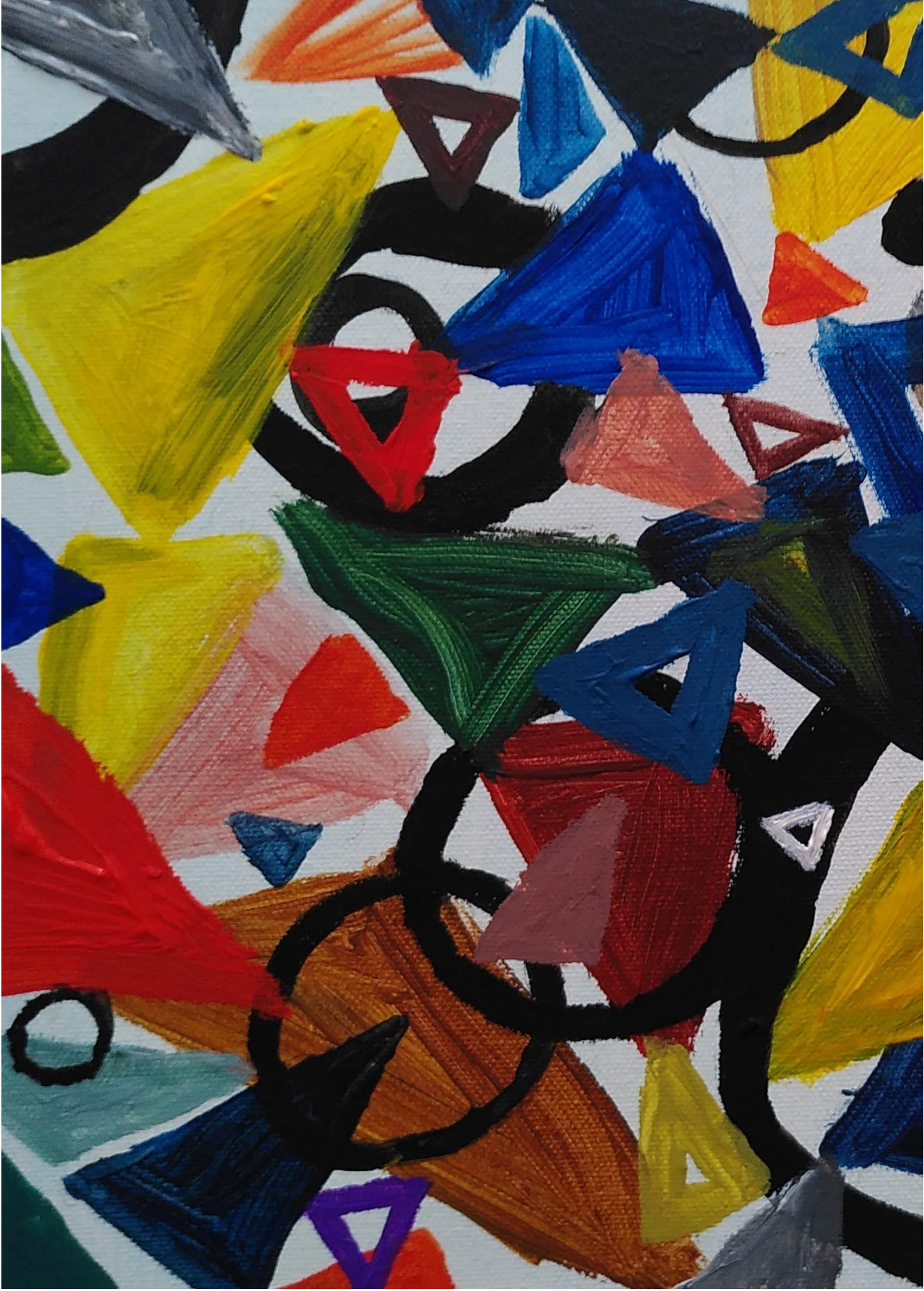
## References

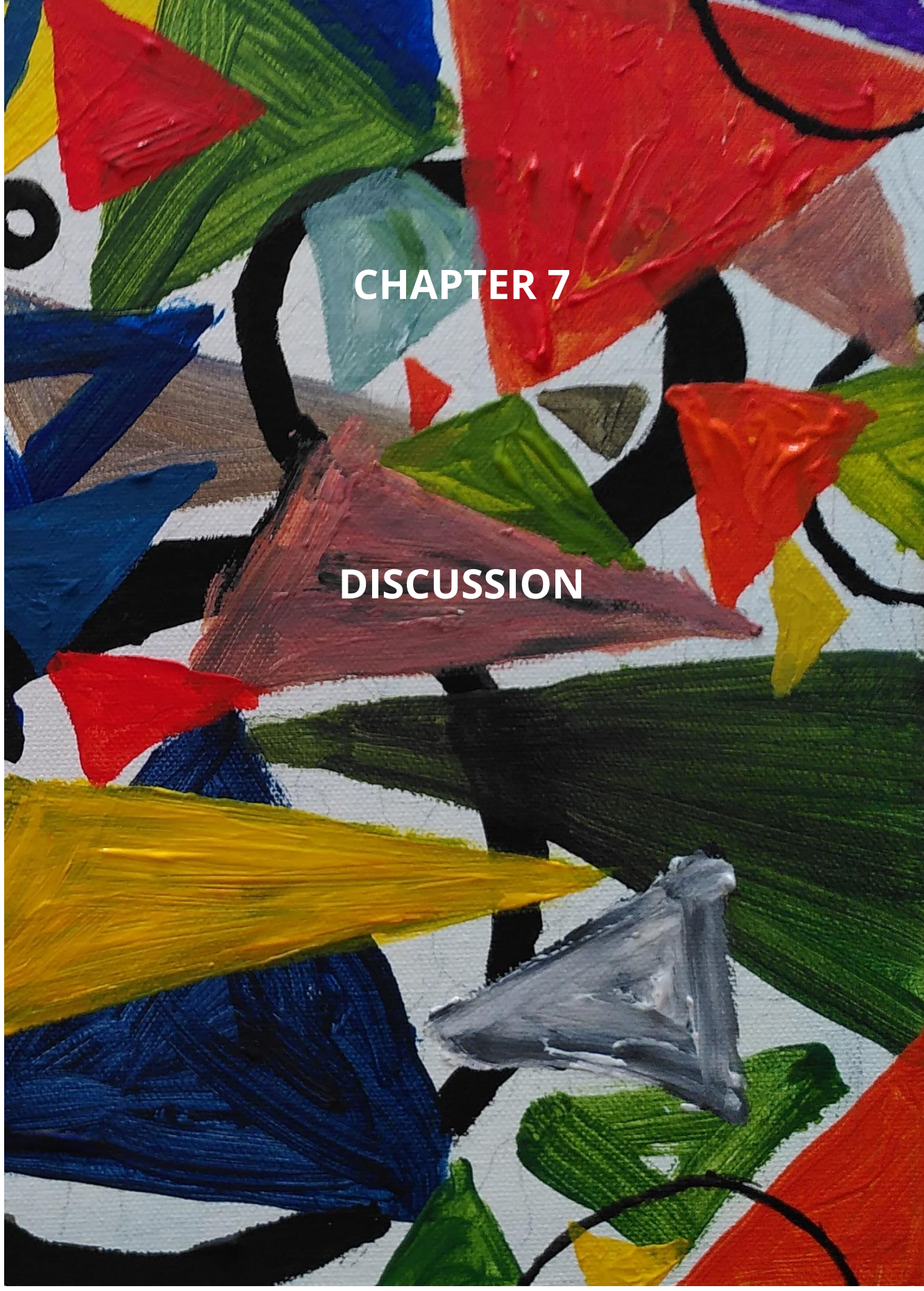
1. The Cancer Genome Atlas Research Network, *Comprehensive molecular profiling of lung adenocarcinoma*. *Nature*, 2014. **511**: p. 543-550.
2. Cappuzzo F, Ciuleano T, Stelmakh L, et al., *Erlotinib as maintenance treatment in advanced non-small-cell lung cancer: a multicentre, randomised, placebo-controlled phase 3 study*. *The Lancet Oncology*, 2010. **11**(6): p. 521-529.
3. Lynch TJ, Bell DW, Sordella R, et al., *Activating mutations in the epidermal growth factor receptor underlying responsiveness of non-small-cell lung cancer to gefitinib*. *N Engl J Med*, 2004. **350**: p. 2129-39.
4. Mok TS, Wu YL, Ahn M, et al., *Osimertinib or Platinum-Pemetrexed in EGFR T790M-Positive Lung Cancer*. *N Engl J Med*, 2017. **376**(7): p. 629-640.
5. Kobayashi S, Boggon TJ, Dayaram T, et al., *EGFR mutation and resistance of non-small-cell lung cancer to gefitinib*. *N Engl J Med*, 2005. **352**: p. 786-92.
6. Yu HA, Arcila ME, Rekhtman N, et al., *Analysis of tumor specimens at the time of acquired resistance to EGFR-TKI therapy in 155 patients with EGFR-mutant lung cancers*. *Clin Cancer Res*, 2013. **19**(8): p. 2240-7.
7. Sequist LV, Waltman BA, Dias-Santagata D, et al., *Genotypic and histological evolution of lung cancers acquiring resistance to EGFR inhibitors*. *Sci Transl Med*, 2011. **3**(75).
8. Bean J, Brennan C, Shih J, et al., *MET amplification occurs with or without T790M mutations in EGFR mutant lung tumors with acquired resistance to gefitinib or erlotinib*. *Proc Natl Acad Sci U S A.*, 2007. **104**(52): p. 20932-7.
9. Westover D, Zugazagoitia J, Cho BC, et al., *Mechanisms of acquired resistance to first- and second-generation EGFR tyrosine kinase inhibitors*. *Ann Oncol*, 2018. **29**: p. 10-19.
10. Balak MN, Gong Y, Riely GJ, et al., *Novel D761Y and common secondary T790M mutations in epidermal growth factor receptor-mutant lung adenocarcinomas with acquired resistance to kinase inhibitors*. *Clin Cancer Res*, 2006. **12**: p. 6494-501.
11. Costa DB, Schumer ST, Tenen DG, et al., *Differential responses to erlotinib in epidermal growth factor receptor (EGFR)-mutated lung cancers with acquired resistance to gefitinib carrying the L747S or T790M secondary mutations*. *J Clin Oncol*, 2008. **26**(7): p. 1182-4.
12. Bean J, Riely GJ, Balak M, et al., *Acquired resistance to epidermal growth factor receptor kinase inhibitors associated with a novel T854A mutation in a patient with EGFR-mutant lung adenocarcinoma*. *Clin Cancer Res*, 2008. **14**(22): p. 7519-25.
13. Zhong J, Li L, Wang Z, et al., *Potential Resistance Mechanisms Revealed by Targeted Sequencing from Lung Adenocarcinoma Patients with Primary Resistance to Epidermal Growth Factor Receptor (EGFR) Tyrosine Kinase Inhibitors (TKIs)*. *J Thorac Oncol*, 2017. **12**(12): p. 1766-1778.
14. Nagano T, Tachihara M, Nishimura Y, *Mechanism of Resistance to Epidermal Growth Factor Receptor-Tyrosine Kinase Inhibitors and a Potential Treatment Strategy*. *Cells*, 2018. **7**: p. 212.
15. Kosaka T, Yatabe Y, Endoh H, et al., *Analysis of epidermal growth factor receptor gene mutation in patients with non-small cell lung cancer and acquired resistance to gefitinib* *Clin Cancer Res*, 2006. **1**(19): p. 5764-9.

16. Xu H, Shen J, Xiang J, et al., *Characterization of acquired receptor tyrosine-kinase fusions as mechanisms of resistance to EGFR tyrosine-kinase inhibitors*. *Cancer Manag Res*, 2019. **11**: p. 6343-6351.
17. Del Re M, Tiseo M, Bordi P, et al., *Contribution of KRAS mutations and c.2369C > T (p.T790M) EGFR to acquired resistance to EGFR-TKIs in EGFR mutant NSCLC: a study on circulating tumor DNA*. *Oncotarget*, 2017. **8**(8): p. 13611-13619.
18. Suda K, Murakami I, Katayama T, et al., *Reciprocal and complementary role of MET amplification and EGFR T790M mutation in acquired resistance to kinase inhibitors in lung cancer*. *Clin Cancer Res*, 2010. **16**(22): p. 5489-98.
19. Izumi H, Yamasaki A, Ueda Y, et al., *Squamous Cell Carcinoma Transformation from EGFR-mutated Lung Adenocarcinoma: A Case Report and Literature Review*. *Clinical Lung Cancer*, 2018. **19**(1): p. e63-e66.
20. Leonetti A, Sharma S, Minari R, et al., *Resistance mechanisms to osimertinib in EGFR-mutated non-small cell lung cancer*. *Br J Cancer*, 2019. **121**: p. 725-737.
21. Le X, Puri S, Negrao MV, et al., *Landscape of EGFR-Dependent and -Independent Resistance Mechanisms to Osimertinib and Continuation Therapy Beyond Progression in EGFR-Mutant NSCLC*. *Clin Cancer Res*, 2018. **24**(24): p. 6195-6203.
22. Yang Z, Yang N, Ou Q, et al., *Investigating Novel Resistance Mechanisms to Third-Generation EGFR Tyrosine Kinase Inhibitor Osimertinib in Non-Small Cell Lung Cancer Patients*. *Clin Cancer Res*, 2018. **24**(13): p. 3097-3107.
23. Oxnard GR, Hu Y, Mileham KF, et al., *Assessment of Resistance Mechanisms and Clinical Implications in Patients With EGFR T790M-Positive Lung Cancer and Acquired Resistance to Osimertinib*. *JAMA Oncol*, 2018. **4**(1527-1534).
24. Piotrowska Z, Isozaki H, Lennerz JK, et al., *Landscape of Acquired Resistance to Osimertinib in EGFR-Mutant NSCLC and Clinical Validation of Combined EGFR and RET Inhibition with Osimertinib and BLU-667 for Acquired RET Fusion Cancer*. *Discov*, 2018. **12**: p. 1529-1539.
25. Chabon JJ, Simmons AD, Lovejoy AF, et al., *Circulating tumour DNA profiling reveals heterogeneity of EGFR inhibitor resistance mechanisms in lung cancer patients*. *Nat Commun*, 2016. **7**: p. 11815.
26. La Monica S, Cretella D, Bonelli M, et al., *Trastuzumab emtansine delays and overcomes resistance to the third-generation EGFR-TKI osimertinib in NSCLC EGFR mutated cell lines*. *J Exp Clin Cancer Res*, 2017. **36**(1): p. 174.
27. van Eijk R, Stevens L, Morreau H, van Wezel T, et al., *Assessment of a fully automated high-throughput DNA extraction method from formalin-fixed, paraffin-embedded tissue for KRAS, and BRAF somatic mutation analysis*. *Exp Mol Pathol*, 2013. **94**(1): p. 121-125.
28. Wu YL, Cheng Y, Zhou J, et al., *Tepotinib plus gefitinib in patients with EGFR-mutant non-small-cell lung cancer with MET overexpression or MET amplification and acquired resistance to previous EGFR inhibitor (INSIGHT study): an open-label, phase 1b/2, multicentre, randomised trial*. *Lancet Respir Med*, 2020. **8**(11): p. 1132-1143.
29. Zhao J and Y Xia, *Targeting HER2 Alterations in Non-Small-Cell Lung Cancer: A Comprehensive Review*. *JCO Precision Oncology*, 2020(4): p. 411-425.

30. Cerami E, Gao J, Dogrusoz U, et al., *The cBio Cancer Genomics Portal: An Open Platform for Exploring Multidimensional Cancer Genomics Data*. *Cancer Discovery*, 2012. **2**(5): p. 401.
31. Gao J, Aksoy BA, Dogrusoz U, et al., *Integrative analysis of complex cancer genomics and clinical profiles using the cBioPortal*. *Sci Signal*, 2013. **6**(269): p. p11.
32. Cohen D, Hondelink LM, Solleveld-Westerink N, et al., *Optimizing Mutation and Fusion Detection in NSCLC by Sequential DNA and RNA Sequencing*. *J Thorac Oncol*, 2020. **15**(6): p. 1000-1014.
33. Benayed R, Offin M, Mullaney K, et al., *High Yield of RNA Sequencing for Targetable Kinase Fusions in Lung Adenocarcinomas with No Mitogenic Driver Alteration Detected by DNA Sequencing and Low Tumor Mutation Burden*. *Clin Cancer Res*, 2019. **25**: p. 4712-4722.
34. Soria JC, Ohe Y, Vansteenkiste J, et al., *Osimertinib in Untreated EGFR-Mutated Advanced Non-Small-Cell Lung Cancer*. *N Engl J Med*, 2017. **378**(2): p. 113-125.





An abstract painting featuring a variety of colors and textures. The composition is dominated by large, expressive brushstrokes in shades of red, green, blue, yellow, and black. There are also several triangular shapes in various colors, including red, orange, yellow, and grey. The background is a mix of white and light grey, with some darker areas. The overall style is dynamic and energetic, with a focus on color and form.

**CHAPTER 7**

**DISCUSSION**

# Chapter 7: Discussion, summary and future challenges

## 7.1 A typical NSCLC patient journey

In the Introduction, a case was described, in which a patient presents with an asymptomatic pulmonary node. (Figure 1) What we can draw from this case is that lung cancer, even in relatively low stages, can have a detrimental and malignant course. Pathologists are prominently involved in the diagnostics and management of NSCLC, as they provide the crucial information in the key treatment decision-making moments.

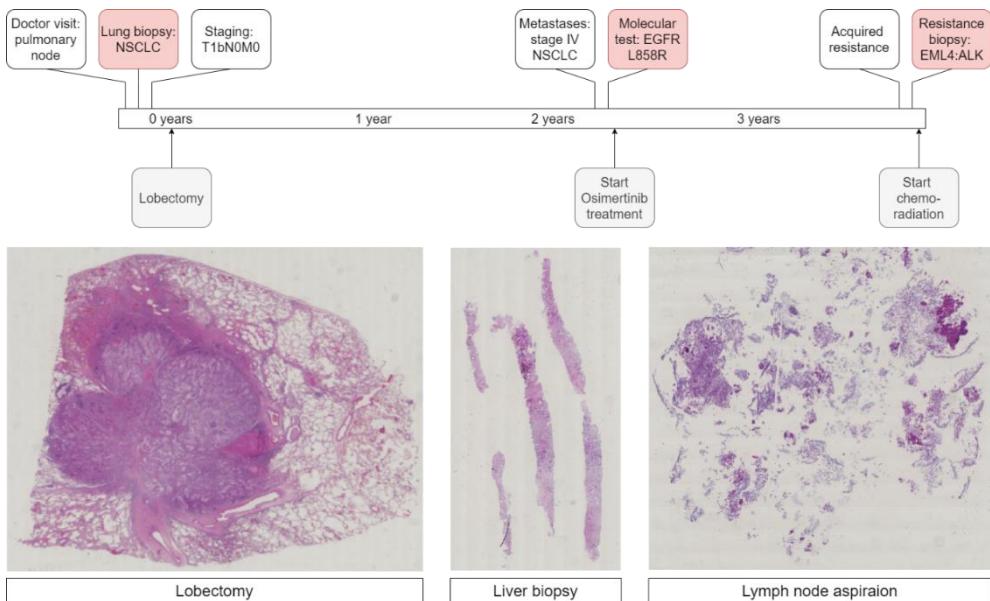


**Figure 1:** Key decision making moments for pathologists in the NSCLC patient journey.

## 7.2 The optimal diagnostic work-up at key decision-making moments in NSCLC: a pathologists' dilemma

If one thing has become clear from both this thesis and the literature on NSCLC, it's that NSCLC is an incredibly heterogeneous, many-faced and deadly disease. No two lung tumors are exactly the same, which is no small feat, as the volume of NSCLC patients is so enormous. A wide variance exists with regard to age, smoking history, tumor grade, TNM-stage, oncogenic driver

mutation, co-mutations, PD-L1 score, anti-tumor immune response, resistance mechanisms, metastatic behavior, treatment response and prognosis. This makes personalizing the diagnosis and management of lung cancer crucial – but also highly complex.

In this thesis, we investigated three key decision-making moments for pathologists in NSCLC: early stage diagnosis (1), late stage diagnosis (2) and acquired *EGFR* TKI resistance (3). We provide a rationale for molecular and immunohistochemical testing sequences at each instance, while taking into account the challenges: tissue scarcity, time constraints, costs of testing and comprehensiveness. Below, we address each of these key decision-making moments, including the specific challenges that a modern day pathologist needs to balance carefully.

### 7.2.1 Key decision making moment 1: Early stage diagnosis

The workup for early stage NSCLC initially did not typically include NGS or IHC. However, with (neo-)adjuvant immunotherapy and adjuvant Osimertinib around the corner, that limited workup is about to change. Additionally, the number of early stage patients will rise in the years to come, due to the imminent implementation of targeted population screening for NSCLC, following data from the NELSON-trial. [1]

With the transition of targeted and immunotherapeutic therapies to the (neo-)adjuvant setting, early stage NSCLC diagnostics will thus become more similar to the treatment-naïve stage IV workup. While this transition to (neo-)adjuvant treatment is ongoing, it's important to take note of how frequent targets occur in early stage tumors, and how these patients and tumors differ from the late stage variants. In **Chapter 2**, we identified *EGFR* mutations in 13% of tumors in stage IIIA or lower, whereas this was 9% in stage IIIB and IV. Especially the earliest stages (stage 0 and stage IA) were enriched for *EGFR* mutations (27% and 18% respectively).

Additionally, as illustrated in **Chapter 2**, there are substantial differences between early stage *EGFR*-mutated and late stage *EGFR*-mutated cancers, including type of *EGFR* mutation, co-mutations, growth pattern and smoking history. This underlines the complex heterogeneity of lung adenocarcinoma, and is an argument in favor of developing comprehensive multi-factorial risk assessment tools instead of current 'one size fits all' protocols.

## 7.2.2 Key decision making moment 2: Late stage diagnosis

In the treatment-naïve stage IV setting, patients need to be screened for PD-L1 expression and targetable mutations. However, with the growing list of targetable mutations, multiple challenges arise: choosing the correct molecular panel, the role of immunohistochemistry for fusion detection, and PD-L1 expression scoring. Each is discussed separately below.

### 7.2.2.1 Molecular diagnostics in stage IV NSCLC

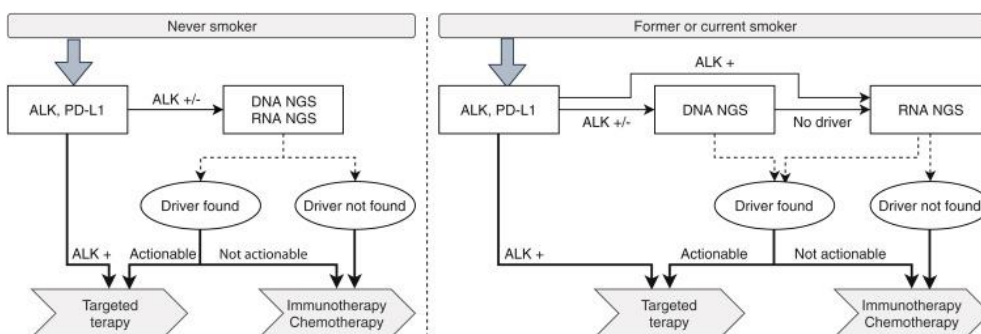
All relevant targets need to be covered by the molecular workup. This seems simple, but in the past years, the number of actionable targets has risen constantly, and will continue to do so. A small targeted panel which only includes targetable alterations, will need to be adjusted with every new target, and is therefore not future-proof. In addition, there are many targets for which an experimental TKI is available via clinical trials, compassionate use or early access programs. Those targets are not officially 'actionable', but finding them can still be worthwhile for individual patients. In addition, selected co-mutations (such as *TP53* and *STK11* – as discussed in **Chapter 2** and **Chapter 6**) are relevant to identify as well, as they can be indicative of the malignant potential and therapy resistance.

The molecular screening in stage IV should thus at least cover (1) the eight currently targetable targets: *EGFR*, *BRAF*, *HER2*, *ALK*, *ROS1*, *RET*, *NTRK* and *MET*; (2) targets for which clinical trials exist, such as *KRAS* G12C and *NRG1*; (3) clinically relevant co-mutations, such as *STK11* and *TP53*. In practice, this means that each specimen should be tested for point mutations, deletions, insertions, amplifications, exon skipping and fusions. Most of these alterations can be detected with small, targeted DNA NGS panels, but for exon skipping and fusion detection, broad DNA NGS panels (such as WGS) or targeted RNA NGS is required.

A major issue with choosing the optimal molecular diagnostics sequence in stage IV is tissue scarcity. In 30% of the treatment-naïve stage IV patients, as discussed in **Chapter 3**, the entire workup needs to be performed on a (small) cytology specimen, often acquired via endoscopic lymph node fine needle aspiration, with a limited number of tumor cells. With broader panels, a higher DNA input is required, which can thus be challenging in these small biopsies and cytology. Taking a new biopsy, with risk of co-morbidity, causes substantial

diagnostic delay, and must be prevented as much as possible. Based on the **Chapter 3** data, we therefore recommend performing targeted DNA NGS first, followed by RNA NGS when no driver is identified. In never-smokers, fusions are far more prevalent (32% of cases, **Chapter 3**) compared to current and former smokers (4% of cases). Therefore, RNA NGS is more relevant for never-smokers, and it should be performed immediately, not only after DNA NGS is driver-negative. (Figure 2) Both of these workups proved relatively tissue-efficient, while covering all required targets.

**Figure 2:** Stage IV NSCLC workup, separate for never-smokers and smokers. (Chapter 3)



### 7.2.2.2 Immunohistochemistry for fusion detection

An exception to the multi-target approach in the molecular stage IV workup is *ALK*. Since *ALK* immunohistochemistry is highly sensitive and specific for *ALK* fusions, fast pre-screening with *ALK* IHC is defensible, and sometimes reduces the turnaround time with several days.

The same exception that can be made for *ALK* immunohistochemistry is not applicable to *NTRK* and *ROS1*. Whereas *ALK* IHC is highly sensitive and specific, *ROS1* IHC has problematic false-positivity (as demonstrated in **Chapter 3**) and *NTRK* IHC – as described in **Chapter 5** – false-negativity and false-positivity. A sequential approach, with pan-TRK immunohistochemistry first and confirming positive cases with RNA NGS, would result in missing 18% of actionable *NTRK* fusions.

### 7.2.2.3 PD-L1 immunohistochemistry

Being the companion biomarker for immunotherapy, the immunohistochemical PD-L1 expression score is mandated in all stage IV

NSCLC workups. However, pathologists should recognize the flaws that this biomarker intrinsically harbors. There is substantial inter- and intraobserver variance around the cutoff point, and PD-L1 expression does not predict response to immunotherapy perfectly – some PD-L1-high patients fail to respond and vice versa. Unfortunately, the search for alternative, more reliable biomarkers has not yet been successful.

Part of the current scientific effort is directed at improving PD-L1 as a biomarker, by reducing interobserver variability and overcoming human scoring bias. In **Chapter 4**, it was demonstrated that automated deep learning algorithms can be reliable, and potentially valuable as a scoring assistant in difficult cases around the 50% cutoff point. As inter- and intraobserver variance is an issue for pathologists in several tasks (Ki67, nuclear grade, Gleason score, ER-expression, etc.), automated, computer-mediated scoring, comparable to PD-L1 scoring as described in **Chapter 4**, could very well be implemented more widely in the near future.

### 7.2.3 Key decision making moment 3: Acquired TKI resistance

With the recent introduction of TKIs into routine NSCLC treatment regimens, pathologists were confronted with a new problem: how to find the resistance mechanism in acquired resistance biopsies? Resistance biopsies – like stage IV biopsies – generally don't contain an abundance of tumor cells, but need to be tested for a wide range of targets. Known resistance mechanisms include: small cell transformation, squamous transformation, *EGFR*, *HER2*, *MET*, *KRAS*, *BRAF*, *PIK3CA*, *ALK*, *RET*, *FGFR*, *ROS1*, *NTRK* and *MET*. The landscape of genomic alterations after TKI resistance thus bears some similarity to the treatment-naïve workup. An important difference however is the clonal heterogeneity in resistance biopsies, which leads to non-mutual exclusivity of resistance mechanisms and impaired amplification detection.

Whereas oncogenic driver mutations such as *BRAF* and *EGFR* are mutually exclusive in treatment-naïve tumors, resistance mechanisms co-occur in resistance biopsies, in at least 7% of cases. A sequential approach, with RNA NGS only when no driver is identified in DNA NGS, as recommended in the treatment-naïve setting, is therefore not comprehensive in resistance biopsies, as resistance mechanisms may co-occur. However, it must be noted that co-occurrence of fusions and exon skipping events with other resistance

mechanisms (except *EGFR* amplification and *PIK3CA*) is rare, so omitting RNA NGS in selected cases could be defensible in case of logistical, tissue-quantity or financial constraints.

Due to clonal heterogeneity, amplification detection with DNA NGS is impaired, as DNA NGS is heavily dependent on the tumor cell percentage for copy number analysis. When not all tumor cells harbor the amplification or the tumor cell percentage is low, the copy number can be underestimated, leading to the missing of amplifications. *MET* and *HER2* amplifications are among the most frequently occurring and (experimentally) targetable resistance mechanisms, so missing those amplifications is not optimal. Our data in **Chapter 6** shows that up to 30% of *HER2* and *MET* amplifications are missed by DNA NGS in the acquired resistance setting. It's therefore important to use additional *MET* and *HER2* testing in resistance biopsies, with *MET* ISH and *HER2* IHC or ISH.

The complete *EGFR* TKI workup therefore includes: morphologic examination, DNA NGS, RNA NGS, *HER2* ISH or IHC and *MET* ISH. (Figure 3)

### 7.3 Future challenges

Although the recommendations throughout this thesis are helpful for choosing the optimal workup in the current NSCLC landscape at key decision-making moments, there is still room for improvement in the treatment and management of future NSCLC patients. Even with the combined research effort of the past decades, most NSCLC patients still die and we still have insufficient knowledge on the biologic mechanisms underlying disease behavior. There are important scientific lacunae that we will need to cover in the coming years, including a different approach to patient risk stratification, improving molecular methods and prevention.

#### 7.3.1 Improved risk stratification

Currently, up to 50% of patients who undergo 'curative' surgical resection die of lung cancer, including the patient in our case at the beginning of this Chapter. This is likely due to the presence of micro-metastases at the time of surgery, which are not detected during routine staging. Current risk assessment in the clinic is based solely on TNM-stage, which is shown to be a relatively poor predictor. A large number of potential biomarkers for

metastasis after surgery have been described already, for example histological differentiation, pleural invasion and specific mutations. [2] However, none of these biomarkers provide a perfect prognostication, and the search for novel and more integrated biomarkers is still ongoing.

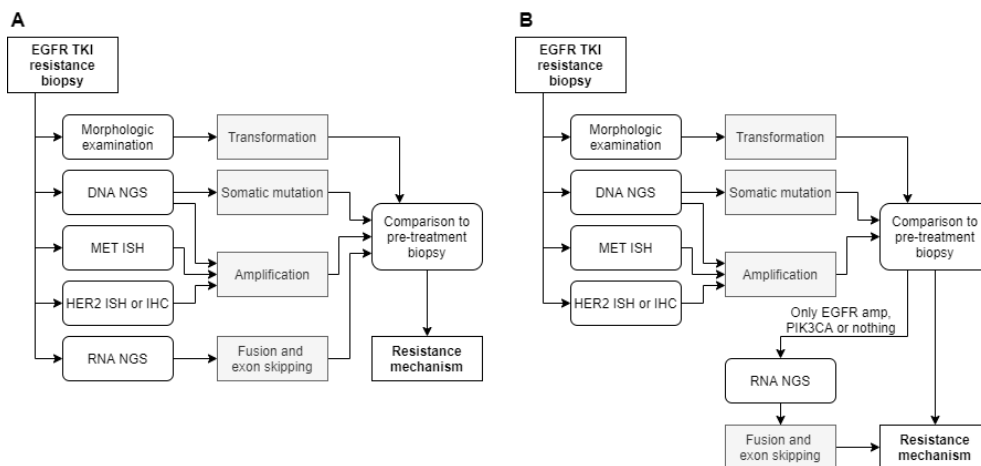


**Figure 3:** Recommended workup for EGFR TKI resistance biopsy testing. (Chapter 6)  
*A: Recommended, comprehensive workup. B: Alternative workup in case of logistical, tissue-quantity or financial constraints.*

Another main challenge that will hopefully be solved in the near future is the selection of patients for immunotherapy. Although some patients respond excellent to immunotherapy, other patients respond barely, or only for a short amount of time. PD-L1 and tumor mutational burden (TMB) are established biomarkers for response, but imperfect ones – some patients with a low PD-L1 and TMB respond remarkably well, and vice versa. Additionally, there is substantial variability between pathologists in PD-L1 assessment and between laboratories in the TMB assessment. An urgent need for novel, better biomarkers for immunotherapy response therefore exists. In recent years, several promising biomarkers have emerged, for example CD8+ tumor infiltrating T-cells, or the presence of tertiary lymphoid structures, [3, 4] but real treatment implications for NSCLC patients are still far away.

In the TKI-treated NSCLC patients, specifically Osimertinib, there is a wide variety in progression-free survival between patients. If we would know in advance what the expected time to resistance would be, treatment and follow-up regimens could be specifically tailored to suit individual patients. This could

potentially reduce the burden of regular screening, give rise to novel treatment innovations, and improve quality of care.

What all these risk stratification problems all have in common is their complex, multi-factorial nature. If we can draw any conclusions from the past decades of cancer research, it's that lung cancer is an incredibly complex, many-faced, capricious disease. Current-day biomarkers such as TNM attempt to simplify all of these biological factors into one biomarker. This approach, although ambitious and hopeful, neglects the incredible complexity and heterogeneity of the biochemical processes that make up the tumor behavior. Any single biomarker is thus by definition a poor representation and it's naive to expect an accurate response prediction from it.

As illustrated by the problems discussed above, there is an urgent clinical need for more comprehensive, multi-factor biomarkers and prediction models. These problems – prediction problems with a large number of potential risk factors – are difficult to solve with plain statistics, but ideal for machine learning. While humans have great difficulty to comprehend 'big data', deep learning models are well-suited for it. In the past several years, there has been an almost exponential increase in the number of biomedical studies utilizing artificial intelligence (AI). There is some hope that this line of research will unlock the problem of risk stratification in NSCLC.

However, although AI is a promising tool, its place in the routine Pathology diagnostics is still only beginning to be established. Although some laboratories are now using fast-throughput scanners for a large portion of the diagnostic load, routine computer-aided diagnostics is still a distant dot on the horizon. The current digital infrastructure in virtually all laboratories is not able to accommodate AI-models yet, which will need to change in years to come. Additionally, the digitalization of laboratories will need to be paralleled with an increase in pathologist's digital awareness. In order to assess the benefit of AI-models, one needs to understand how AI-models work and be aware of the pitfalls. Currently however, AI has no place in the curriculum of pathologists-in-training.

Another challenge in the field of digital pathology and machine learning is domain adaptation. (Figure 4) It's well known that the performance of AI-models is often domain-specific, and models don't generalize well to other

laboratories. Small differences in cutting technique, scanner settings or staining methods (domain differences) can have substantial consequences for model performance. This will become an issue in long-term model use as well, as most laboratories purchase new laboratory equipment every few years. Data scientists need to come up with easy-to-implement domain adaptation models, and should work together with pathologists to determine a standardized, periodic quality assessment protocol for AI-tools.

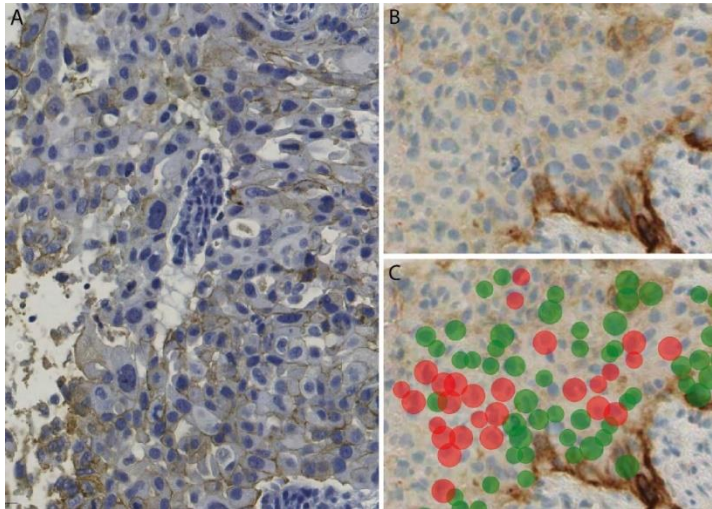


**Figure 4:** Domain adaptation example. A: PD-L1 slide from LUMC, using 22C3 antibody. B: PD-L1 slide from Erasmus MC, using SP263 antibody and a different immunostainer. C: Predictions from LUMC-trained PD-L1 algorithm on Erasmus MC slide, failing to correctly detect most cells due to domain differences.

### 7.3.2 Towards whole genome sequencing for all?

In the near future, whole genome sequencing (WGS) and liquid biopsy will be used more often. Whereas WGS is now inefficient for lung cancer biopsies and cytology due to tissue scarcity, the techniques involving WGS are becoming more tissue-efficient. Tissue scarcity is therefore unlikely to remain a limitation for long. In addition, WGS is becoming less expensive each year, which promotes the availability worldwide. Eventually, we will perform WGS on more often, regardless TNM stage.

In addition, liquid biopsy is now used only in selected cases. Although liquid biopsy still has some problematic limitations, such as the inability to detect

fusions, exon skipping and copy number alterations, it could be useful in selected cases, such as the TKI resistance setting. In **Chapter 6**, we demonstrated that *EGFR* TKI resistance cases have substantial intratumor genomic heterogeneity. In the 43-49% of resistance cases, no mechanism is identified, which could be caused by sampling error and potentially solved by liquid biopsy. For patients with acquired resistance to Osimertinib, liquid biopsy could thus become a meaningful addition.

### 7.3.3 Smoking eradication

Although future research will undoubtedly improve lung cancer diagnostics and mortality by using the most novel, cutting-edge techniques, their combined benefits are insignificant compared to what we would win when tobacco would be eradicated. Smoking is the main cause of lung cancer, and up to 90% of lung adenocarcinomas occur in former or current smokers. (**Chapter 3**) However, as discussed in **Chapter 1**, smoking prevalence is only slowly decreasing, and still rising in some countries.

The first anti-tobacco campaign originated from 1604, when King James I of England argued that smoking was “A custome lothsome to the eye, hatefull to the Nose, harmefull to the braine, dangerous to the Lungs, and in the blacke stinking fume thereof, neerest resembling the horrible Stigian smoke of the pit that is bottomelesse”. [5]

Statistical evidence for the detrimental effects of smoking was first reported to the public much later, in 1950, when epidemiologists Doll and Hill indisputably demonstrated a causal relation between smoking and lung cancer, first with their study in the London oncology wards, and later with their British Doctors Study. In their initial study, they proved that smoking was 25 times more prevalent in lung cancer patients compared to patients in the non-oncology ward. [6] They followed up their study with a prospective questionnaire study amongst British doctors, and demonstrated a much higher lung cancer related death rate in heavy smoking doctors. [7] The link between second-hand smoke and lung cancer was demonstrated in the 1980s, [8, 9] and the harmful effects of third-hand smoke are currently becoming more clear. [10, 11]

Since the poetic allegations of King James I and the thorough epidemiologic research of Doll and Hill, smoking prevention measures have increased in both quantity and quality. Currently, there are multiple evidence-based smoking

cessation interventions for individuals, including nicotine replacement, pharmacological treatment with bupropion and varenicline and behavioral interventions. These measures combined yield a 24% success rate 1 year after smoking cessation attempt, which is much better than the 3-5% when patients try to stop themselves, but still disappointingly low. [12]

Currently, there are many evidence-based population-level public health interventions, including: heavy taxes on tobacco products, [13] advertisement bans, [14] increasing the minimum age for legal access, [15, 16] reducing tobacco retailer density, [17] prohibiting smoking in public [18, 19] and awareness campaigns. [20] The main aim of these interventions is to reduce the number of people – especially children and young adults – who initiate smoking.

Historically, all (plans for) smoking prevention interventions are met with strong opposition from the tobacco industry, by means of misinformation and manipulation. When Doll and Hill first published about the causal relation between lung cancer and tobacco smoking in 1950, [6] their findings – although epidemiologically sound – were disputed by the tobacco industry, who fabricated contradictory studies and flooded the media with enlisted doctors claiming that Doll and Hills' research was controversial and lacked proof. [21] It wasn't until 1954, after Doll and Hill had repeated their study prospectively, on an even larger scale and with the same results, [7] that the link was finally acknowledged. Jeffrey Wigand, former vice-president of research and development at Brown & Williamson and one of the most influential whistleblowers in history, exposed that 'big tobacco' had, in fact, known about the detrimental health effects of smoking for decennia and was actively working towards making smoking even more addictive. He received several death threats and lawsuits.

In the Netherlands and the European Union, there is still evidence, today, that the tobacco industry influences politicians to delay or adjust plans for smoking prevention, [22] and routinely bypasses advertisement bans, for example via the use of social media influencers. [23]

However, it's still possible for decades-long traditions to change. New Zealand was recently internationally commended for announcing a comprehensive package of smoking prevention interventions at once. Their plan is to

completely eradicate smoking, in order to make their current 14-year-olds unable to ever buy tobacco products in their lifetime, and the first of a truly smoke-free generation. However promising, New Zealand is still the only country to make such far-reaching policy changes. Other countries – including the Netherlands – sluggishly struggle politically with the tobacco lobby, the idea of limiting people’s ‘free choice’ to smoke, and losing substantial income from tobacco taxes. Although a complete ban on smoking reduces healthcare costs substantially in the long run, it’s a painful financial choice in the short term.

Bradford Hill, confronted with the limited acknowledgement following their first paper in 1950, argued to Richard Doll that “the researchers’ job is to report, not campaign”, but this viewpoint has shifted significantly since the 1950s. CanMEDS roles ‘Maatschappelijk handelen’ and ‘Gezondheidsbevorderaar’ are now included in the Dutch medical curriculum as important capacities of a modern doctor, with an emphasis on prevention, [24] and doctors have become increasingly active in the media, backing anti-tobacco activists. This is a crucial development in the long run, as the best treatment for cancer patients is obviously to keep them from becoming sick in the first place.

#### 7.4 Conclusion

At the end of this thesis, we are a small step closer to optimizing and personalizing the diagnosis and treatment of NSCLC, by providing a rationale for each of the three key decision-making moments in NSCLC management. For lung cancer pathologists however, the journey toward precision medicine is far from over. The discovery of novel treatments, interventions and biomarkers are following each other up more rapidly than ever before, by which the scientific beast that is our collective academic knowledge has slowly begun to move NSCLC towards the categories of ‘preventable’, ‘curable’ and ‘manageable’. The lung cancer pathologist thus has a crucial and central role to play in the next decades: navigating new diagnostic challenges, learning to work with novel and unexpected innovations, and working together more intensively than ever before with molecular biologists, clinicians and radiologists. These new circumstances might ask more of lung cancer pathologists than ever before in history, but their effort – although enormous –

could just make it possible to provide a brighter future for the cancer patients of tomorrow.

## References

1. de Koning HJ, Van der Aalst CM, De Jong PA, et al., *Reduced Lung-Cancer Mortality with Volume CT Screening in a Randomized Trial*. N Engl J Med, 2020. **382**(6): p. 503-513.
2. Uramoto H and Tanaka F, *Recurrence after surgery in patients with NSCLC*. Transl Lung Cancer Res, 2014. **3**(4): p. 242-249.
3. Bai R, Lv Z, Xu D, et al., *Predictive biomarkers for cancer immunotherapy with immune checkpoint inhibitors*. Biomark Res, 2020. **8**: p. 34.
4. Giraldo NA, Sanchez-Salas R, Peske JD, et al., *The clinical role of the TME in solid cancer*. Br J Cancer, 2019. **120**(1): p. 45-53.
5. King James I of England, *A Counterblaste to Tobacco*. 1604.
6. Doll R and Hill AB, *Smoking and carcinoma of the lung; preliminary report*. Br Med J, 1950. **2**(4682): p. 739-748.
7. Doll R and Hill AB, *The mortality of doctors in relation to their smoking habits; a preliminary report*. Br Med J, 1954. **1**(4877): p. 1451-1455.
8. Hirayama T, *Non-smoking wives of heavy smokers have a higher risk of lung cancer: a study from Japan*. Br Med J (Clin Res Ed), 1981. **282**(6259): p. 183-5.
9. Trichopoulos D, Kalandidi A, Sparros L, et al., *Lung cancer and passive smoking*. Int J Cancer, 1981. **27**(1): p. 1-4.
10. Sleiman M, Gundel LA, Pankow JF, et al., *Formation of carcinogens indoors by surface-mediated reactions of nicotine with nitrous acid, leading to potential thirdhand smoke hazards*. Proc Natl Acad Sci U S A, 2010. **107**(15): p. 6576-81.
11. Jacob P 3rd, Beonwitz NL, Destailats H, et al., *Thirdhand Smoke: New Evidence, Challenges, and Future Directions*. Chem Res Toxicol, 2017. **30**(1): p. 270-294.
12. Laniado-Laborín R, *Smoking cessation intervention: an evidence-based approach*. Postgrad Med, 2010. **122**(2): p. 74-82.
13. Bader P, Boisclair D and Ferrence R, *Effects of tobacco taxation and pricing on smoking behavior in high risk populations: a knowledge synthesis*. Int J Environ Res Public Health, 2011. **8**(11): p. 4118-4139.
14. Saffer H and Chaloupka F, *The effect of tobacco advertising bans on tobacco consumption*. J Health Econ, 2000. **19**(6): p. 1117-37.
15. Millett C, Lee JT, Gibbons DC, et al., *Increasing the age for the legal purchase of tobacco in England: impacts on socio-economic disparities in youth smoking*. Thorax, 2011. **66**(10): p. 862-5.
16. *Public Health Implications of Raising the Minimum Age of Legal Access to Tobacco Products*, Bonnie RJ, Stratton K and Kwan LY. Editors. 2015, National Academies Press (US), Washington (DC).
17. Lee JGL, Kong AY, Sewell KB, et al., *Associations of tobacco retailer density and proximity with adult tobacco use behaviours and health outcomes: a meta-analysis*. Tob Control, 2021: p. tobaccocontrol-2021-056717.
18. Lemstra M, Neudorf C and Opondo J, *Implications of a public smoking ban*. Can J Public Health, 2008. **99**(1): p. 62-5.
19. Catalano MA and DB Gilleskie, *Impacts of local public smoking bans on smoking behaviors and tobacco smoke exposure*. Health Econ, 2021. **30**(8): p. 1719-1744.

20. Farrelly MC, Davis KC, Duke J, et al., *Sustaining 'truth': changes in youth tobacco attitudes and smoking intentions after 3 years of a national antismoking campaign*. Health Educ Res, 2009. **24**(1): p. 42-8.
21. Gardner MN and Brandt AM, *"The doctors' choice is America's choice": the physician in US cigarette advertisements, 1930-1953*. Am J Public Health, 2006. **96**(2): p. 222-232.
22. *Marlboro-fabrikant is slimmer dan de concurrentie (en de politiek)*, in *Follow The Money*. 2020: <https://www.ftm.nl/artikelen/philip-morris-concurrentie-politiek>.
23. Kaplan S, *Big Tobacco's Global Reach on Social Media*, in *The New York Times*. 2018.
24. Scheele F, Teunissen P, Van Luijk S, et al., *Introducing competency-based postgraduate medical education in the Netherlands*. Med Teach, 2008. **30**(3): p. 248-53.





An abstract cubist artwork featuring a complex composition of geometric shapes, primarily in shades of blue, white, and orange, with black outlines. The composition is dense and layered, with various forms overlapping and intersecting. The overall style is reminiscent of mid-20th-century abstract art.

# APPENDICES

## Nederlandse samenvatting

Voor niet-kleincellig longcarcinoom (NSCLC) zijn er meer behandel mogelijkheden dan ooit tevoren, wat ervoor zorgt dat het kiezen voor de juiste behandeling steeds complexer wordt. Longpathologen zijn verantwoordelijk voor het testen van NSCLC-patiënten voor een groot aantal moleculaire veranderingen en het voorspellen van immunotherapie-gevoeligheid. Hiervoor gebruiken ze een aantal testmethoden: immunohistochemie (IHC), in situ hybridisatie (ISH), DNA sequencing (DNA NGS) en RNA sequencing (RNA NGS). Echter, in het constant veranderende veld van moleculair onderzoek en onco-immunologie is het niet altijd duidelijk wat de beste testmethode is. Er wordt steeds gezocht naar een balans tussen weefsel-efficiëntie, tijd, kosten en uitgebreidheid van verschillende tests.

Het doel van dit proefschrift is daarom om retrospectief de huidige testmogelijkheden te onderzoeken, en de optimale testmogelijkheden te selecteren voor NSCLC-patiënten, specifiek op 3 cruciale diagnostische momenten:

1. Vroeg-stadium NSCLC (zonder uitzaaiingen)
2. Laat-stadium NSCLC, dat nog niet behandeld is
3. Laat-stadium NSCLC, na resistentie voor behandeling.

**Hoofdstuk 2** beschrijft de opbrengsten van moleculair onderzoek bij vroeg-stadium NSCLC. **Hoofdstuk 3** beschrijft de beste moleculaire work-up bij laat-stadium onbehandelde NSCLC. **Hoofdstuk 4** beschrijft de rol van kunstmatige intelligentie (AI) bij *programmed death ligand 1* immunoscore. **Hoofdstuk 5** beschrijft de sensitiviteit van NTRK immunohistochemie, en of dat gebruikt zou moeten worden in de routine diagnostiek. **Hoofdstuk 6** beschrijft de moleculaire work-up na resistentie voor EGFR-remmers.

## List of publications

Cohen D, Hondelink LM, Solleveld-Westerink N, et al. *Optimizing mutation and fusion detection in NSCLC by sequential DNA and RNA sequencing*. J Thorac Oncol. 2020 Jun;15(6):1000-1014.

Hondelink LM, Hüyük M, Postmus PE, et al. *Development and validation of a supervised deep learning algorithm for automated whole-slide programmed death-ligand 1 tumour proportion score assessment in non-small cell lung cancer*. Histopathology. 2022 Mar;80(4):635-647.

Hondelink LM, Jebbink M, Von der Thüsen JH, et al. *Real-world approach for molecular analysis of acquired EGFR tyrosine kinase inhibitor resistance mechanisms in NSCLC*. JTO Clin Res Rep. 2021 Nov 1;2(12):100252.

Butter R, Hondelink LM, van Elswijk L, et al. *The impact of a pathologist's personality on the interobserver variability and diagnostic accuracy of predictive PD-L1 immunohistochemistry in lung cancer*. Lung Cancer. 2022 Apr;116:143-149.

Hondelink LM, Schrader AMR, Asri Aghmuni G, et al. *The sensitivity of pan-TRK immunohistochemistry in solid tumours: a meta-analysis*. Eur J Cancer. 2022 Sep;173:229-237.

Hondelink LM, Ernst SM, Atmodimedjo P, et al. *Prevalence, clinical and molecular characteristics of early stage EGFR-mutated lung cancer in a real-life west-European cohort: implications for adjuvant therapy*. Eur J Cancer. 2023 Mar;181:53-61.

Song Q, Muller KE, Hondelink LM, et al. *Non-metastatic axillary lymph nodes have distinct morphology and immunophenotype in obese breast cancer patients at risk for metastasis*. MedRxiv. 2023 Apr 17:2023.04.14023288545.

Doeleman T, Hondelink LM, Vermeer MH, et al. *Artificial intelligence in digital pathology of cutaneous lymphomas: a review of the current state and future perspectives*. Semin Cancer Biol. 2023 Sep;94:81-88.

## **Curriculum vitae**

Coornhert-gymnasium Gouda (2006 – 2011)

Bachelor Geneeskunde Universiteit Leiden (2011 – 2014)

Master Geneeskunde Universiteit Leiden (2016 – 2020)

PhD-kandidaat afdeling Pathologie Leids Universitair Medisch Centrum (2020 – 2021)

Arts in opleiding tot patholoog Leids Universitair Medisch Centrum (2021 – heden)

## Dankwoord

Tessa  
Neetish  
Golzar  
Casper  
Sander  
Tobias  
Iza  
Michiel  
Nadia

Isa  
Kyra  
Maaike  
Willem  
Mariska  
Zaza  
Amy  
Manon  
Onno

Mathies  
Laurens  
Shay  
Sam  
Ro  
Wessel  
Max  
Diana  
Belcalis





Stellingen behorende bij het proefschrift getiteld 'Diagnostic challenges of today's lung cancer pathology: Personalizing therapy by immunohistochemical and molecular biomarkers'

- 1 Programmed death ligand 1 immunohistochemistry is a problematic biomarker for immunotherapy response. (this thesis)
- 2 Lung cancer in never smokers should be seen as a distinct entity, and a different molecular testing sequence should be used for never-smokers. (this thesis)
- 3 There is no place for pan-TRK and ROS1 immunohistochemistry in the NSCLC workup. (this thesis)
- 4 Targeted hotspot DNA NGS can never stand alone to identify HER2 and MET amplifications in the EGFR TKI acquired resistance setting. (this thesis)
- 5 Cell free DNA sequencing can replace part of the molecular diagnostics for NSCLC.
- 6 In treatment resistance management and prediction, the model of tumor evolution should be the central hypothesis.
- 7 Novel methods, including artificial intelligence, methylation, tumor-immune microenvironment profiling and RNA expression are promising potential new biomarkers for both prognostication and therapy selection in NSCLC.
- 8 Similar to the pan-cancer treatment indication for NTRK-rearranged stage IV tumors, a target-specific approach should be considered for other mutations.
- 9 The best treatment for NSCLC is prevention; more (societal and scientific) effort should go into smoking eradication and prevention.
- 10 Similar to the tobacco industry, scientists and universities should cut ties with the fossil fuel industry.